TRANSPORTATION RESEARCH RECORD
566

Vehicle Barrier Systems

8 reports prepared for the 54th Annual Meeting of the Transportation Research Board

TRB
TRANSPORTATION RESEARCH BOARD
NATIONAL RESEARCH COUNCIL
Washington, D. C., 1976

Transportation Research Record 566
Price $6.00
Edited for TRB by Joan B. Silberman

Subject areas
22 highway design
51 highway safety

The project that is the subject of this report was approved by the Governing Board of the National Research Council, whose members are drawn from the councils of the National Academy of Sciences, the National Academy of Engineering, and the Institute of Medicine. The members of the committee responsible for the report were chosen for their special competence and with regard for appropriate balance.

This report has been reviewed by a group other than the authors according to procedures approved by a Report Review Committee consisting of members of the National Academy of Sciences, the National Academy of Engineering, and the Institute of Medicine.

LIBRARY OF CONGRESS CATALOGING IN PUBLICATION DATA

National Research Council. Transportation Research Board.
Vehicle barrier systems.

(Transportation research record; 566)
1. Roads–General fences–Addresses, essays, lectures. 2. Roads–Crash cushions–Addresses, essays, lectures. 3. Bridge railings–Addresses, essays, lectures. I. Title. II. Series.
TE7.H5 no. 566 [TE228] 380.5'08s [625.7'95]
ISBN 0-309-02476-5 76-15253

CONTENTS

FOREWORD

The eight papers in this RECORD cover a variety of topics in the area of roadside safety devices. Bridge rail behavior under heavy vehicle impact is discussed in three papers: Two deal with analytical simulation, and one deals with a specific design concept. Construction of an energy-absorbing bridge rail, scale-model and pendulum testing techniques, and full-scale test results of a guardrail system and a crash cushion are reported on.

Labra, Rudd, and Ravenscroft present an analytical modeling technique to simulate possible rollover vaulting of heavy vehicles impacting traffic railings. Such behavior is always possible with heavy vehicles because of their relatively high center of gravity, and the simulation model presented is intended to provide estimates of this type of behavior for single-unit vehicles.

Calculation procedures to assess the potential of proposed designs of flexible bridge railings are reported by Cantor and Bloom. These procedures were derived to provide guidance for initial evaluation of flexible bridge railings intended to safely contain impacting vehicles ranging from subcompacts to large single-unit trucks. Limited validation cases of this calculation method are presented.

Helm, Free, Warner, and Frandsen investigated the effects of friction at the car-barrier interface in angular collisions by using scale-model techniques. For the specific barrier design examined, significant changes in gross vehicle behavior were noted over the range of friction values studied in modeled 60-mph (97-km/h), 25-deg impacts.

An energy-absorbing bridge railing using the plastic deformation of steel rings is reported on by Kimball, Bronstad, Michie, Wentworth, and Viner. The development program included full-scale crash testing and the use of the BARRIER VII computer program. The results of the full-scale crash tests ranging from 2,000-lb (907-kg) subcompacts to 40,000-lb (18 144-kg) buses and tractor-trailers are discussed.

Nordlin, Stoker, and Stoughton report on strong post guardrail tests in which three post designs are compared. In the specific system examined, both smaller sized wood posts and blocks and steel posts and blocks were found to be acceptable alternates to the previous California design for metal beam guardrails.

Pendulum tests of a single breakaway sign support leg using rigid and crushable pendulum striking faces are reported by Bronstad, Michie, and White. Both conventional base-bolting assemblies and torque-limiting nuts were included in the test series.

Kasinskas and Dougan describe the construction of an energy-absorbing bridge rail using frangible tubes as the primary energy absorber. Specific design changes from the tested version of this railing made for the specific installation site are noted.

Marquis, Hirsch, and Nixon report on four tests with tire-sand inertia barriers. Such barriers are intended for sites where debris scatter from sand tires is not likely to fall on the paved roadway.

—John G. Viner

ROLLOVER-VAULTING ALGORITHM FOR SIMULATING VEHICLE-BARRIER COLLISION BEHAVIOR

John J. Labra, James Rudd, and J. Ravenscroft, ENSCO, Inc., Springfield, Virginia

Because of the relatively high center of gravity of most heavy vehicles, the possibility of rollover vaulting is always present when a heavy vehicle collides with a median or bridge barrier. There have been various investigations made on vehicle-barrier response using simulation models that are either too simplified or extremely costly to run. The algorithm developed in this paper incorporates a comprehensive, three-dimensional model of the vehicle-barrier interaction and is very inexpensive to operate. In this algorithm, the vehicle-barrier interaction is assumed to take place in three phases: (a) the initial impulsive impact with the barrier; (b) a continuous, nonimpulsive translational and angular motion during redirection; and (c) a second impulsive impact when the rear of the vehicle swings around and strikes the barrier. The algorithm enables the user to monitor all the important vehicle dynamic parameters, including the angular orientation of the vehicle during redirection and the magnitude of the initial impulsive impact forces between vehicle and barrier. The program is applied to investigate the vaulting potential of passenger and heavy vehicles with various barriers at speeds and impact angles covering the expected range.

•VARIOUS investigations have been made into the behavior of vehicles interacting with median and bridge barriers (1, 2, 3, 4, 5, 6, 7). Because of the relatively high center of gravity (c.g.) of most of these heavy vehicles, the possibility of rollover vaulting is always present when such a vehicle collides with a barrier. A relatively simple mathematical procedure for determining the possibility of rollover vaulting has been developed by Dunlap (8). This approach essentially is limited to the case of the vehicle impacting the barrier broadside so that all points along the length of the vehicle impact the barrier simultaneously. In reality, the initial impact of the vehicle is usually restricted to the front corner nearest the barrier. Dunlap (8) extrapolates his method to cover this oblique condition by using certain worst case values for the vehicle's initial kinematic conditions during the interval of redirection. However no general methods for obtaining values of these worst case conditions were presented.

There are two other limitations with the aforementioned procedure (8). First, only rollover potential about the barrier's longitudinal axis is checked. However, the vehicle may be more likely to roll about another axis (lying between the barrier and vehicle axes), and this would not be revealed by Dunlap's analysis. Second, the procedure computes an angular velocity parameter $\dot{\Phi}_f$ at each time step during redirection derived from an impulse principle. This assumption is only valid during the initial impulsive contact with the barrier and not during the smooth redirection phase.

In an effort to remove the aforementioned limitations, an improved rollover-vaulting algorithm (RVA) has been developed. In this algorithm, the vehicle-barrier interaction is assumed to take place in three phases: (a) the initial impulsive impact with the barrier at a given angle; (b) a continuous, nonimpulsive translational and rolling motion during redirection; and (c) a second impulsive impact when the rear of the vehicle swings around and impacts the barrier. This third step could conceivably be eliminated by assuming a nonimpulsive motion after the initial impact and redirection. However, although this would simplify the procedure, observations of full-scale tests and past simulation results based on the BARRIER VII program (9) reveal that a second impulsive impact situation does indeed occur. Specifically, the RVA program can monitor the following:

1. The angular orientation of the vehicle during and after the initial impact,
2. The respective angular rates of the vehicle during redirection,
3. The trajectory of the vehicle center of gravity during redirection,
4. The magnitude of the initial impulse between the vehicle and the barrier, and
5. The tire-suspension reaction forces during redirection of the vehicle.

In the algorithm, a vehicle fixed reference frame and an inertial reference frame as shown in Figure 1 are used. The vehicular reference frame origin O, located at the contact point, is assumed to traverse at a constant speed in the plane of the barrier. After the initial impact at O, the vehicle is assumed to rotate about this moving impact point during the redirection phase.

To maintain low computer costs when implementing the RVA program, certain simplifying assumptions have been made. These include

1. A six degree of freedom, rigid body representation for the vehicle without separate degrees of freedom for the wheels;
2. A single impact point moving with a constant velocity during redirection;
3. A representation of a linear spring and dashpot tire-suspension force; and
4. An undeformable vehicle-barrier interface.

As a result, the computer run time for evaluating a typical impact is extremely short (approximately 2 sec of CP time on a CDC 6000 Series machine). Thus, reliable rollover-vaulting information can be obtained at a fraction of the cost required for other existing three-dimensional vehicle-barrier simulations.

With the RVA program, vaulting potential for any single-unit vehicle may be investigated by inserting the relevant weight and geometric parameters. The program was used to investigate impacts of a 45,500-lb (20 638-kg) truck, a 40,000-lb (18 144-kg) bus, and a 4,000-lb (1814-kg) car with a rigid barrier of variable height for various impact conditions. For the truck, the results indicated no vaulting for the 10 and 15-deg impact angles for barrier heights ≥ 30 in. (76.2 cm). However, rollover vaulting was predicted for the 25-deg impact. For the car, the results indicated no vaulting for any of the runs. This is attributed to the relatively low center of gravity position with respect to the barrier's longitudinal roll axis. In the case of the bus simulations, vaulting was predicted with the 27-in. (68.6-cm) barrier at 60 mph (96.5 km/h) and the 25-deg impact angle. However, for the 39-in. (99.1-cm) barrier, no vaulting occurred during the run at 60 mph (96.5 km/h) and 25 deg. Further applications of the RVA program to investigate rollover vaulting in the case of flexible barriers are discussed later.

INITIAL IMPACT

In the RVA program when the vehicle first impacts the barrier, an impulsive situation is assumed to exist. Based on the angular momentum principle about the vehicle's c.g., the angular velocity components ω_1, ω_2, and ω_3 about their respective vehicle fixed axes x, y, and z, assumed to be zero before impact, are defined by the following:

$$\| I_{ij}^{c.g.} \| \begin{vmatrix} \omega_1 \\ \omega_2 \\ \omega_3 \end{vmatrix} = \bar{r} \times \hat{P} \qquad (1)$$

where

$\| I_{ij}^{c.g.} \|$ = the vehicle's moment of inertia matrix about its c.g.,

Figure 1. Vehicle impacting barrier.

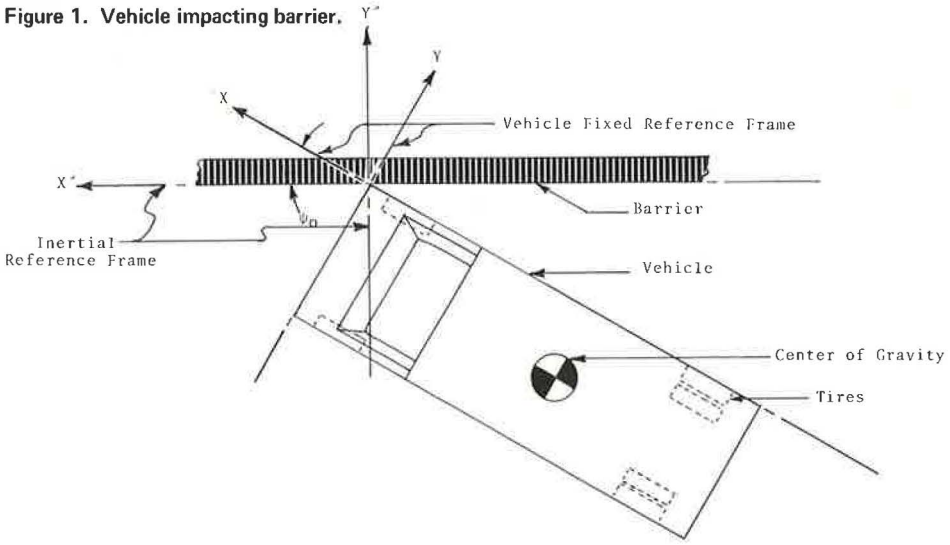

Figure 2. Side and bottom views of vehicle.

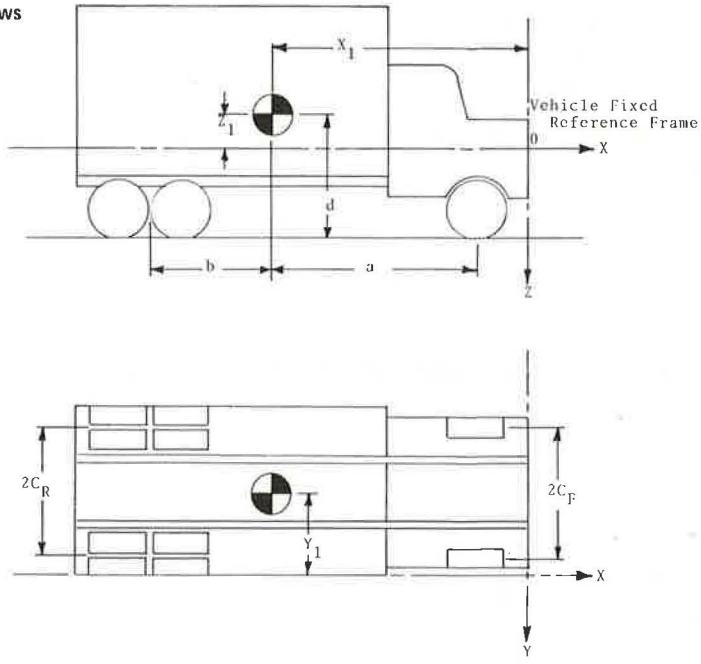

Table 1. Vehicle parameters.

Parameters	Car	Bus	Truck	Parameters	Car	Bus	Truck
M, lb	4,000	40,000	45,500	a, in.	59	240	136
x_1, in.				b, in.	57	101	42
39-in. barrier	-91	-270	-172	C_F, in.	30	36	40
27-in. barrier	-91	-270	-172	C_R, in.	30	36	36
y_1, in.				d, in.	24	55	55
39-in. barrier	-37	-48	-38	α_{RF} and α_{LF}, lbf-sec/in.	3.5	4.16	4.16
27-in. barrier	-37	-48	-38	α_{RR} and α_{LR}, lbf-sec/in.	3.9	4.16	0
z_1, in.				β_{RF} and β_{LF}, lbf	55	2,200	1,100
39-in. barrier	15	-16	-16	β_{RR} and β_{LR}, lbf	50	2,200	2,200
27-in. barrier	3	-28	-28	ϵ_{LF} and ϵ_{RF}, in./sec	0.001	0.001	0.001
I_{ij}^{*}, lbf-sec^2-in.				ϵ_{LR} and ϵ_{RR}, in./sec	0.001	0.001	0.001
I_{xx}	4,500	211,000	126,536	k_{RF} and k_{LF}, lbf/in.	131	4,700	2,300
I_{yy}	25,000	2,509,000	385,543	k_{RR} and k_{LR}, lbf/in.	192	4,700	4,700
I_{zz}	39,000	2,500,000	487,358				
I_{xz}	0	0	0				

Note: 1 lb = 0.45 kg, 1 in. = 2.54 cm, 1 lbf-sec^2-in. = 11.29 N-s^2-cm, 1 lbf-sec/in. = 1.75 N-s/cm, 1 lbf = 4.45 N, 1 lbf/in. = 175.1 N/m.

$\bar{r}$ = the moment arm from the vehicle's c.g. to the impact point O on the barrier, and
$\hat{P}$ = the impulsive force between vehicle and barrier.

Based on the linear momentum principle during this initial impact phase, we also obtain

$$\left.\begin{aligned} M(v_x' - v_x) &= -\hat{P}_x \\ M\, v_y' &= -\hat{P}_y \\ M\, v_z' &= -\hat{P}_z \end{aligned}\right\} \tag{2}$$

where

v_x, O, O = the initial translational velocity of the c.g. before impact in the vehicle fixed longitudinal direction;
v_x', v_y', v_z' = the c.g. velocity components immediately after impact, with respect to the vehicle fixed coordinate system;
$\hat{P}_x$, $\hat{P}_y$, $\hat{P}_z$ = the impulsive force components in the negative vehicle fixed x, y, z directions; and
M = the mass of the vehicle.

Assuming that the component of the impulsive force in the plane of the barrier can be ignored, we have

$$\left.\begin{aligned} \hat{P}_x \cos\psi_o - \hat{P}_y \sin\psi_o &= 0 \\ \hat{P}_z &= 0 \end{aligned}\right\} \tag{3}$$

where ψ_o is the initial yaw angle between the vehicle and the barrier.

In addition, the relationship between the vehicle c.g. velocity and the contact point velocity is

$$\begin{vmatrix} v_x' \\ v_y' \\ v_z' \end{vmatrix} = \begin{vmatrix} v_{px} \\ v_{py} \\ v_{pz} \end{vmatrix} + \begin{vmatrix} \omega_2 z_1 - \omega_3 y_1 \\ \omega_3 x_1 - \omega_1 z_1 \\ \omega_1 y_1 - \omega_2 x_1 \end{vmatrix} \tag{4}$$

where

v_{px}, v_{py}, v_{pz} = the components of the contact point O velocity in the vehicle fixed system, and
x_1, y_1, z_1 = the components of the vector from point O to the c.g.

Furthermore, the components V_{px}, V_{py}, and V_{pz} of the contact point velocity in the inertial reference frame may be written as

$$\begin{vmatrix} V_{px} \\ V_{py} \\ V_{pz} \end{vmatrix} = \| A \| \begin{vmatrix} v_{px} \\ v_{py} \\ v_{pz} \end{vmatrix} \tag{5}$$

where

$$\|A\| = \begin{vmatrix} \cos\theta\cos\psi & -\cos\psi\sin\psi + \sin\phi\sin\theta\cos\psi & \sin\phi\sin\psi + \cos\phi\sin\theta\cos\psi \\ \cos\theta\sin\psi & \cos\phi\cos\psi + \sin\phi\sin\theta\sin\psi & -\cos\psi\sin\phi + \cos\phi\sin\theta\sin\psi \\ -\sin\theta & \cos\theta\sin\phi & \cos\theta\cos\phi \end{vmatrix},$$

which is the transformation matrix from the vehicle fixed to the inertial reference frame, and

θ, ϕ, ψ = the pitch, roll, and yaw angles for the vehicle.

Finally, if we now assume the vehicle remains in contact with the barrier at point O during redirection, we also have the following additional constraint:

$$V_{py} = 0 \tag{6}$$

Coupling this constraint with equations 1, 2, 3, 4 and 5 yields the resulting angular and translational velocities of the vehicle after the initial impact. These velocities then define the initial conditions for the second phase of the impact discussed in the next section.

MOTION DURING REDIRECTION

After the initial impact with the barrier, the vehicle is assumed to remain in contact with the barrier at point O. In addition, the contact point is assumed to traverse at a constant velocity. Through this assumption, the rotational equations of motion about the point O have the form of the Euler equations of motion:

$$\|I^{o}_{ij}\| \cdot \begin{vmatrix} \dot{\omega}_1 \\ \dot{\omega}_2 \\ \dot{\omega}_3 \end{vmatrix} = |E| + \begin{vmatrix} \Sigma M_\phi \\ \Sigma M_\theta \\ \Sigma M_\psi \end{vmatrix} \tag{7}$$

where

$\|I^{o}_{ij}\|$ = the vehicle's moment of inertia matrix about the vehicle-barrier contact point O,

$\begin{vmatrix} \Sigma M_\phi \\ \Sigma M_\theta \\ \Sigma M_\psi \end{vmatrix}$ = the resulting moments about point O due to the tire-suspension reaction forces (Appendix).

$$|E| = \begin{vmatrix} -\omega_2\Omega_3 + \omega_3\Omega_2 + MgA_1 \\ +\omega_1\Omega_3 - \omega_3\Omega_1 - MgA_2 \\ -\omega_1\Omega_2 + \omega_2\Omega_1 + MgA_2 \end{vmatrix} \tag{8}$$

are the nonlinear inertial terms in the equations of motion, where

$$\Omega_1 = I_x\omega_1 - I_{xy}\,\omega_2 - I_{xz}\,\omega_3,$$

$$\Omega_2 = I_y\omega_2 - I_{yx}\,\omega_1 - I_{yz}\omega_3,$$

$$\Omega_3 = I_z\omega_3 - I_{zx}\,\omega_1 - I_{zy}\,\omega_2,$$

$$A_1 = y_1 \cos\theta\,\cos\phi - z_1 \sin\phi\,\cos\theta,$$

$$A_2 = x_1 \cos\theta\,\cos\phi + z_1 \sin\theta, \text{ and}$$

$$A_3 = x_1 \sin\phi\,\cos\theta + y_1 \sin\theta.$$

The initial value of angles θ, ϕ, and ψ in equation 8 are taken to be those defined for the vehicle before impact (e.g., $\theta = \phi = 0$; $\psi = \psi_o$). The initial angular velocities ω_1, ω_2, and ω_3, on the other hand, are those values obtained from equation 1. In addition, during the period of redirection, the forces assumed to act about the contact point are the tire-suspension reaction forces (Appendix) and the vehicle's weight. To solve equation 7 for each time increment Δt, values of angles θ, ϕ, and ψ for time t are required. These are obtained from the following:

$$\left.\begin{aligned} \dot{\psi} &= \frac{1}{\cos\theta}\,[\omega_2 \sin\phi + \omega_3 \cos\phi] \\ \dot{\phi} &= \omega_1 + \omega_2 \sin\phi \tan\theta + \omega_3 \cos\phi \tan\theta \\ \dot{\theta} &= \omega_2 \cos\phi - \omega_3 \sin\phi \end{aligned}\right\} \qquad (9)$$

By integrating the solutions to equations 7 and 9 and by using in both equations the previous values for ω_1, ω_2, ω_3 and θ, ϕ, ψ, one obtains the vehicle angular velocity and corresponding angle orientations for any time t.

When the vehicle has been redirected to a position where the yaw angle ψ is zero, the second impulsive impact is assumed to occur.

SECONDARY IMPACT

From observations of full-scale tests and simulation results, it became apparent that, after the impacting vehicle redirects parallel to the barrier, a second impulsive situation exists. This was noted especially for the longer and heavier vehicles such as trucks and buses.

For simulation of this second impulsive impact, the vehicle's orientation is monitored during redirection until the yaw angle ψ between vehicle and barrier is zero. At this point, the second impact is assumed to take place. Impulse principles are again used to determine the resulting motion. Here it is assumed that after impact the resulting angular motion is purely about the barrier longitudinal axis X. Based on this assumption, the equation of motion is

$$\|\,I^*_{ij}\,\| \begin{vmatrix} \dot{\Phi} \\ 0 \\ 0 \end{vmatrix} - \begin{vmatrix} 0 \\ \hat{T}_2 \\ \hat{T}_3 \end{vmatrix} = \|\,I^*_{ij}\,\| \begin{vmatrix} \omega_1^* \\ \omega_2^* \\ \omega_3^* \end{vmatrix} \qquad (10)$$

where

$\| I^*_{ij} \|$ = the inertia matrix of the vehicle about the contact point O with respect to the inertial XYZ coordinate system,
$\omega^*_1, \omega^*_2, \omega^*_3$ = the vehicle angular velocity components immediately before impact with respect to the inertial reference frame,
$\dot{\Phi}, 0, 0$ = the resulting vehicle angular velocity vector immediately after impact about the inertial X axis, and
$0, \hat{T}_2, \hat{T}_3$ = the impulsive torque components.

To determine if the resulting angular velocity $\dot{\Phi}$ about the barrier's longitudinal axis is sufficient to cause rollover vaulting of the vehicle, the critical angular velocity $\dot{\Phi}_{RV}$ for vaulting is first evaluated. This is found by using the conservation of energy principle after the second impulsive impact:

$$KE_f + PE_f = KE_i + PE_i \tag{11}$$

where

KE = kinetic energy,
PE = potential energy, and
i, f = subscripts indicating initial and final respectively.

The initial potential energy after secondary impact is

$$PE_i = W_v D \tag{12}$$

where

W_v = the weight of the vehicle, and
D = the vertical height of the c.g. with respect to the inertial reference frame, at the instant of secondary impact.

The initial kinetic energy after impact is simply

$$KE_i = \tfrac{1}{2} I^*_x \dot{\Phi}^2 \tag{13}$$

where I^*_x is the vehicle's moment of inertia about the barrier's longitudinal axis (inertial X axis).

The limiting case of rollover vaulting occurs when KE_f is zero at the instant the vehicle c.g. is vertically above the barrier. In this case,

$$\Phi + \beta = 90 \text{ deg} \tag{14}$$

where

$$\beta = \tan^{-1} [(-z_1 \cos\theta_o)/y_1], \text{ and} \tag{15}$$

θ_o = pitch orientation of the vehicle at the instant of secondary impact.

Determination of the vertical height of the c.g. in this configuration is obtained by substituting Φ from equation 14 into the third row of the transformation matrix $\| A \|$, that is,

$$D_1 = (a_{31}, a_{32}, a_{33}) \begin{vmatrix} x_1 \\ y_1 \\ z_1 \end{vmatrix} \tag{16}$$

The potential energy at this instance is then

$$PE_f = W_v D_1 \tag{17}$$

Substituting equations 12, 13, and 17 into equation 11, we obtain, for the critical angular velocity,

$$\dot{\Phi}_{RV} = \sqrt{\frac{2W_v(D_1 - D)}{I_x^*}} \tag{18}$$

Thus, if the roll rate $\dot{\Phi}$ obtained from equation 10 is equal to or greater than $\dot{\Phi}_{RV}$, i.e.,

$$\dot{\Phi}/\dot{\Phi}_{RV} \geq 1 \tag{19}$$

then rollover vaulting will take place.

IMPLEMENTATION OF RVA PROGRAM AND SIMULATION RESULTS

The foregoing theoretical developments were amalgamated into an algorithm and coded for placement on a CDC 6400 system. Using the RVA program, simulations were made for a car, an inner-city truck, and a bus impacting a rigid barrier. The vehicular speeds and impact angles initially considered were (1 mph = 1.6 km/h):

1. 60 mph/7 deg,
2. 60 mph/15 deg, and
3. 60 mph/25 deg.

Corresponding to these impact conditions, two configurations of barriers were initially considered, consisting of a 27-in. (68.6-cm) concrete parapet with and without a 12-in.-high (30.5-cm) steel railing [heights of 39 in. (99.1 cm) and 27 in. (68.6 cm) respectively]. The vehicle geometric parameters, as shown in Figures 1 and 2, and tire-suspension force parameters (as defined in the Appendix) are given in Table 1.

With the vehicle parameters given in Table 1 for a car, bus, and inner-city truck, a series of simulations were made by using the RVA program. The results for the various impacts are given in Table 2 and are shown in Figure 3.

From the above defined simulations, all runs at the 7 and 10-deg impact angles resulted in satisfactory nonvaulting vehicle behavior. In addition, the 15 and 25-deg-angle impacts for the automobile also resulted in satisfactory behavior modes. However, the bus vaulted the 27-in. (68.6-cm) barrier at 60 mph (96.5 km/h) and 25 deg, and the truck vaulted the 27-in. (68.6-cm) barrier at 60 mph (96.5 km/h) and 15 deg.

Since there is no energy dissipation through vehicle sheet metal or barrier deformation in the RVA program, the ratio value (Table 2) of 1.0 should be considered only as an estimate of vehicle vaulting potential. This is further emphasized when one considers that, under full-scale test conditions, when a vehicle impacts a contoured rigid

Table 2. Potential of vehicles to vault barriers at various speeds and impact angles.

Item	Barrier Height (in.)	60 mph and 7 Deg		60 mph and 10 Deg		60 mph and 15 Deg		60 mph and 25 Deg	
		Position	Ratio[a]	Position	Ratio[a]	Position	Ratio[a]	Position	Ratio[a]
Car	39	Stable	-0.42			Stable	-1.39	Stable	-3.89
	27	Stable	-0.07			Stable	-0.22	Stable	-0.51
Bus	39	Stable	0.18			Stable	0.08	Stable	0.52
	27	Stable	0.20			Stable	0.52	Vault	1.58
Truck	27	Stable	0.52			Vault	1.11	—	—
	30			Stable	0.41	Stable	0.93	Vault	3.02
	31			Stable	0.38	Stable	0.87	Vault	2.77
	32			Stable	0.34	Stable	0.81	Vault	2.55
	33			Stable	0.31	Stable	0.75	Vault	2.33
	35			Stable	0.25	Stable	0 63	Vault	1.95
	37			Stable	0.23	Stable	0.52	Vault	1.61
	39			Stable	0.21	Stable	0.41	Vault	1.31
	41			Stable	0.19	Stable	0.30	Vault	1.03

Note: 1 mph = 1.61 km/h. 1 in. = 2.54 cm.

[a] $\dot{\Phi}/\dot{\Phi}_{RV}$. If greater than unity, the truck vaults when impacting a noncontoured parapet or a flexible barrier.

Figure 3. Rollover-vaulting potential for 45,500-lb (20 638-kg) inner-city truck.

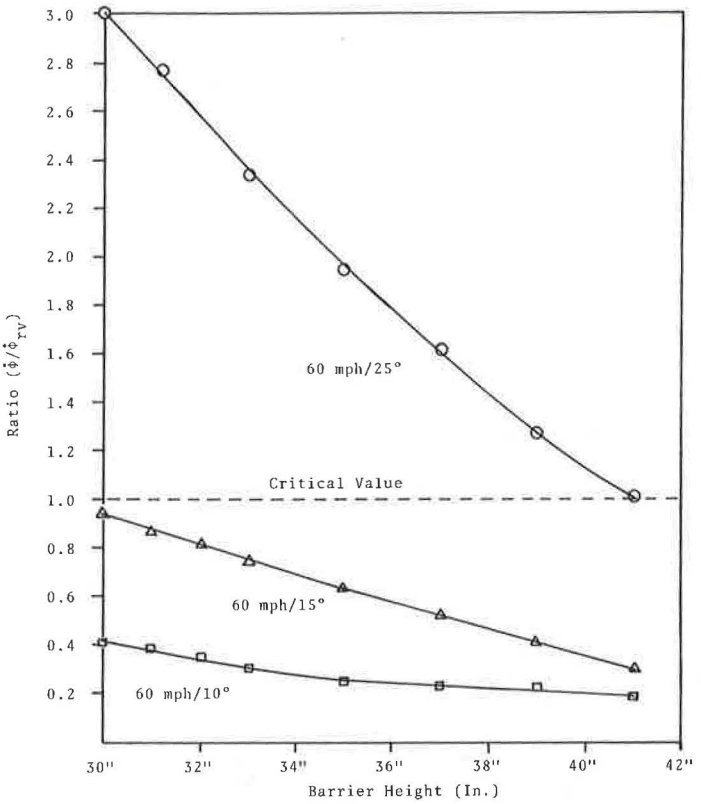

Table 3. Vehicle orientation at secondary impact.

Item	Barrier Height (in.)	60 mph and 7 Deg			60 mph and 15 Deg			60 mph and 25 Deg		
		ϕ (deg)	θ (deg)	$\dot{\Phi}$ (deg/sec)	ϕ (deg)	θ (deg)	$\dot{\Phi}$ (deg/sec)	ϕ (deg)	θ (deg)	$\dot{\Phi}$ (deg/sec)
Car	39	-0.3	0.1	-67.6	-15.5	0	-188.3	-27.8	3.6	-384.7
	27	-1.4	0	-15.2	-3.1	0.3	-46.4	-5.3	0.9	-105.3
Bus	39	-0.6	0	24.5	0.4	0.3	11.3	11.5	1.2	76.2
	27	-1.4	0.1	24.2	9.4	0.9	64.0	28.0	1.9	195.4
Truck	39	-0.6	0.1	31.0	2.2	0.3	61.4	8.5	0.4	183.0
	27	2.2	0.2	61.7	7.2	0.6	130.5	—	—	—

Note: 1 mph = 1.6 km/h. 1 in. = 2.54 cm.

parapet, the redirectional properties of the contoured parapet will reduce the vehicle's potential for vaulting. However, the degree to which the contour will aid in redirecting an impacting vehicle will depend in part on the size of the vehicle. For a large single-unit vehicle, the redirectional properties of a New Jersey type of contour parapet would be minimal. This was verified by our use of the highway vehicle object simulation model (1) to simulate heavy vehicle-rigid barrier impacts. We found that at 60 mph (96.5 km/h) and 15 deg a 33-in.-high (83.8-cm) contoured parapet was sufficient to prevent rollover vaulting of a 45,500-lb (20 638-kg) single-unit vehicle. However at 60 mph (96.5 km/h) and 15 deg, a 27-in.-high (68.6-cm) parapet resulted in the vehicle vaulting the barrier. These findings compare well with the results from the RVA simulations (Table 2), which do not consider the contour of the parapet. Hence, as seen in Figure 3, a rigid concrete parapet over 30 in. high (76.2 cm) should be sufficient to prevent vaulting of a 45,500-lb (20 638-kg) single-unit vehicle at 60 mph (96.5 km/h) and 15 deg. In the case of flexible barriers that have the potential of lying down, thereby ramping the vehicle, a minimum height of 39 in. (99.1 cm) is recommended to prevent vaulting of the same vehicle under the same impact conditions.

In addition to the evaluation of whether a vehicle would vault the barrier, the results of the simulations demonstrated the importance of the final roll position ϕ and roll-angular velocity $\dot{\Phi}$ at the instant of secondary impact. In the case of the impacting automobile, the roll orientation and negative roll velocity at the instant of secondary impact (Table 3) had a stabilizing effect in preventing the vehicle from vaulting. Contrary to this, in the case of the bus impacting the 27-in. (68.6-cm) barrier (Table 3), the relatively high roll angle (ϕ = 28 deg) and roll velocity ($\dot{\Phi}$ = 195.4 deg/sec) toward the barrier resulted in the bus vaulting at 60 mph (96.5 km/h) and 25 deg.

A complete comparison of the roll ϕ and pitch θ positions for all three vehicles and the resulting angular velocity $\dot{\Phi}$ after the secondary impact are given in Table 3 for specific simulations.

FURTHER APPLICATIONS

The RVA algorithm can be used to investigate the possibility of rollover vaulting for various vehicle-barrier combinations. In vehicles, this includes the various automobile models (e.g., compact, full-sized sedan) and the heavier single-unit vehicles (e.g., inner-city truck, bus). The barriers modeled can be both the rigid type (e.g., California type 20 bridge barrier, Texas CMB-70) and the flexible type (e.g., Texas T-1, aluminum barrier).

When a rigid barrier with a contoured parapet is modeled, the effect of the parapet in redirecting the vehicle by assuming a nonzero initial roll and pitch orientation can be determined before the initial impact. (This requires a simple modification of equation 1). If a felxible barrier is modeled, the location of the inertial X axis may be varied to account for the lowering of the impact point O and the axis of rotation due to barrier torsional deflections. In this instance, the top and bottom of the undeformed barrier may be considered as the inertial X axis, and this results in an upper and lower bound on the probability of rollover vaulting.

Furthermore, if the energy dissipation through vehicle and barrier deformation is neglected, the results of this algorithm will be conservative in nature. However, considering the flexible barrier phenomena of torsional deflections and the possibility of vehicular ramping, the findings of the study have a nonconservative aspect. As a result of this, the RVA program should be used as a tool for quickly estimating the vaulting potential during vehicle-barrier interaction. Its findings should not, however, be taken as rigid guidelines without proper verification through full-scale testing.

REFERENCES

1. R. R. McHenry and N. J. Deleys. Vehicle Dynamics in Single Vehicle Accidents: Validation and Extension of a Computer Simulation. Cornell Aeronautical Laboratory, Rept. VJ-2251-V-3, Dec. 1968.

2. T. J. Hirsch, G. G. Hayes, and E. R. Post. Vehicle Crash Test and Evaluation of Median Barriers for Texas Highways. Texas Transportation Institute, Texas A&M Univ., Research Rept. 146-4, June 1972.
3. R. D. Young, H. E. Ross, Jr., and R. M. Holcomb. Simulation of Vehicle Impact With the Texas Concrete Median Barrier. Texas Transportation Institute, Texas A&M Univ., Research Rept. 140-5, Vol. 1, June 1972.
4. T. J. Hirsch and E. R. Post. Truck Tests on Texas Concrete Median Barrier. Texas Transportation Institute, Texas A&M Univ., Research Rept. 146-7, Aug. 1972.
5. M. P. Jurkat and J. A. Starrett. Automobile-Barrier Impact Studies Using Scale Model Vehicles. Highway Research Record 174, 1967, pp. 30-41.
6. E. F. Nordlin, R. N. Field, and R. P. Hackett. Dynamic Full-Scale Impact Test of Bridge Barrier Rails. Highway Research Record 83, 1965, pp. 132-168.
7. E. F. Nordlin and R. H. Field. Dynamic Tests of Steel Box Beam and Concrete Median Barriers. Highway Research Record 222, 1968, pp. 53-88.
8. D. F. Dunlap. Curb-Guardrail Vaulting Evaluation. Highway Research Record 460, 1973, pp. 10-19.
9. G. H. Powell. Computer Evaluation of Automobile Barrier Systems. Univ. of California, Berkeley, Rept. UC SESM 70-17, Aug. 1970.

APPENDIX

TIRE-SUSPENSION REACTION FORCES

During the interval of vehicle redirection after the initial impact with the barrier, the roll and pitch orientations are determined by the vehicle dynamic system. These changes result from the vehicle's initial velocity conditions, weight, and the tire-suspension system's reaction forces during redirection.

The tire-suspension forces are assumed to amount to linear springs with viscous and coulomb damping, that is,

$$F'_{IJ} = k_{IJ} Z'_{IJ} + \alpha_{IJ} \dot{Z}'_{IJ} + \beta_{IJ} \tag{20}$$

where

- IJ = the subscripts for right front (RF), left front (LF), right rear (RR), and left rear (LR) tire locations on the vehicles,
- k_{IJ} = the equivalent tire-suspension system spring stiffnesses for each wheel,
- α_{IJ} = the viscous damping coefficients for the individual wheels,
- β_{IJ} = the coulomb damping coefficients for the individual wheels,
- Z'_{IJ} = the individual vertical tire displacements in the inertial coordinate system, and
- $\dot{Z}'_{IJ}$ = the individual vertical tire velocities in the inertial coordinate system.

Although the k_{IJ} and α_{IJ} are constant, the β_{IJ} terms are defined as

$$\beta_{IJ} = \begin{cases} 0 \text{ for } |\dot{Z}'_{IJ}| \leq \xi_{IJ} \\ \beta_{IJ} \operatorname{sgn}(\dot{Z}'_{IJ}) \text{ for } |\dot{Z}'_{IJ}| > \xi_{IJ} \end{cases} \tag{21}$$

where

β_{IJ} = the constant damping coefficients, and
ξ_{IJ} = the friction-lag coefficients for the front and rear suspensions.

These tire-suspension reaction forces are assumed, for simplicity, to be in the negative inertial Z direction. Hence, equation 20 may be transformed to the vehicle fixed reference frame by using the transformation matrix, that is,

$$\begin{vmatrix} F_{IJX} \\ F_{IJY} \\ F_{IJZ} \end{vmatrix} = \| A^{-1} \| \begin{vmatrix} 0 \\ 0 \\ -F'_{IJZ} \end{vmatrix} \tag{22}$$

These reaction forces result in restoring moments about the impact point O as the vehicle redirects. These moments are included in the equations of motion and are, as previously defined in equation 7,

$$\begin{aligned} \Sigma M_{\phi} = {} & (F_{RFY} + F_{LFY} + F_{RRY} + F_{LRY})(z_1 + d) \\ & + F_{RRZ}(y_1 + C_R) + F_{RFZ}(y_1 + C_F) \\ & + F_{LFZ}(y_1 - C_F) + F_{LRZ}(y_1 - C_R) \end{aligned} \tag{23}$$

$$\begin{aligned} \Sigma M_{\theta} = {} & (F_{RFX} + F_{LFX} + F_{RRX} + F_{LRX})(z_1 + d) \\ & - (F_{RFZ} + F_{LFZ})(x_1 + a) \\ & - (F_{RRZ} + F_{LRZ})(x_1 - b) \end{aligned} \tag{24}$$

$$\begin{aligned} \Sigma M_{\psi} = {} & -F_{LFX}(y_1 - C_F) - F_{LRX}(y_1 - C_R) \\ & - F_{RRX}(y_1 + C_R) - F_{RFX}(y_1 + C_F) \\ & + (F_{RFY} + F_{LFY})(x_1 + a) \\ & + (F_{RRY} + F_{LRY})(x_1 - b) \end{aligned} \tag{25}$$

where a, b, C_F, C_R, and d are vehicle parameters as shown in Figure 2.

SIMPLIFIED CRITERIA FOR EVALUATING FLEXIBLE BRIDGE RAIL PERFORMANCE

Clarence Cantor and Jeffrey Bloom, ENSCO, Inc., Springfield, Virginia

Simplified criteria are derived for evaluating the capability of a flexible bridge railing system to safely contain impacting vehicles ranging in size from subcompacts to heavy trucks. The evaluation is based on comparison of the static force versus deflection characteristic of the railing system with an associated integral characteristic that is easily obtained. The criteria have been applied to typical high-performance bridge railing designs such as the collapsing ring barrier and another hybrid barrier system. The barrier performance predicted by the simplified criteria agrees well with the dynamic results obtained from full-scale tests and computer simulations. The simplified criteria should prove valuable to the highway engineer in evaluating current and proposed designs of flexible bridge railings and in providing a guide to design improvements if required.

•THE present standards of the American Association of State Highway and Transportation Officials for bridge rails are intended to ensure the containment of 4,000-lb (1814-kg) passenger vehicles. However, the satisfaction of these standards does not necessarily imply that the bridge rail will safely redirect an errant passenger vehicle; the most common failing is that the vehicle occupant (especially at the higher velocities and impact angles) will experience intolerably high deceleration levels. In the case of heavy vehicles [weights ≥ 40,000 lb (18 144 kg)], it is unlikely that the same bridge rails will even contain the vehicle. Consequently, there is a need to generate new standards for bridge rails that will overcome the above-mentioned deficiencies. In essence, bridge performance criteria are required that will ensure the safe containment and redirection of all classes of vehicles, from the subcompact level [2,250 lb (1021 kg)] to the heavy, articulated tractor-trailer vehicle [≥40,000 lb (18 144 kg)].

The standards developed by ENSCO cover the required performance of both flexible (or semirigid) bridge rails and rigid concrete bridge parapets. Because of the different modes of operation of these two types of barriers, a single set of standards does not suffice for both types. However, both involve some type of containment criteria. The containment criteria to be discussed in this paper relate to some of the major performance requirements of flexible bridge rails. Criteria covering all of the major performance requirements, for both flexible and rigid barriers, are discussed elsewhere (1).

The overriding requirement for a high-performance, flexible bridge rail is that it safely redirect all vehicles (within a certain weight range) that impact the barrier with impact conditions up to some worst case [probably 60 mph (97 km/h) and 15 deg]. This implies that the lateral motion of the impacting vehicle must be halted without excessive lateral deceleration and that the barrier deflection must not exceed some maximum associated with the barrier and its location.

It would be extremely useful if simple criteria were available to evaluate the ability of a given barrier to satisfy this containment requirement, for any given set of performance requirements, such as the range of impacting vehicles to be contained, maximum allowable lateral deceleration, and maximum allowable barrier deflection for impact conditions in the worst case. The criteria developed in this paper are intended to meet this objective.

HYPOTHESES BASED ON EMPIRICAL OBSERVATIONS

Extensive simulation studies of vehicle impacts with typical flexible railings, performed by ENSCO (1), have yielded two empirical results that are important to this work:

1. The maximum lateral force experienced by the impacting vehicle of mass m occurs at about the maximum dynamic deflection δ_m experienced by the barrier (for that impact), and this force is approximately equal to the associated value given by the point static barrier characteristic $F(\delta)$. This implies that inertia and damping forces for typical barriers are small compared with the static force generated by the barrier; furthermore, the contact area at peak barrier deflection appears limited so that the vehicle-barrier force levels are about the same as those predicted by the point static characteristic for the same maximum deflection.
2. The strain energy under the point static characteristic $F(\delta)$ up to $\delta = \delta_m$ is typically some constant fraction α of the vehicle's initial lateral kinetic energy $\frac{1}{2} mv_t^2$ (the remainder being dissipated in occurrences such as vehicle crush, vehicle-roadway interaction, barrier friction, and barrier deformations at more than one location). A value of $\alpha = \frac{1}{2}$ seems to more or less fit a wide range of vehicles and impact conditions; however, to allow for more general application, the criteria development uses the constant α.

Based on these hypotheses, simplified criteria have been developed for evaluating the point static characteristic $F(\delta)$ of a given barrier, which can be used to predict barrier performance and to determine whether the barrier can safely contain impacting vehicles ranging in mass from m_o to M. [The static force versus deflection characteristic $F(\delta)$ can be determined either experimentally, theoretically, or from a computer model such as BARRIER VII (5).] The validity of the resulting criteria (and of the underlying hypotheses) has been spot-checked by comparing the performance predicted by the criteria with that obtained from full-scale tests and computer simulations, for a few typical high-performance bridge railing designs. This is discussed subsequently.

DERIVATION OF SIMPLIFIED CRITERIA

The foregoing hypotheses imply that for any vehicle of mass m the corresponding peak barrier deflection δ_m satisfies the relationship

$$\int_0^{\delta_m} F(\delta)d\delta = \alpha \tfrac{1}{2} mv_t^2 \tag{1}$$

The maximum lateral force experienced by this vehicle is $F(\delta_m)$. Then by Newton's Law, the maximum lateral acceleration experienced by the vehicle is

$$a_{max} = \frac{F(\delta_m)}{m} \tag{2}$$

We require that this maximum acceleration be less than or equal to some predetermined tolerable acceleration limit, a_{tol}, or

$$\frac{F(\delta_m)}{m} \leq a_{tol} \tag{3}$$

From equation 1, we obtain

$$m = \frac{2}{\alpha v_L^2} \int_0^{\delta_m} F(\delta)d\delta \tag{4}$$

Substituting this expression for m in inequality in equation 3 yields

$$F(\delta_m) \leq \frac{2a_{tol}}{\alpha v_L^2} \int_0^{\delta_m} F(\delta)d\delta \tag{5}$$

We require that this inequality be satisfied for all values of δ_m in the interval (δ_{m_o}, δ_M), where δ_{m_o} is the maximum barrier deflection corresponding to the smallest vehicle m_o and δ_M is the maximum deflection corresponding to the largest vehicle M. This will ensure that all vehicles in the range from m_o to M will experience peak lateral decelerations less than a_{tol}.

Let us define an integrated barrier characteristic $P(\delta_m)$ by

$$P(\delta_m) \triangleq \frac{2a_{tol}}{\alpha v_L^2} \int_0^{\delta_m} F(\delta)d\delta \tag{6}$$

Then inequality in equation 5 can be expressed as

$$P(\delta_m) \geq F(\delta_m) \quad \text{for } \delta_{m_o} \leq \delta_m \leq \delta_M \tag{7}$$

From equations 6 and 4, we obtain

$$P(\delta_m) = m\, a_{tol} \tag{8}$$

Hence,

$$P(\delta_{m_o}) = m_o\, a_{tol} \tag{9}$$

and

$$P(\delta_M) = M\, a_{tol} \tag{10}$$

Then for any barrier, inequality in equation 7 can be easily checked by plotting $F(\delta_m)$ and $P(\delta_m)$ on the same graph and determining the interval of interest (δ_{m_o}, δ_M) from

equations 9 and 10. [The intersection of a horizontal line of value $m_o a_{tol}$ with $P(\delta_m)$ occurs at δ_{m_o}; similarly, a horizontal line of value $M a_{tol}$ intersects $P(\delta_m)$ at δ_M.]

One more criterion must be satisfied to ensure satisfactory barrier lateral performance, namely, that the peak barrier deflection δ_M, corresponding to the maximum vehicle M, does not exceed some predetermined maximum deflection δ_{tol} that is allowable from barrier strength or space considerations. This is readily determined from the same graph since δ_M is directly available from equation 10 as indicated previously.

The physical significance of the criterion in equation 7 can be summarized as follows. For a given barrier, the associated integral characteristic $P(\delta_m)$ yields the maximum allowable force ($m a_{tol}$) associated with the peak deflection δ_m caused by a vehicle of mass m. The actual peak force experienced by this vehicle is simply $F(\delta_m)$. If this is less than $P(\delta_m)$, then the actual peak acceleration of m will be less than the allowable value a_{tol}. If this condition holds true for all peak displacements between δ_{m_o} and δ_M (as obtained from equations 9 and 10), then all vehicles in the range from m_o to M will experience peak accelerations less than a_{tol}. Thus $P(\delta_m)$ forms a kind of tolerable limit curve associated with the static characteristic $F(\delta_m)$. The final criterion for satisfactory barrier performance is simply that the peak displacement δ_M associated with the maximum vehicle M be less than a predetermined limit δ_{tol}.

Note that the maximum deflection δ_m caused by a vehicle of mass m is independent of the allowable acceleration a_{tol}. Referring to equations 6 and 4, we see that

$$\frac{P(\delta_m)}{a_{tol}} = \frac{2}{\alpha v_L^2} \int_0^{\delta_m} F(\delta)d\delta = m \qquad (11)$$

Thus we could plot m versus δ_m directly to determine the maximum barrier deflection associated with any mass. However, this same information is available from the curve of $P(\delta_m)$ versus δ_m since the ordinate in this case equals $m a_{tol}$ where a_{tol} is some constant. Furthermore, the same curve $P(\delta_m)$, when compared to $F(\delta_m)$ in the interval of interest (δ_{m_o}, δ_M), determines whether or not the peak decelerations are acceptable for the range of vehicles under consideration. Thus the single curve $P(\delta_m)$ yields the maximum deflection δ_m for any m and, when compared to $F(\delta_m)$, also determines whether the peak decelerations are less than a_{tol} for vehicles in the range of interest.

Besides facilitating the foregoing simplified criteria, the $P(\delta_m)$ and $F(\delta_m)$ curves also yield much additional information. Regardless of whether or not the limit criterion of equation 7 is satisfied, these curves can be used to predict the peak deflection and acceleration for any vehicle. Equation 8 states that the peak deflection δ_m of any vehicle can be obtained from the intersection of the $P(\delta_m)$ curve with a horizontal line whose value is equal to $m a_{tol}$. When this value of δ_m is used, the peak force $F(\delta_m)$ can be directly obtained from the $F(\delta_m)$ curve. Then, the peak acceleration of the given vehicle is simply $F(\delta_m)/m$.

The foregoing implies that the first intersection of the $P(\delta_m)$ and $F(\delta_m)$ curves can define the smallest vehicle m_o that will experience tolerable deceleration levels. The reason for this is that $P(\delta_m)$, formed by integrating $F(\delta)$, must always start below the $F(\delta_m)$ curve. As δ_m is increased, $P(\delta_m)$ will increase at a faster rate than $F(\delta_m)$ and finally cross $F(\delta_m)$. By defining the intersection coordinates as (δ_{m_o}, $m_o a_{tol}$), we have ensured tolerable deceleration levels for the corresponding value of m_o. As we take larger values of δ_m, the $P(\delta_m)$ curve will generally lie above the $F(\delta_m)$ curve; this indicates acceptable levels of peak acceleration for these larger vehicles as well. However, it is possible to define a barrier characteristic such that the $F(\delta_m)$ curve rises above the $P(\delta_m)$ curve for some large vehicle of mass M. In any event, the range of vehicles from m_o to M that will experience tolerable peak accelerations can be obtained directly from the intersections of the $P(\delta_m)$ and $F(\delta_m)$ curves.

GUIDE TO USE OF CRITERIA

The use of the above-derived criteria can be illustrated by the following example. Figure 1 shows an arbitrary barrier static characteristic $F(\delta_m)$ that is linear up to 100,000 lbf (445 kN) at 30 in. (0.76 m) and is constant thereafter. The assumed impact conditions for the worst case are 60 mph (97 km/h) and 15 deg from which the lateral velocity v_L is calculated to be 273.4 in./sec (6.94 m/s). The assumed value of α is 0.5, and the tolerable acceleration limit is chosen as 10 g. The integral characteristic $P(\delta_m)$ defined by equation 6 is then

$$P(\delta_m) = 0.207 \text{ in.}^{-1} \int_0^{\delta_m} F(\delta)d\delta$$

In the general case, the integration of $F(\delta)$ would be done either numerically (by a computer program) or graphically (by a planimeter). In this simple example, however, the integration can be done analytically since $F(\delta)$ is known in analytic form. Therefore, we have

$$F(\delta) = \begin{cases} 3{,}333 \text{ lbf/in.} \times \delta & \text{for } 0 \leq \delta \leq 30 \text{ in.} \\ 100{,}000 \text{ lbf} & \text{for } \delta > 30 \text{ in.} \end{cases}$$

Hence for $\delta_m \leq 30$ in. (0.76 m),

$$P(\delta_m) = 0.207 \text{ in.}^{-1} \times 3{,}333 \text{ lbf/in.} \; (\delta_m^2/2)$$

or

$$P(\delta_m) = 345 \text{ lbf/in.}^2 \times \delta_m^2$$

For $\delta_m > 30$ in. (0.76 m),

$$P(\delta_m) = 345 \text{ lbf} \times (30)^2 + 0.207 \text{ in.}^{-1} \times 100{,}000 \text{ lbf} \; (\delta_m - 30 \text{ in.})$$

or

$$P(\delta_m) = 310{,}500 \text{ lbf} + 20{,}700 \text{ lbf/in.} \; (\delta_m - 30 \text{ in.})$$

(Note: In the above equations 1 lbf = 4.45 N, 1 lbf/in. = 175.1 N/m, and 1 in. = 2.54 cm.)

The integral characteristic $P(\delta_m)$, as in the equations above, is also shown in Figure 1. An examination of the two curves shows that the intersection occurs at an estimated force level of 32,200 lbf (143 kN). Setting that equal to 10 $m_v g$, we see that vehicles greater than 3,220 lb (1461 kg) would experience peak lateral accelerations less than 10 g.

If we are interested in containing vehicles up to 40,000 lb (18 144 kg), we can check the barrier deflection corresponding to that maximum vehicle. A horizontal line of value, 40,000 lb/g (18 144 kg/g) × 10 g, or 400,000 lbf (1779 kN), intersects $P(\delta_m)$ at a value of δ_m equal to about 34.3 in. (0.87 m). If this is less than the maximum allowable barrier deflection δ_{tol}, then the barrier would be judged acceptable for containing vehicles up to 40,000 lb (18 144 kg). Conversely, if δ_{tol} is less than 34.3 in. (0.87 m), say for example 30 in. (0.76 m), then the intersection of a vertical line at δ_{tol} = 30 in. (0.76 m) with $P(\delta_m)$ will inherently define the maximum vehicle capability of the barrier. As in Figure 1, such a line would intersect $P(\delta_m)$ at a force level of about M a_{tol} = 310,000 lbf (1379 kN) so that the maximum vehicle M that the barrier could contain would be about 31,000 lb (14 061 kg).

We can explore this example further to show the potential of the $P(\delta_m)$ criteria for providing guidelines to barrier design modifications. Suppose we would like a modification that would make the barrier performance satisfactory for vehicles as small as 2,250 lb (1021 kg). The modified $F(\delta_m)$ curve of Figure 2 [for 60 mph (97 km/h) and 15 deg, α = 0.5, and a_{tol} = 10 g] is one solution. Here, we have introduced a stiff initial characteristic up to 22,500 lbf (100 kN), which then remains constant at this value until it joins the original $F(\delta_m)$ curve (of Figure 1). The associated $P(\delta_m)$ curve for the new characteristic is also shown in Figure 2. The intersection of the two curves now occurs at a force level of 22,500 lbf (100 kN), which corresponds to an m_o of 2,250 lb (1021 kg). The modification provides a more rapid buildup of $P(\delta_m)$ and, at the same time, limits $F(\delta_m)$ to a value of $m_o a_{tol}$ until the two curves can cross.

Interestingly enough, this modification not only results in a tolerable peak acceleration for all vehicles greater than 2,250 lb (1021 kg) but also results in a slightly smaller peak barrier deflection δ_M for the maximum vehicle M under consideration. For M = 40,000 lb/g (18 144 kg/g) the corresponding value of δ_M is about 33.6 in. (0.85 m), or about 0.7 in. (0.02 m) less than the original value.

Another option open to the designer would be the further reduction of peak deflection δ_M without producing unsafe levels of deceleration for any vehicle under consideration. Since $P(\delta_m)$ is considerably higher than $F(\delta_m)$ for large δ_m, as shown in Figure 2, we could increase the stiffness of the barrier characteristic beginning at some δ_m without affecting the deceleration behavior for smaller vehicles. This type of modification is shown in Figure 3 [for 60 mph (97 km/h) and 15 deg, α = 0.5, and a_{tol} = 10 g]. The associated integral characteristic $P(\delta_m)$ is still above $F(\delta_m)$. This ensures safe containment of all vehicles under consideration. However, the peak barrier deflection δ_M, for M = 40,000 lb/g (18 144 kg/g), has now been reduced to 30 in. (0.76 m).

The static characteristic of a given barrier may differ from one point to another. For example, the static characteristic of a barrier taken at a point midway between two posts may be softer than the characteristic taken at a post. For the barrier performance to be judged satisfactory, it must satisfy the criteria when applied to both the softest and stiffest characteristics of the barrier. In general, these two characteristics will have to be reasonably close to one another if the barrier performance is to satisfy the criteria. This will inherently provide some protection against pocketing as well; however, separate criteria to ensure against pocketing are described elsewhere (1).

APPLICATION TO TYPICAL HIGH-PERFORMANCE BARRIERS

The $P(\delta_m)$ criteria have been applied to some typical high-performance bridge barriers. These include the collapsing ring barrier and the ENSCO-designed, two-stage, New York-T1 barrier.

The collapsing ring barrier was designed by the Federal Highway Administration and has been extensively tested by Southwest Research Institute (2). The barrier consists of a box section bump rail attached by 18-in.-diameter (0.46-m) steel rings to a strong backup rail. The rings partially collapse during minor impacts; more severe impacts totally collapse the rings, and the vehicle is restrained by the stiff backup rail. The barrier demonstrates a graduated force-deflection characteristic providing restraint

Figure 1. Application of criteria to theoretical barrier 1.

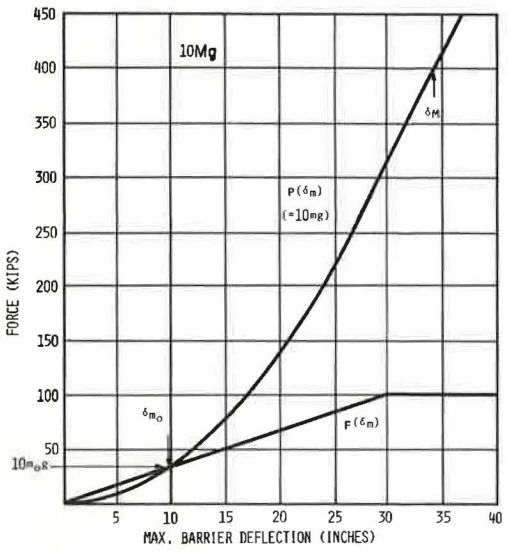

Figure 2. Application of criteria to theoretical barrier 2.

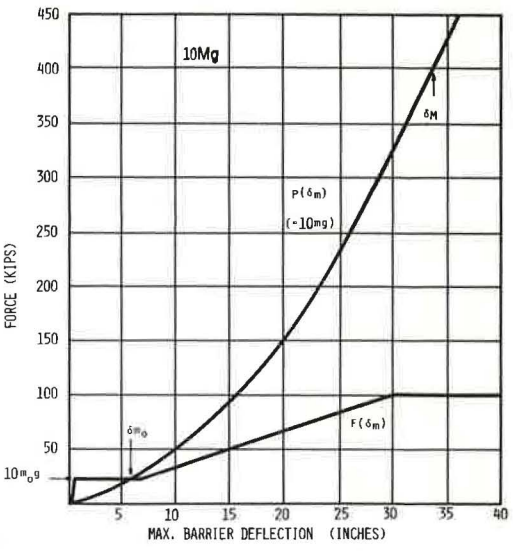

Figure 3. Application of criteria to theoretical barrier 3.

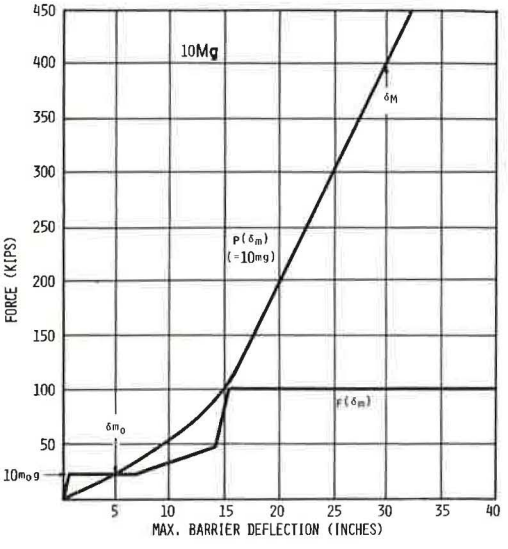

Figure 4. Application of criteria to collapsing ring barrier.

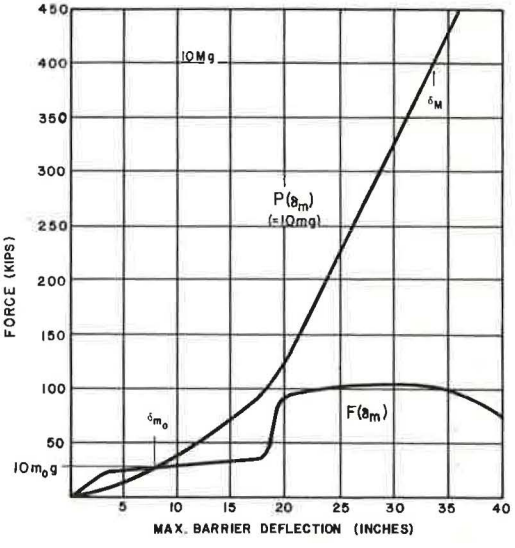

for heavy vehicles [40,000 lb (18 144 kg)] combined with low deceleration for both light and heavy vehicles.

The two-stage, New York-T1 barrier is a hybrid design using the New York box beam barrier (3) as a traffic rail and a modified version of the Texas T-1 (4) (or thrie beam) barrier as a backup rail. The New York box beam barrier consists of a strong box section rail mounted on weak 3S5.7 posts and provides low-force levels for light vehicles. When this barrier is mounted 14 in. (0.36 m) in front of the modified T-1D barrier [two overlapping W-beam rails mounted on 38-in.-high (0.97-m) 10W21 posts], the combination provides a behavior similar to that of the collapsing ring barrier.

To determine the static force-deflection curve $F(\delta)$ for the barriers, the BARRIER VII computer simulation was used (5). This program provides a two-dimensional simulation of vehicle-barrier impacts and contains a highly sophisticated barrier model. When a lateral point load is applied to the barrier and barrier mass and damping are removed, the overall static force-deflection characteristic can be obtained from the program. The $F(\delta_s)$ curves together with the corresponding $P(\delta_s)$ curves [for 60 mph (97 km/h) and 15 deg, $\alpha = 0.5$, and $a_{tol} = 10\ g$] are shown in Figure 4 (collapsing ring barrier) and Figure 5 (New York-T1 barrier).

As shown in Figure 4, the two curves intersect at a force level of about 25,000 lbf (111 kN), which shows that vehicles as small as 2,500 lb (1134 kg) would experience peak accelerations less than or equal to 10 g. A 40,000-lb (18 144-kg) vehicle would produce a peak deflection δ_M of about 33.5 in. (0.85 m), which is acceptable for this barrier. The collapsing ring barrier incorporates some of the desirable characteristics discussed in the preceding section, namely a stiff initial characteristic up to a value corresponding to 10 g for a light vehicle [2,500 lb (1134 kg)] a flattening out near this value until the $P(\delta_s)$ curve can reach and cross this value, and a stiff characteristic beginning at some larger value of δ_s to minimize peak barrier deflection δ_M.

The $F(\delta_s)$ characteristic for the combination New York box beam and Texas T-1 barrier (New York-T1 barrier) and the associated $P(\delta_s)$ characteristic are shown in Figure 5. The intersection of the two curves occurs at a force level of about 12,500 lb (56 kN), which implies tolerable peak accelerations for vehicles as small as 1,250 lb (567 kg). However, the deflection δ_M required to contain a 40,000-lb (18 144-kg) vehicle is about 37 in. (0.94 m), which may be more than can be tolerated. The performance of the two-stage New York-T1 barrier can be classified as similar to that of the collapsing ring barrier.

CHECK OF CRITERIA VALIDITY

As discussed earlier, the simplified $P(\delta_s)$ criteria are based on certain hypotheses that have been gleaned from empirical results. The validity of these hypotheses and the criteria can be checked by comparing the peak acceleration and barrier deflection for many different vehicle-barrier impacts with the corresponding results of actual full-scale tests or computer dynamic simulations. This has been done to a certain extent in the case of the collapsing ring barrier and the two-stage, New York-T1 barrier. Although more corroborative evidence is necessary to establish criteria validity (or the realm in which the criteria are valid), the results of these comparisons to date have been encouraging.

Data from three of the full-scale tests of the collapsing ring barrier [those with $\frac{3}{8}$-in.-thick (0.01-m) BR5-6-8 rings] performed at Southwest Research Institute have been compared with results predicted by the simplified criteria. Maximum deflection and maximum deceleration from the test data and from the criteria are given in Table 1. Only permanent maximum deflections were available from the full-scale test data; therefore, when these data are compared with the maximum dynamic deflections predicted by the criteria, allowance should be made for elastic springback. The results compare well for all three tests that involved vehicles ranging from 2,090 to 19,000 lb (948 to 8618 kg).

Table 2 compares maximum barrier deflection and maximum deceleration as predicted by the criteria with those of computer-simulated impacts with the collapsing ring barrier. The BARRIER VII simulation was used to simulate impacts of vehicles from 2,250 lb (1021 kg) to 40,000 lb (18 144 kg). Table 3 gives a similar comparison based on the New York-T1 barrier. Again in both cases, good correlation was obtained.

Note that the test conditions given in Tables 1, 2, and 3 are not all for 60 mph (97 km/h) and 15 deg. Thus, the $P(\delta_s)$ curves of Figures 4 and 5 were appropriately scaled to reflect the actual lateral velocity in each case (equation 6) so that predicted results could be obtained from the criteria. The value of $\alpha = 0.5$ was left unchanged; the fact that this still produced good agreement with full-scale and computer-simulated tests indicates that α may be considered constant over a fairly wide range of test conditions.

Figure 5. Application of criteria to combination New York-T1 barrier.

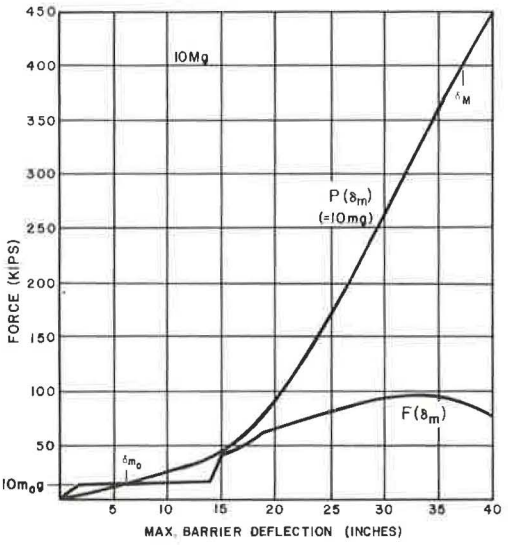

Table 1. Full-scale test results versus results predicted by criteria for collapsing ring barrier.

Test Number[a]	Vehicle Type	Vehicle Mass (lb)	Impact Speed (mph)	Impact Angle (deg)	Maximum Lateral Deflection (in.) Actual[b]	Maximum Lateral Deflection (in.) Predicted by Criteria[c]	Maximum Lateral Deceleration *(g)* Actual	Maximum Lateral Deceleration *(g)* Predicted by Criteria
BR6	Car	2,090	55.7	23.5	4.38	9.80	13.06	13.25
BR5	Car	3,910	56.1	23.9	14.25	16.95	8.60	8.90
BR8	Bus	19,000	60.9	13.9	20.44	22.50	4.02	5.20

Note: 1 lb = 0.45 kg, 1 mph = 1.6 km/h, 1 in. = 0.0254 m.
[a]Southwest Research Institute. [b]Permanent relaxed. [c]Dynamic.

Table 2. Simulated test results versus results predicted by criteria for collapsing ring barrier.

Vehicle Type	Vehicle Mass (lb)	Impact Speed (mph)	Impact Angle (deg)	Maximum Lateral Deflection (in.) Simulated[a]	Maximum Lateral Deflection (in.) Predicted by Criteria	Maximum Lateral Deceleration *(g)* Simulated[a]	Maximum Lateral Deceleration *(g)* Predicted by Criteria
Car	2,250	60	15	5.20	6.70	10.53	10.09
Car	2,250	60	25	14.42	13.50	17.11	13.55
Car	4,000	60	15	8.16	10.00	6.58	6.87
Bus	19,000	59	15	25.30	22.50	4.40	5.20
Bus	40,000	55	15	32.40	30.50	3.23	2.55

Note: 1 lb = 0.45 kg, 1 mph = 1.6 km/h, 1 in. = 0.0254 m.
[a]BARRIER VII.

Table 3. Simulated test results versus results predicted by criteria for New York-T1 barrier.

Vehicle Type	Vehicle Mass (lb)	Impact Speed (mph)	Impact Angle (deg)	Maximum Lateral Deflection (in.) Simulated[a]	Maximum Lateral Deflection (in.) Predicted by Criteria	Maximum Lateral Deceleration *(g)* Simulated[a]	Maximum Lateral Deceleration *(g)* Predicted by Criteria
Car	2,250	60	15	7.74	9.20	8.83	6.13
Car	4,000	60	15	11.84	14.50	5.51	7.25
Car	4,000	60	25	18.32	20.60	12.30	17.03
Truck	40,000	60	15	38.27	36.90	3.68	2.36

Note: 1 lb = 0.45 kg, 1 mph = 1.6 km/h, 1 in. = 0.0254 m.
[a]BARRIER VII.

The term good agreement, used to describe how predicted results compare with actual or computer-simulated test results, may disturb some readers, who see a few cases of wide differences, in Tables 1, 2, and 3. However, considering the variability of full-scale and computer-simulated test results, even for relatively small changes in vehicle-barrier initial conditions, the results given in Tables 1, 2, and 3 are indeed considered to be in good agreement. In the majority of cases, the predicted peak deflections and accelerations are within 25 percent of those obtained from full-scale and computer-simulated tests. In no case did this difference exceed 40 percent. (The apparently larger difference in the case of comparison with the deflection of full-scale test BR6 in Table 1 is attributable to the fact that peak dynamic deflection was not measured. Considering the likely magnitudes of elastic springback, the results given in Table 1 are in good agreement.)

CONCLUSIONS

The simplified criteria given in this paper for evaluating the containment performance of bridge railing systems appear to be quite effective. The peak deflections and accelerations predicted by these criteria agree well with those obtained from full-scale and computer-simulated tests of a few typical high-performance barrier systems. Although this limited sample of results is not sufficient for a complete validation of the criteria, there is sufficient evidence to suggest that the criteria can be a useful tool for evaluating and improving current and proposed designs of high-performance barrier systems.

Further investigation of the potential of these simplified criteria is certainly warranted. Some possible areas for future study are the following:

1. Comparison of results predicted by the criteria with those of full-scale tests and computer-simulated impact tests, for many different barriers.
2. Determination of whether two or three different values of α might be desirable to obtain closer correspondence with full-scale and simulated test results, for the extremely wide range of vehicle types and impact conditions.

ACKNOWLEDGMENTS

This work was performed by ENSCO, Inc. and sponsored by FHWA. We gratefully acknowledge the guidance and support provided by James Rudd of ENSCO and James Wentworth of FHWA.

REFERENCES

1. T. J. Rudd, J. A. Bloom, and J. J. Labra. Establishment of Interim Guidelines for Barriers Required to Contain Heavy Vehicles. ENSCO, Inc., Final Rept., Nov. 1974.
2. J. D. Michie, M. E. Bronstad, and C. E. Kimball. Development of a New Energy-Absorbing Bridge Railing. Southwest Research Institute, Jan. 1974.
3. E. F. Nordlin. Dynamic Tests of Steel Box Beam and Concrete Median Barriers. Highway Research Record 222, 1968, pp. 53-68.
4. R. M. Olson et al. Texas T-1 Bridge Rail Systems. Texas Transportation Institute, Final Rept., Nov. 1971.
5. G. H. Powell. BARRIER VII—A Computer Program for Evaluation of Automobile Barrier Systems. Rept. FHWA-RD-73-, March 1973.

SCALE-MODEL EVALUATION OF FRICTIONAL EFFECTS AND REDIRECTION MECHANISMS FOR ANGLE BARRIER IMPACTS

Brent R. Helm, Joseph C. Free, Charles Y. Warner, and Greg B. Frandsen,
Department of Mechanical Engineering,
Brigham Young University and Eyring Research Institute

The effects of friction at the car-barrier interface in angular collisions have been investigated by using a 1/24 scale model. Results demonstrate that interface friction can have a great effect on both vehicle trajectory and predicted damage to car and barrier. Friction thresholds for successful redirection are related to vehicle and barrier stiffness, impact angle, and impact speed, but low-friction values show promise of improving accidental barrier impacts at all speeds and angles tested.

•WHEN an automobile collides with a guardrail or gore barrier at 60 mph (96.6 km/h) and 25 deg, seemingly insignificant design details can have tremendous effects on the outcome. The snagging of the vehicle on guardrail or barrier should probably be avoided more than any other peril except penetration through the barrier. (In some installations penetration is possibly less dangerous than snagging.) The influence of the tangential force in the barrier (Figure 1) is significant in the overall vehicle dynamics of such an impact, since it introduces an unstable moment on the vehicle which, if not counteracted, leads to snagging or, at best, dangerous trajectories.

The importance of friction, as defined here, has been acknowledged in the development of traffic barriers. The use of the blockout and rub rails on the MB4 median barrier was recommended to avoid the frictional force of snagging vehicle tires against barrier posts (4, 5). However, this is not the kind of friction that can be easily handled by lubrication. Successful design must provide good force-distribution structures, to limit local stresses at sliding interfaces to reasonable levels. When this is done, lubrication methods can be considered for improvements.

In actual practice, the dynamic interfacial effects are somewhat more imposing than those normally connoted by the term friction. They can range all the way from paint scraping to shearing off a complete front wheel and suspension. Management of these forces in practice is complicated by diverse geometry in vehicle and barrier design, by the wide diversity in significant vehicle dynamic characteristics, and by the more subtle nondesign that results in more or less random load paths within automobile bodies of different makes and models. The advent of federal motor safety standards may be expected to reduce the broad scatter of automobile crash dynamics somewhat with stiffer bumpers already on the street (1) and stiffer substructure to come (2, 3).

Figure 2 shows an example, from scale-model testing, of the catastrophic redirectional trajectory that is a result of high friction. The objective of this paper is to demonstrate that proper management of interfacial friction can have tremendous effect on the severity of a side-angle impact and to identify rough guidelines for improvement in barrier design.

SCALING LAWS AND MODEL PARAMETERS

The scale-modeling procedure has previously been applied successfully to complex dynamic impact situations (6, 15). Given the complex interactions of the angle barrier crash, it is perhaps the best single technique for engineering insight at low cost.

In their development of a planar, rigid-car model for frontal impact attenuator

Figure 1. Idealized forces in horizontal place, car-barrier angle impact.

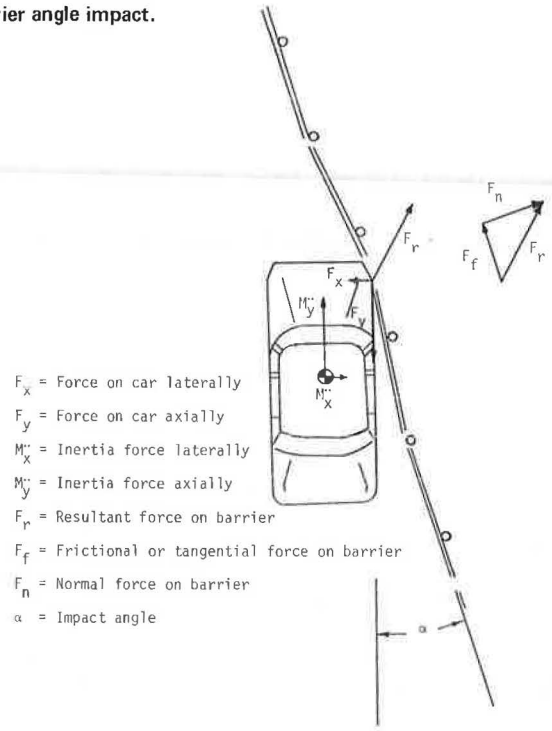

Figure 2. Trajectory at 58 mph (93.3 km/h) and 25 deg as a result of high friction.

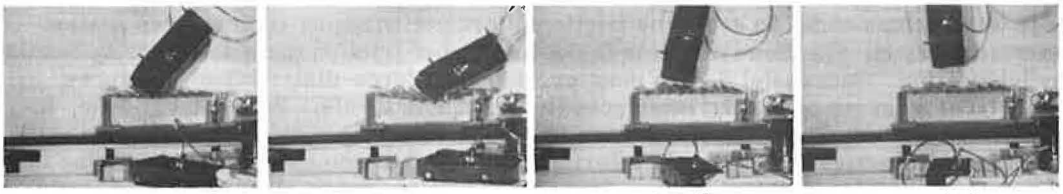

Figure 3. Model-vehicle body and chassis.

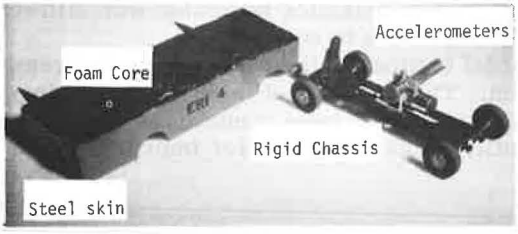

Figure 4. Measurement of vehicle crush.

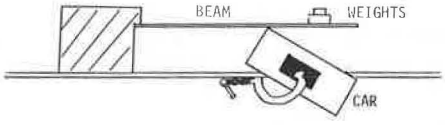

crashes, Fay and Wittrock (9) have developed appropriate scaling laws from dimensional analysis. This process was extended in the present study to include a representation of vehicle deformation by using the frontal crash characteristics [linear ramp; slope of 12 *g*/ft (12 *g*/m)] recommended by Emori (10). The model was then constructed with a solid core enclosed in a viscoelastic foam body with a 0.004-in. (0.01-cm) steel skin (Figure 3). For experimental convenience, the length scale was $\frac{1}{24}$, and the acceleration scale was set equal to one. From these two selections, the time scale was calculated. The mass scale was selected to match barrier cable force and deflection. The static force-deflection behavior of the model was measured as shown in Figure 4. The resulting force-deflection curves are shown in Figure 5.

Since the phenomena under investigation are expected to be largely two dimensional, the pitch and yaw moments of inertia were deemed to be quite important. These were scaled to prototype equivalents by weighing the rigid core of the vehicle and by proper accelerometer placement. Mass moments of inertia of model roll, pitch, and yaw were determined by calibrating a torsional pendulum with a rod of known moment of inertia and then by suspending the car at the center of gravity along each axis and measuring the natural frequency of the car. The mass moment of inertia was obtained by using the equation:

$$I = \frac{K}{\omega^2} \tag{1}$$

where

I = mass moment of inertia in slug-inch^2 (kilogram · meter^2),
K = torsional spring constant in pound-force-inch/radian (newton · meter/radian), and
ω = natural frequency in radians/sec.

A summary of the scaling factors used is given in Table 1.

Table 2 gives scaled parameters for the car and barrier with the maximum scaling error. The large error in wheel weight of the vehicle was not considered significant because its rotational energy was less than 6 percent of the total vehicle energy.

Verification of the model car was done by a scale-model simulation, similar to the profile developed by New Jersey (18), of actual full-scale impacts of the type 50 prestressed concrete median barrier. Figure 6 correlates the longitudinal and lateral acceleration traces for the model and the full-sized vehicle for an impact at 25 deg and 60 mph (96.5 km/h). The plots are in general agreement.

Model vehicle and barrier surfaces were matched in the following ways to obtain a range of friction coefficients:

1. For low friction, a clear plastic cover was placed over the fish scales with a lightweight bearing oil sandwiched between, and a painted surface was used on the car body. The resulting static coefficient of friction was about 0.1.
2. For medium friction, surfaces were painted on the fish scales, and a surface was painted on the car body. The resulting static coefficient of friction was about 0.85.
3. For friction, medium-grade sandpaper squares were glued to fish scales, and the car body was covered with silicone rubber. The resulting static coefficient of friction was about 1.35.

The coefficients of friction were determined by placing the proper surfaces together, by using a known weight to produce a lateral force F, and by using another known weight to produce a normal force N.

When the correct forces F and N were applied so that the frictional surfaces were just on the verge of slippage, the coefficient of friction was calculated by using the equation,

Figure 5. Force-deflection curve for model-vehicle crush.

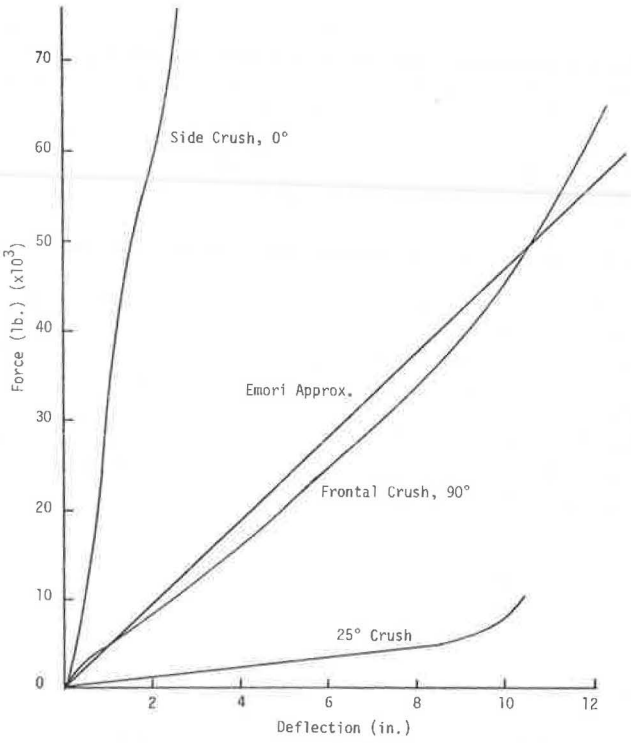

Table 1. Scaling factors.

Item	Measurement
Length	$\frac{1}{24}$
Time	$(\frac{1}{24})^{0.5} = 0.204$
Mass	8.0295×10^{-5}
Acceleration	1
Velocity	0.204
Force	8.0295×10^{-5}
Mass moment of inertia	1.394×10^{-7}
Force versus deflection	1.927×10^{-3}

Table 2. Vehicle and barrier parameter scaling.

Parameter	Prototype	Model	Maximum Error (percent)
Vehicle weight, lb	4,700	0.377	5
Track width, in.	70	2.9	5
Wheel base, in.	120	5	5
Roll, lbf-in.-sec^2	4,989	0.0006958	1
Pitch, lbf-in.-sec^2	25,641	0.00379	1
Yaw, lbf-in.-sec^2	34,335	0.003942	4
Frontal crush, lbf/ft	56,400	144.9	10

Note: 1 lb = 0.45 kg. 1 in. = 2.54 cm. 1 lbf-in.-sec^2 = 11.29 N-cm-s^2. 1 lbf/ft = 14.6 N/m.

Figure 6. Verification of model test results.

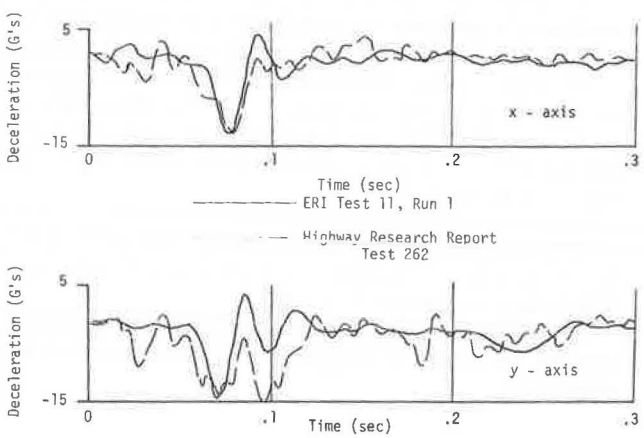

$$\mu = F/N \quad (2)$$

TEST PROCEDURE

Tests were conducted on a 5 by 9-ft (1.5 by 2.7-m) table. The model vehicle was accelerated to impact velocity by a tow cable passed around guide pulleys and into a network of multiplying pulleys attached to a weight (Figure 7). The weight was held suspended until the beginning of the test and then was released by an electric solenoid. A cable trailing the vehicle released the tow cable just before impact. The vehicle velocity was determined by recording the time interval between electrical impulses generated by two metal bands on the tow cable that were positioned to pass an electromagnetic pulse generator just before the tow cable was released.

Vehicle accelerations were obtained by two piezoelectric accelerometers mounted at the vehicle's center of gravity. Low noise data lines were trailed behind the vehicle.

Barrier cable loads were obtained from a piezoelectric load cell mounted in the barrier. Data from the piezoelectric transducers were amplified by charge amplifiers. Velocity-time impulses and amplified transducer data were recorded simultaneously on a four-trace oscilloscope picture and on a computer data acquisition system that uses a minicomputer to record the data through an analog-to-digital converter.

The data were scaled and digitally filtered through a fourth-order Butterworth filter with a cutoff frequency of 200 Hz and were plotted by the digital data acquisition system. Data were from high-speed movie film shot at 500 frames/sec. A mirror system was used to obtain simultaneous top and side views.

TEST RESULTS

Figures 2, 8, and 9 show the details of the vehicle-barrier interaction for situations of high, medium, and low friction.

Figure 10 shows the catastrophic behavior as a result of high friction when the vehicle exits at about 90 deg into parallel traffic lanes. The comparison in Figure 10 shows that the barrier cable forces resulting from high friction were approximately 1.5 times those resulting from medium friction and 2.0 times those resulting from low friction. These higher forces have implications for actual barrier designs since they would induce further failure of a barrier structure. It appears that, if the force on the vehicle parallel to the barrier is high enough to induce an angular velocity (CCW in this case), no recovery is possible. The higher forces thus generated cause a moment that increases the angular velocity.

Although the high-speed film data of Figures 8 and 9 show a similar qualitative behavior for medium and low friction, the comparison of deceleration rates as shown in Figure 11 shows that axial decelerations for low friction were less than 50 percent of those for medium friction. These reductions in deceleration imply that for actual crash situations vehicle crush and front wheel damage in low-friction situations would be reduced, damage repair costs would be reduced, and postcrash maneuverability would be improved.

Average pulse decelerations for three runs each at medium and low friction are given in Table 3. The axial decelerations are consistently lower for low friction, and the average of the lateral decelerations is 20 percent higher for low friction. However, these high lateral loads occur during the secondary lateral impact of the side and rear of the vehicle and are thus unlikely to cause significant damage or deviant trajectories. The time shift of the axial pulse and the lateral pulse is shown in Figure 11.

CONCLUSIONS

For the scaled velocities tested and a cable-plate type of redirecting system interacting with a scaled 4,700-lb (2130-kg) vehicle of the stiffness profile shown in Figure 5, the

Figure 7. Scale-model test facility.

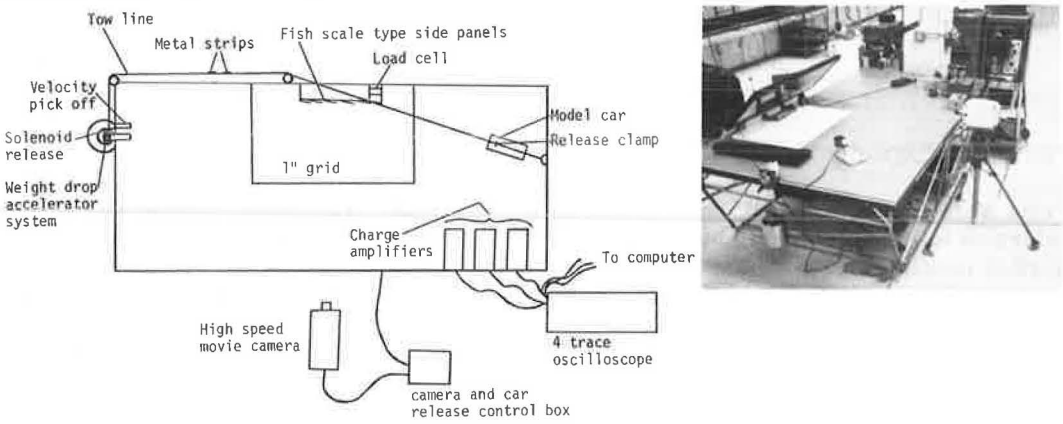

Figure 8. Trajectory at 61 mph (98.2 km/h) and 25 deg as a result of medium friction.

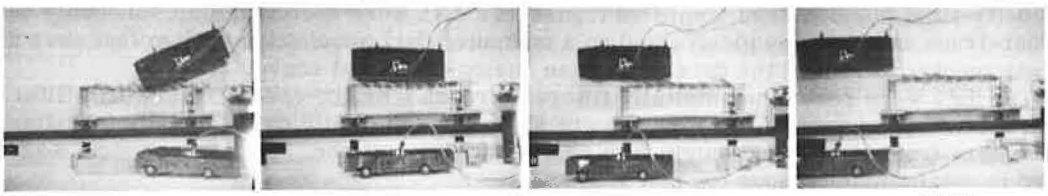

Figure 9. Trajectory at 61 mph (98.2 km/h) and 25 deg as a result of low friction.

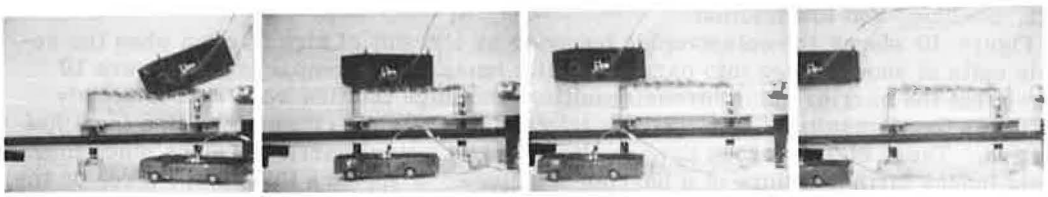

Figure 10. Barrier load versus time.

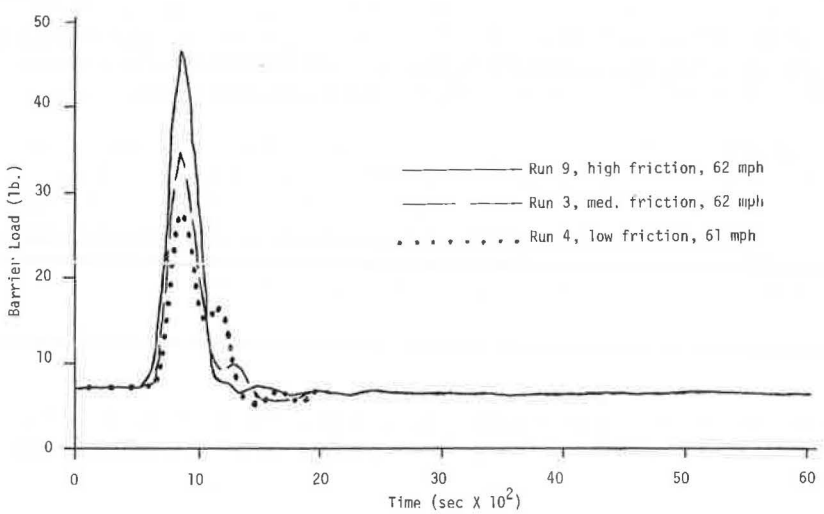

Figure 11. Deceleration rate versus time.

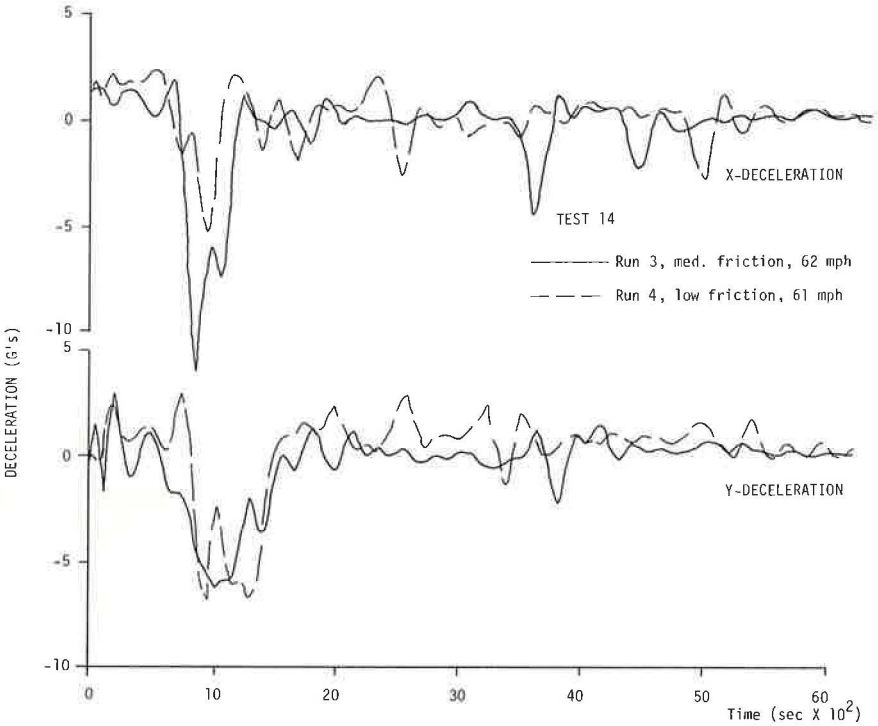

Table 3. Average pulse deceleration for medium- and low-friction tests.

Run No.[a]	Friction	Impact Speed (mph)	Average Pulse Deceleration[b] (*g*) Axial (X)	Lateral (Y)
1	Medium	61	4.97	1.96
2	Medium	62	4.00	3.08
3	Medium	62	5.46	2.60
4	Low	61	2.10	3.35
5	Low	61	2.81	3.06
6	Low	59	1.60	3.85

Note: 1 mph = 1.6 km/h.

[a]Test 14.

[b]Mean deceleration during period of pulse with 2-*g* cut-off level.

influence of the frictional forces at the vehicle-barrier interface is important. High-friction coefficients (μ = 1.35) are catastrophic in their effect, and low-friction coefficients (μ = 0.10) significantly reduce axial deceleration levels below those for medium-friction coefficients (μ = 0.85).

The influence of these factors for velocities ranging from 47 to 62 mph (76 to 100 km) has been investigated. The influence of the stiffness of the barrier structure has not been evaluated, but the influence of friction is believed to have more effect on lower stiffness structures because of the increased pocketing potential. Results of full-scale tests on concrete median barriers smeared with grease indicated no apparent difference in performance as compared with ungreased median barriers (16, 17). However, low-friction coefficients are not likely to be obtained in this manner since fluid pressures in the grease cannot be maintained unless adequate contact area can be developed to contain the fluid pressures. Deforming vehicle surfaces would most probably pierce the lubrication film.

This study implies that redirecting appurtenances should be designed for low values of vehicle interface-surface friction.

ACKNOWLEDGMENTS

This study was conducted at Brigham Young University. It was part of the development of high-performance crash barriers being conducted by Eyring Research Institute. The support of the Federal Highway Administration, U.S. Department of Transportation is gratefully acknowledged.

REFERENCES

1. Federal Motor Vehicle Safety Standards and Regulations, With Amendments and Interpretations Issued Through July 1974. National Highway Traffic Safety Administration, Standard 215, Aug. 1974.
2. Proposal for 45-50 mph Frontal Crashworthiness by Early 1980's. National Highway Traffic Safety Administration, Docket 74-14, Notice 1, March 19, 1974.
3. C. Y. Warner and D. Friedman. Automobiles and Highway Crash Attenuators: System Design Considerations. Transportation Research Record 488, 1974, pp. 19-23.
4. J. D. Michie and M. E. Bronstad. Location, Selection, and Maintenance of Highway Traffic Barriers. NCHRP Rept. 118, 1971.
5. J. L. Beaton and R. N. Field. Dynamic Full-Scale Tests of Median Barriers. HRB Bulletin 266, 1960, pp. 78-125.
6. B. S. Holmes and G. Sliter. Scale Modeling of Vehicle Crashes—Techniques, Applicability, and Accuracy; Cost Effectiveness. SAE, 3rd National Conference on Occupant Protection, Troy, Mich., Paper 740586, 1974.
7. B. S. Holmes and J. D. Colton. Scale Model Experiments for Safety Car Development. Trans., SAE, Paper 730073, 1973.
8. R. J. Fay and M. A. Kaplan. Energy-Absorbing Corrugated Metal Highway Buffer. Highway Research Record 460, 1973, pp. 20-29.
9. R. J. Fay and E. P. Wittrock. Scale-Model Test of an Energy-Absorbing Barrier. Highway Research Record 343, 1971, pp. 75-82.
10. R. I. Emori. Scale Model of Auto Collision With Breakaway Obstacles. Experimental Mechanics, Vol. 13, No. 2, Feb. 1973.
11. R. I. Emori. Scale Model Study Vehicle Collision Into Fixed Objects. Univ. of California, Los Angeles, Rept. UCLA-ENG-7106, Jan. 1971.
12. R. I. Emori. Analytical Approach to Automobile Collisions. SAE Annual Meeting, Detroit, Paper 680016, Jan. 1968.
13. M. P. Jurkat and J. A. Starrett. Automobile-Barrier Impact Studies Using Scale Model Vehicles. Highway Research Record 174, pp. 30-41.
14. H. L. Langhaar. Dimensional Analysis and Theory of Models. John Wiley, New York, 1951.
15. G. Murphy. Similitude and Engineering. Ronald Press, New York, 1950.
16. L. C. Lundstrom, P. C. Skeels, B. R. Englund, and R. A. Rogers. A Bridge Parapet Designed for Safety? General Motors Proving Ground Circular Test Track Project. Highway Research Record 83, 1965, pp. 169-187.
17. J. S. Starrett and I. R. Ehrlich. Highway Center-Barrier Investigation—Part 2. Davidson Laboratory, Stephens Institute of Technology, Rept. 1139, June 1967.
18. E. F. Nordlin et al. Dynamic Tests of a Prestressed Concrete Median Barrier Type 50, Series XXVI. State of California, Research Rept. CA HY MR 6588-1-73-06, March 1973.

DEVELOPMENT OF A NEW COLLAPSING-RING BRIDGE RAIL SYSTEM

C. E. Kimball, M. E. Bronstad, and J. D. Michie, Southwest Research Institute; and J. A. Wentworth and J. G. Viner, Federal Highway Administration

An energy-absorbing bridge rail system that uses the plastic deformation of steel rings as the primary impact energy absorber has been developed through full-scale crash testing and the use of the BARRIER VII computer program. The system design not only is capable of withstanding impacts by large vehicles such as buses and trucks but also does not impart high accelerations to impacting smaller vehicles. Ten full-scale crash tests were performed with vehicles ranging from 2,000 to 40,000 lb (907 to 18 144 kg). Redirection of high-speed [55 mph (89 km/h)], 40,000-lb (18 144-kg) vehicles (articulated and nonarticulated) impacting at a 19-deg angle was demonstrated. No significant elastic rebound of the rails and energy-absorbing rings was evident during the test. Vehicle damage was limited to mostly sheet metal damage of the impacting front quadrant and side panels with limited suspension damage at the same quadrant. Bridge rail damage ranged from slight for the subcompact vehicle impact to extreme for heavy vehicle impacts. Tests were documented by strain gauge, vehicle accelerometer, and high-speed movie data as well as permanent deformation measurements.

•A NEED exists for a bridge rail design that not only is capable of withstanding impacts by large vehicles such as buses and trucks but that also does not impart high accelerations to impacting smaller vehicles. Accordingly, this paper presents information on the development of a concept known as the collapsing-ring bridge rail system (CRBRS), which appears to be capable of fulfilling that need. Although this system represents an advance in state of the art in bridge rail design, it is constructed with conventional materials and barrier elements that are currently used in highway construction.

BACKGROUND

The idea of using steel rings as a primary energy-absorbing device for the bridge rail system described was conceived by the staff of the Offices of Research and Development of the Federal Highway Administration. It was recognized that vehicle impact energy could be dissipated in thick-walled rings by their partial or complete collapse. Initial analysis and testing of the rings were performed by Perrone (1) to determine the required ring geometry and material characteristics. After these initial studies, the bridge rail system that incorporated the collapsing-ring concept as shown in Figure 1 was designed by FHWA, and a vehicle crash test program was initiated.

The following performance goals were established for the design of this new system:

1. Reduction in impact severity, as compared with that in conventional nondeflecting bridge rail designs, for vehicles weighing from 2,000 to 4,000 lb (907 to 1814 kg) when impacting the system at 60 mph (97 km/h) and 25 deg. This is achieved through the use of the plastic deformation of the collapsing ring. The complete collapse of at least one ring without excessive vehicle contact with the elements of the outer railing system was desired for 4,000-lb (1814-kg) vehicle, 60-mph (97-km/h), 25-deg impacts.
2. Redirection of vehicles in impacts as severe as a 25,000-lb (11 340-kg) school bus

Figure 1. Collapsing-ring bridge rail system.

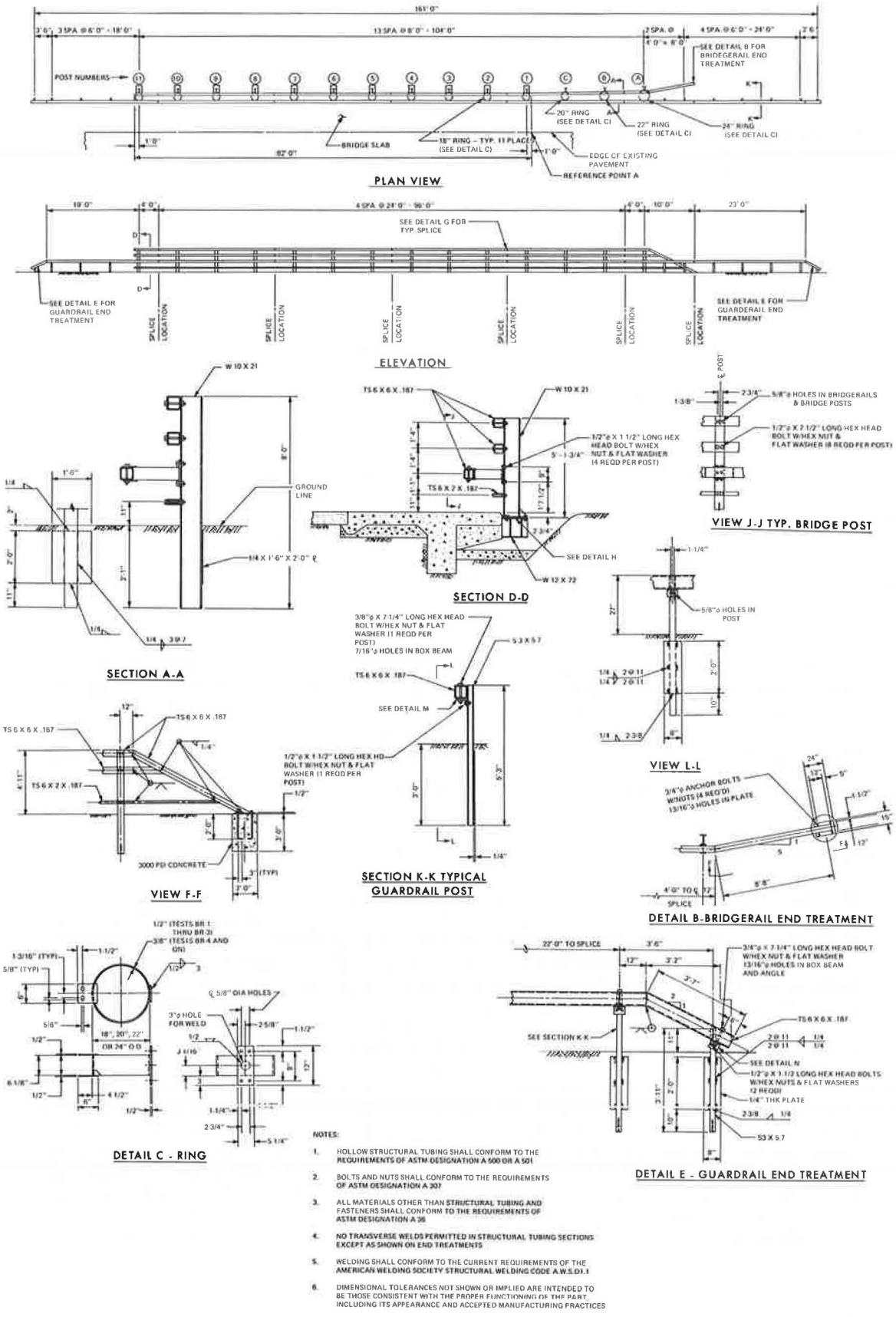

Figure 1. Continued.

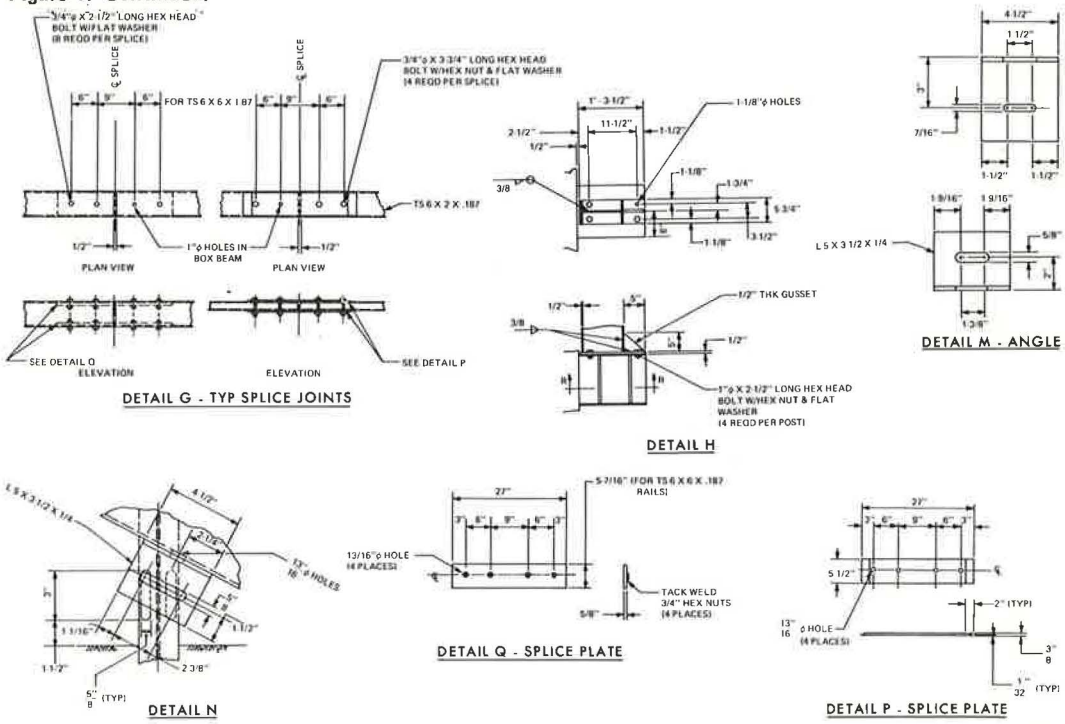

Table 1. Vehicle crash results.

Test No.	Vehicle Weight (lb)	Impact Speed (mph)	Impact Angle (deg)	Vehicle Exit Conditions: Angle (deg) Measured	Angle (deg) Predicted	Speed (mph) Measured	Speed (mph) Predicted	Maximum Avg Vehicle Acceleration[a]: Longitudinal (y) Measured	Longitudinal (y) Predicted	Lateral (x) Measured	Lateral (x) Predicted	Maximum Permanent Ring Deflection (in.) Measured	Maximum Permanent Ring Deflection (in.) Predicted
BR-1	19,000	34.4	7.5	0.6		27		-0.86		0.40		0.5	
BR-2	19,000	56.0	7.3	2	3.2	56	53	-1.26	-0.89	2.67	3.29	3.4	1.02
BR-3	3,960	60.0	24.7	12	19.6	43	42	-6.05	-6.32	8.46	18.17	7.06	13.27
BR-4	4,097	60.0	25.9	5.6	19.9	36	42	-6.81	-6.35	6.56	18.19		13.31
BR-5	3,910	56.1	23.9	12	18.7	42	38	-5.61	-5.72	6.58	18.50	13.75	11.76
BR-6	2,090	55.7	23.5	13	45	41	39	-6.15	-4.55	12.24	16.91	4.0	5.44
BR-7	4,230	56.7	29.1	10	32	41	34	-5.57	-5.53	8.18	21.78	18.0	17.33
BR-8	19,000	60.9	13.9	2	1	54	52	-2.09	-2.00	3.90	7.03	16.38	10.42[b]
BR-9	40,000	54.3	19.1	13	6.6	42	53	-1.42	-0.43	2.63	1.24	54.0	34.0[b]
BR-10	40,000	55.1	19.0	11	6.6	44	53	-3.55	-0.43	8.86	1.24	23.25	28.0[b]

Note: 1 lb = 0.45 kg. 1 mph = 1.6 km/h.

[a]Maximum acceleration over 50-msec duration obtained from high-speed movie film. [b]Rail deflections.

Figure 2. Results of full-scale crash test BR-5.

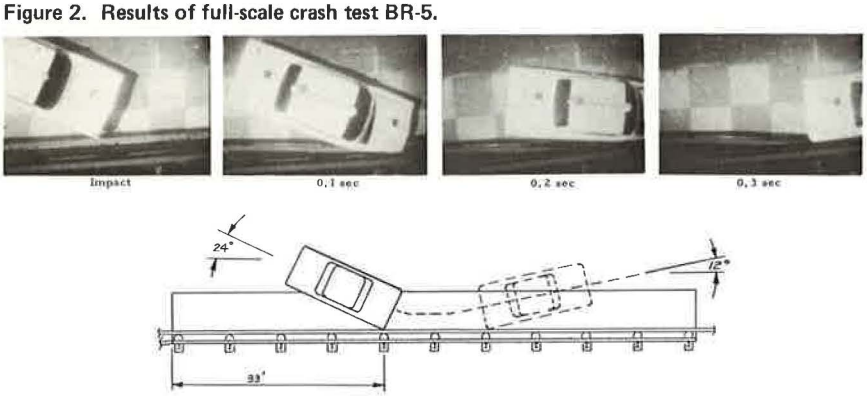

impacting the railing at 60 mph (97 km/h) and 20 deg. In such impacts, behavior of the outer railing system elements as a conventional nondeflecting bridge was desired.

3. Approach rail-bridge rail transition design to be capable of handling 60-mph (97-km/h) collisions with 4,000-lb (1814-kg) vehicles in impacts of 60 mph (97 km/h) and 25 deg.

As the program progressed, it appeared that the capability of the system to handle heavy vehicle impacts might significantly exceed initial design goals if dynamic displacement of the backup posts could occur with some form of limit on the leaning of the system during impact. This would require a somewhat predictable failure mode of the post at the baseplate connection, such as a tension failure of the anchor bolts. Computer runs made with the BARRIER VII program (2) indicated that collisions as severe as a 40,000-lb (18 144-kg) intercity bus or a 40,000-lb (18 144-kg) tractor-trailer rig at 60 mph (97 km/h) and 15 deg might be handled in such a manner. Accordingly 60-mph (97-km/h), 15-deg tests with these vehicles were added to the program.

TEST PROGRAM

Ten full-scale crash tests with vehicles ranging from 2,100 to 40,000 lb (952 to 18 144 kg) were conducted to examine the dynamic performance of the system in terms of the stated performance goals. Only one design change was made to the system during this test program. An initial ring thickness of ½ in. (12.7 mm), used in tests BR-1 to BR-3, was finalized to a thickness of ⅜ in. (9.5 mm) and then was evaluated by tests BR-4 to BR-10, which included standard-sized and small vehicles impacting at large angles, and large vehicles impacting at moderate angles. In addition, one test evaluated dynamic performance of the approach guardrail-bridge rail transition. Test procedures and data reduction methods are discussed elsewhere (3).

COMPUTER SIMULATION

The BARRIER VII (2) computer program was developed to predict the behavior of an automobile striking a protective barrier. The barrier is idealized as a structural framework of arbitrary configuration, and the automobile as a body surrounded by a cushion of springs. Large displacements and inelastic behavior, including hysteresis effects on unloading, are considered in the barrier structure. The automobile slides along the barrier, and the effects of normal forces, friction forces, and wheel drag forces are considered in determining its motions. The program and its capabilities are described in detail in another report (2).

In the modeling of the CRBRS, only two of the structural members available in the BARRIER VII program were used. These were the beam and the post. Post elements were used to model all posts in the system, and various beam elements were used to model the rail sections and the collapsing ring. The collapsing rings were modeled by a combination of two simple beam elements in parallel.

The BARRIER VII program was used to predict the collision outcome for each test in the test series. Vehicle trajectories and accelerations and barrier responses were predicted with varying degrees of accuracy. From the BARRIER VII program, in conjunction with the photographic and accelerometer data gathered during full-scale testing, the forces and moments on and displacements of key system elements were evaluated over the duration of the collision process.

TEST RESULTS

Results of the test series are given in Table 1. Theoretical predictions of the vehicle and barrier behavior computed by the BARRIER VII program are compared to experimentally derived values for the 10 tests. Comparisons are made for vehicle exit angle,

exit speed, and maximum average accelerations and for maximum permanent barrier ring deflection.

In test BR-1, a test abort was unsuccessfully attempted resulting in a 34-mph (55-km/h) impact compared to a 60-mph (97-km/h) target speed. Test BR-2 was therefore designed to meet the target conditions of BR-1. From test BR-3, it was determined that the rings were too stiff (i.e., the design goal of complete collapse of one ring under the test conditions was not met), and a design change was initiated. Test BR-4 was scheduled to provide data on system performance using the new $^3/_8$-in.-thick (9.5-mm) rings (which were used for all subsequent tests). During test BR-4, a failure of the front rail at a butt-welded joint, which was neither authorized by the design drawings nor observed before the test, occurred. Test BR-5 was a repeat of test BR-4. Tests BR-6 through BR-10 were conducted as given in Table 1. Further details on these tests are given elsewhere (3), and a description of the more significant tests in this series follows. Data for vehicles and the collapsing-ring bridge rail for tests BR-5 through BR-10 are given in Table 2. The data for rails, rings, and pavement condition, which were the same for each of these tests, are as follows (1 in. = 25.4 mm and 1 ft = 0.3 m):

Item	Measurement
Bridge rail, in.	TS 6 × 6 × 0.1875
Post, ft	W 10 × 21 × 5.15
Bridge post spacing, ft	8
Installation length, ft	82
Steel rings	
Thickness, in.	0.375
Outside diameter, in.	18.0
Length, in.	6.12
Pavement condition	Dry

Test BR-2

The vehicle in test BR-2 was a 1962 Ward school bus weighing 12,050 lb (5480 kg) when empty and 19,000 lb (8618 kg) when ballasted with three sections of 20-in. (508-mm) internal-diameter steel tubing rigidly attached to the vehicle structure. The bus impacted the front rail at post 2 (posts on the simulated bridge deck are numbered consecutively beginning upstream as shown in Figure 1) with a speed of 56 mph (90 km/h) and an impact angle of 7.3 deg. The bus was redirected almost parallel to the rail; it rolled 13.8 deg toward the rail and then 10 deg away from the rail. Maximum 50-msec average accelerations were 1.3 *g* (longitudinal) and 2.60 *g* (lateral); maximum permanent ring deflection was 3.4 in. (86.4 mm) at post 2.

Test BR-5

The 3,910-lb (1773-kg) 1964 Chevrolet Impala sedan impacted the front rail at post 5 with a speed of 56 mph (90 km/h) and an impact angle of 24 deg and was smoothly redirected as shown in Figure 2. Figure 3 shows the condition of the vehicle and the rail barrier after the impact. The design goal of complete collapse of one ring without excessive vehicle contact with other elements of the system with the given impact conditions was met with the $^3/_8$-in.-thick (9.5-mm) rings. The comparison of predicted and experimental results is shown in Figure 4.

Test BR-6

The 2,090-lb (948-kg) 1972 VW subcompact sedan impacted the front rail between posts

Figure 3. Condition of vehicle and collapsing-ring bridge rail after impact in test BR-5.

Figure 4. Results of BARRIER VII simulation versus those of actual test BR-5.

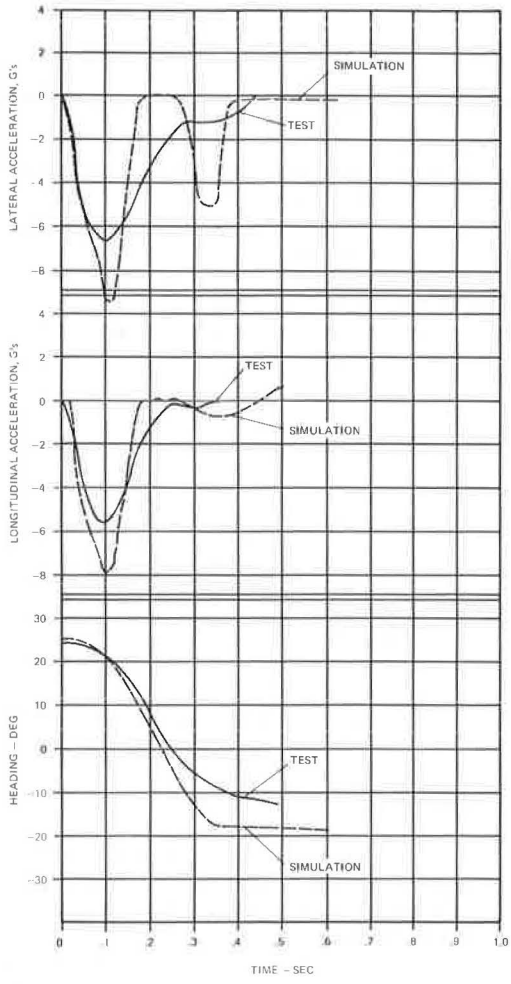

Figure 5. Results of full-scale crash test BR-6.

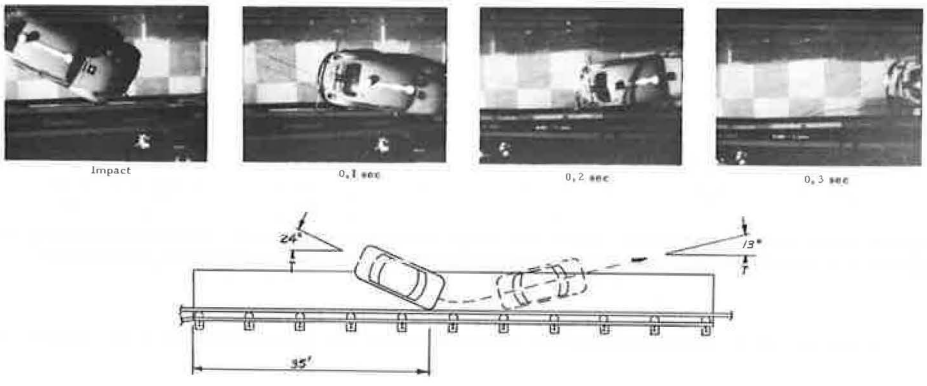

5 and 6 with a speed of 56 mph (90 km/h) and an impact angle of 24 deg and was smoothly redirected as shown in Figure 5. Vehicle and barrier damage is shown in Figure 6, and the comparison of predicted and experimental results is shown in Figure 7.

Test BR-7

The 4,230-lb (1018-kg) sedan impacted the approach guardrail-bridge rail transition with a speed of 57 mph (92 km/h) and an impact angle of 29 deg. As shown in Figure 8, the vehicle impacted the guardrail, completely collapsed the first ring (resulting in backup rail translation of the soil), mounted posts A, B, and C at the end of the bridge rail, and was then smoothly redirected. Maximum permanent deflection of this post was 22.9 in. Vehicle and barrier damage is shown in Figure 9.

Test BR-8

The 19,000-lb (8618-kg) school bus impacted the front rail at post 8 with a speed of 61 mph (98 km/h) and an impact angle of 14 deg. As shown in Figure 10, the bus rolled toward the rail to a maximum roll angle of 15 deg, and the rear of the bus impacted the two upper rails before being redirected. For the first time in the test series, two bridge posts sustained damage: Posts 7 and 8 sustained baseplate bending, and the two bolts nearest the bridge deck in post 8 failed in tension. Vehicle and installation damage are shown in Figure 11. The comparison of experimental and theoretical vehicle dynamics is shown in Figure 12.

Test BR-9

The scenicruiser intercity bus ballasted to 40,000 lb (18 144 kg) with 10,200 lb (4627 kg) of sand bags in the baggage compartment impacted the front rail at post 2 with a speed of 54 mph (87 km/h) and an impact angle of 19 deg. As shown in Figure 13 and Figure 14, the bus completely collapsed rings in the impact zone, rolled toward the rail, and the rear of the bus impacted the three-rail system. The redirected bus reached a maximum roll angle of 20 deg (toward the rail) before returning to an upright position. The significance of the vehicle's c.g. being lowered by the ballast and of the ballast spilling free of the vehicle is not clearly defined. In the extreme case, had the vehicle been redirected in a manner that raised the c.g., a rollover might have occurred.

The bottom rail (rub rail) failed completely. Considerable post damage was sustained: Posts 2 through 5 failed in bending and torsion with all four baseplate bolts fractured; posts 1, 6, and 7 sustained baseplate bending, and the two bolts nearest the bridge deck failed in tension. In addition, all three soil-mounted posts upstream of the bridge deck were displaced laterally with a maximum permanent displacement of approximately 26 in. (660 mm). The comparison of experimental and theoretical vehicle dynamics is shown in Fgiure 15.

Test BR-10

The 40,000-lb (18 144-kg) tractor-trailer truck impacted the front rail at post 4 with a speed of 55 mph (89 km/h) and an impact angle of 20 deg. As shown in Figure 16, the truck tractor impacted the front rail and initiated a roll toward the barrier as it was redirected. The roll continued as the trailer impacted the two upper rails and ended when both the tractor and the trailer rolled on their right sides. The tractor had nearly recovered to a 0-deg roll attitude before trailer momentum initiated the final roll sequence of the complete rig. Little damage was sustained by the tractor cab because of the roll. Bridge posts 2 through 5 sustained baseplate bending, and the two bolts nearest the bridge deck failed in tension. This damage is shown in Figure 17.

Figure 6. Condition of vehicle and collapsing-ring bridge rail after impact in test BR-6.

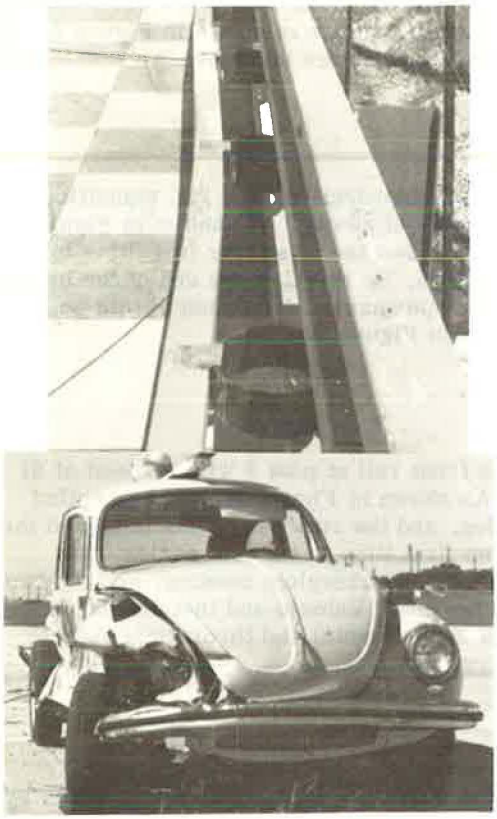

Figure 7. Results of BARRIER VII simulation versus those of actual test BR-6.

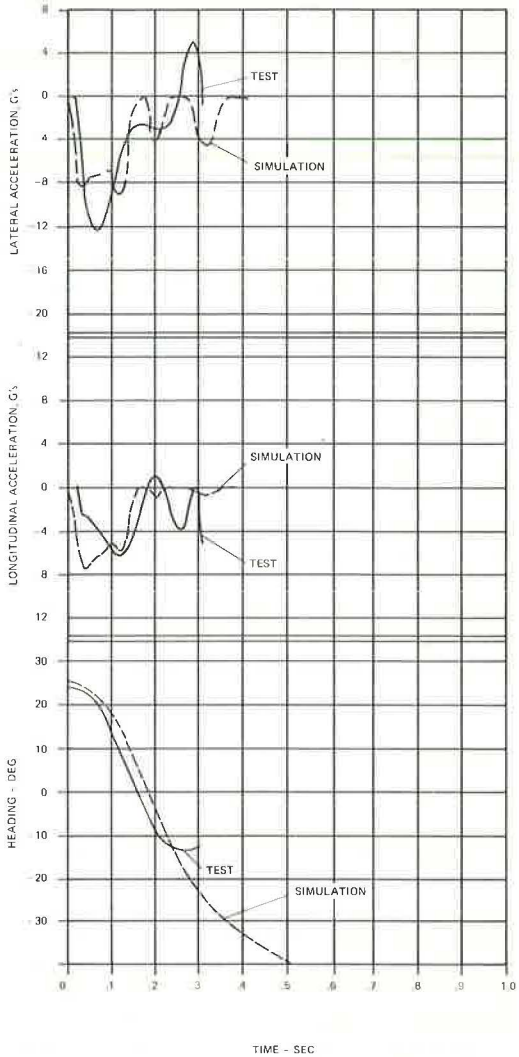

Figure 8. Results of full-scale crash test BR-7.

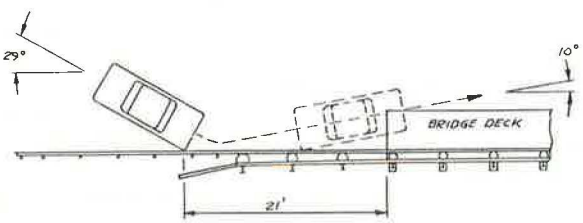

Figure 9. Condition of vehicle and collapsing-ring bridge rail after impact in test BR-7.

Table 2. Data for vehicles and barriers for impact tests.

Test	Maximum Permanent Ring Deflection (in.)			Vehicle Weight[a] (lb)	Impact		Exit Angle (deg)	Vehicle Acceleration[b] (g)		Vehicle Rebound Distance (ft)
	Front Rail	Midrail	Top Rail		Speed (mph)	Angle (deg)		Lateral	Longi-tudinal	
BR-5	13.75			3,910	56.1	23.9	12.0	6.58	-5.61	20
BR-6	4.0			2,090	55.7	23.5	13.0	12.24	-6.15	10
BR-7	18.0			4,230	56.7	29.1	10.0	8.18	-5.57	12
BR-8	16.4	1.8	2.4	19,000	60.9	13.9	2.0	3.90	-2.09	25
BR-9	24	38	42.5	40,000	54.3	19.1	13.2	2.63	-1.42	30
BR-10	23.3	30.8	35.8	40,000	55.1	19.0	11.0	8.86	-3.55	25

Note: 1 in. = 25.4 mm. 1 lb = 0.45 kg. 1 ft = 0.3 m.

[a]With instrumentation. [b]For the top rail, 50-msec average.

Figure 10. Results of full-scale crash test BR-8.

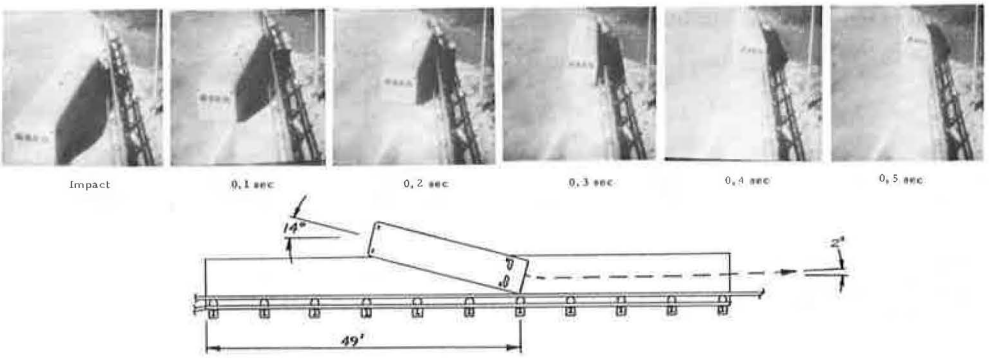

Figure 11. Condition of vehicle and collapsing-ring bridge rail after impact in test BR-8.

Figure 12. Results of BARRIER VII simulation versus those of actual test BR-8.

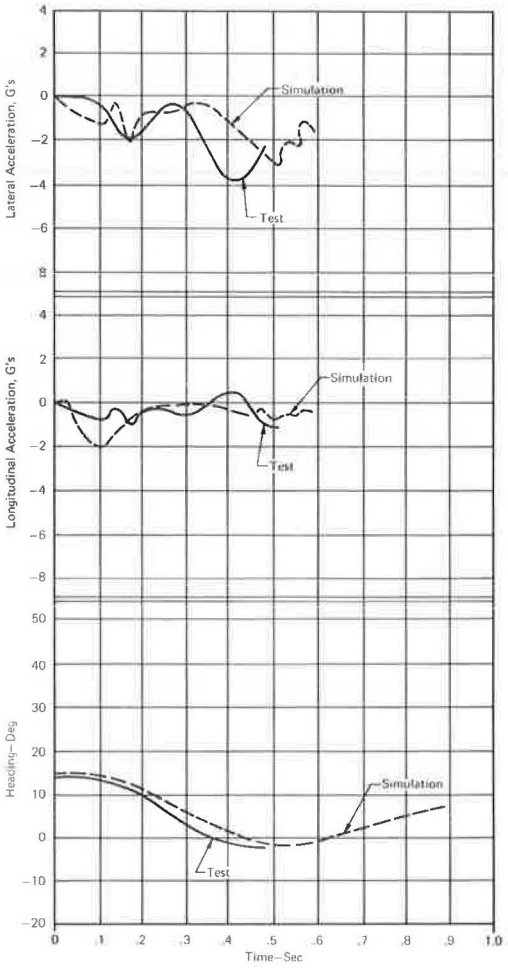

Figure 13. Results of full-scale crash test BR-9.

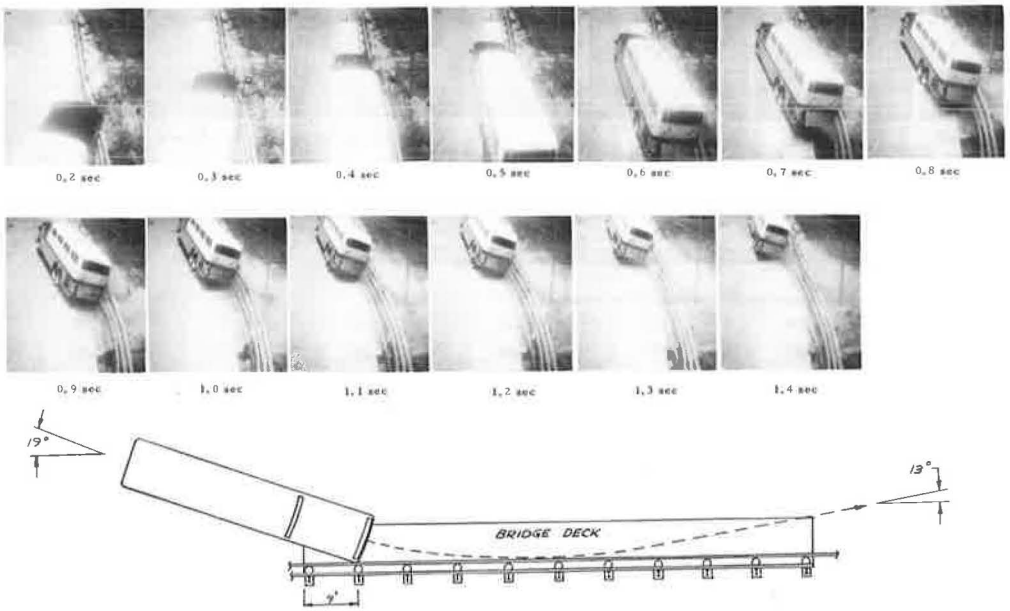

Figure 14. Condition of vehicle and collapsing-ring bridge rail after impact in test BR-9.

Figure 15. Results of BARRIER VII simulation versus those of actual test BR-9.

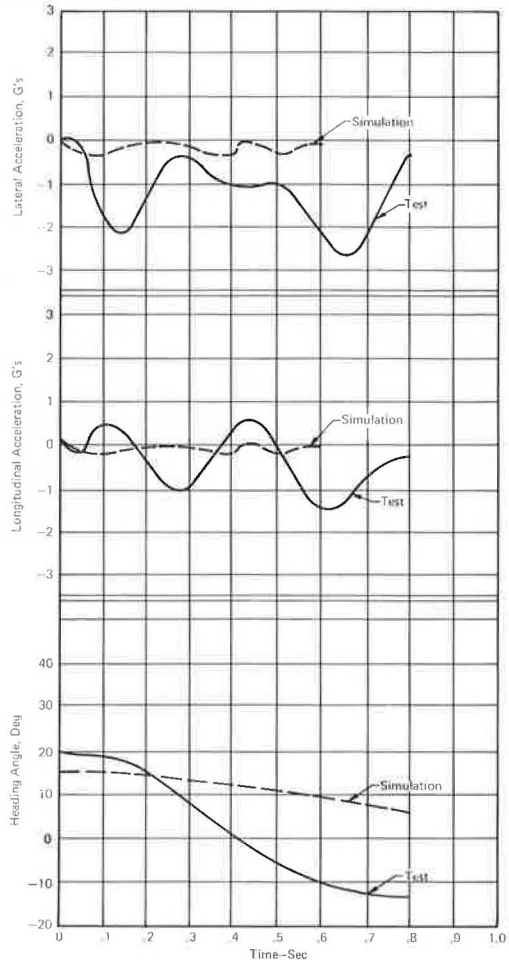

Figure 16. Results of full-scale crash test BR-10.

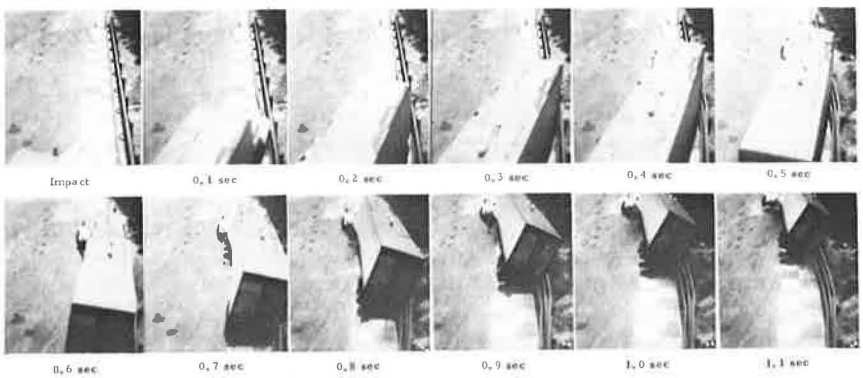

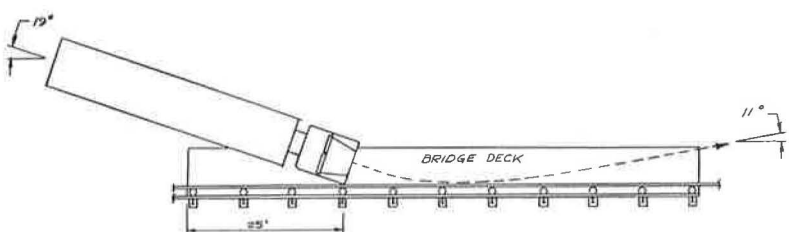

Figure 17. Condition of vehicle and collapsing-ring bridge rail after impact in test BR-10.

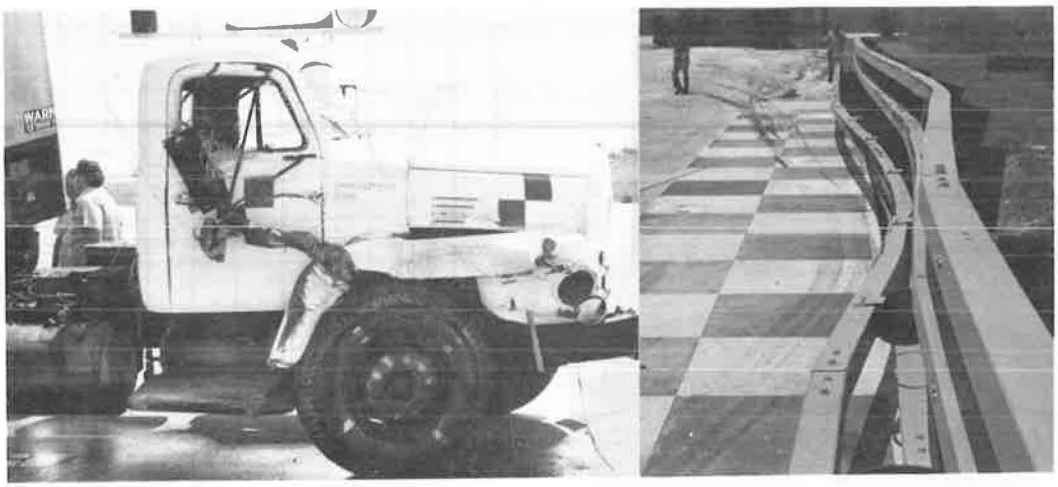

DISCUSSION OF RESULTS

Tests conducted in this program demonstrated that the following design goals were met with the use of $^{3}/_{8}$-in.-thick (9.5-mm) rings:

1. Reduction in impact severity, as compared with that in conventional nondeflecting bridge rail designs, was shown in test BR-5, in which 13.8 in. (350.5 mm) of permanent deformation occurred in one collapsing ring that was impacted by a 3,900-lb (1770-kg) vehicle at 56 mph (90 km/h) and 24 deg and in test BR-6, in which 4.0 in. (101 mm) of permanent deformation occurred in one collapsing ring that was impacted by a 2,090-lb (948-kg) VW at 56 mph (90-km/h) and 24 deg. The vehicle was driven away from the impact zone after test BR-6.
2. A 19,000-lb (8618-kg) school bus was successfully redirected by the bridge rail system in a 61-mph (98-km/h) impact at 14 deg (test BR-8), and a 2.4-in. (61-mm) maximum permanent deflection occurred in the outer railing elements. This shows that, in the outer backup railing, elements behaved much as conventional nondeflecting designs under impacts near the upper limit of their ultimate resistance. In test BR-8, the maximum dynamic load impacting the barrier was in the order of 75,000 lb (34 119 kg), and few conventional railings are designed to withstand forces of this magnitude.
3. Successful redirection of a 40,000-lb (18 144-kg) scenicruiser bus impacting the system at 54 mph (87 km/h) and 19 deg was demonstrated in test BR-9, and a maximum permanent deflection of 42.5 in. (1079.5 mm) of the top rail of the outer rail elements occurred.
4. A 40,000-lb (18 144-kg) tractor-trailer rig was retained and redirected in a 55-mph (89-km/h), 20-deg impact (test BR-10); however, the vehicle rolled on its side. Maximum permanent post displacement was 35.8 in. (909.7 mm) at the height of the top rail and 23.3 in. (591.8 mm) at the height of the collapsing ring. System design changes aimed at reducing leaning of the posts in such impacts may help reduce such roll-over events.
5. Satisfactory redirection was obtained when the approach rail transition was impacted with a 4,200-lb (1905-kg) vehicle at 57 mph (92 km/h) and 20 deg. This resulted in a maximum permanent ring deflection of 18 in. (457 mm) (test BR-7).

No significant elastic rebound of the rails and the energy-absorbing rings was evident during the tests. For a large number of moderate impacts expected in actual service, it is anticipated that the system could be restored by a maintenance crew using a hydraulic jack. Rings with less than 4-in. (101-mm) permanent deformation were succes-

fully restored and reused in this program. In cases where significant ring deformation and rail deformation occur, replacement of these elements will be required.

REFERENCES

1. N. Perrone. Thick-Walled Rings for Energy-Absorbing Bridge Rail Systems. Rept. FHWA-RD-73-49, Dec. 1972.
2. G. H. Powell. BARRIER VII—A Computer Program for Evaluation of Automobile Barrier Systems. Rept. FHWA-RD-73-, March 1973.
3. J. D. Michie, M. E. Bronstad, C. E. Kimball, J. A. Wentworth, and J. G. Viner. Development of a Collapsing Ring Bridge Railing System. Federal Highway Administration.

DYNAMIC TESTS OF METAL BEAM GUARDRAIL

E. F. Nordlin, J. R. Stoker, and R. L. Stoughton,
Division of Construction and Research, California Department of Transportation

The results of four vehicle impact tests into metal beam guardrail using three types of posts and blocks are reported. The then current (1971) California standard plans for metal beam guardrail required 8 by 8-in. (203 by 203-mm) nominal douglas fir posts and blocks. We wanted to determine whether smaller sized wood posts and blocks could be used and whether steel posts and blocks could be used in place of the 8 by 8-in. (203 by 203-mm) blocks to reduce guardrail costs. We also wanted to obtain another permissible post material besides wood. It was concluded that 6 by 8-in. (152 by 203-mm) nominal douglas fir wood posts and blocks were an acceptable substitute and that wide-flange 6-in. by 8.5-lb/ft (152-mm by 12.7-kg/m) steel posts and blocks could be used provided W-section backup plates were used at alternate posts where no beam splice occurred and a positive connection was used at the end-anchor cable in place of cable clips. All four tests conducted used 4,960-lb (2250-kg) passenger vehicles with nominal impact speeds and angles of 65 mph (105 km/h) and 25 deg respectively.

•IN 1964, the California Division of Highways performed a series of full-scale impact tests on the metal beam guardrail. Those tests (1) resulted in the adoption of a design that featured a 12-gauge (2.66-mm) W-section steel beam mounted on 8 by 8-in. (203 by 203-mm) douglas fir (DF) wood posts and blockout blocks that were spaced 6.25 ft (1.9 m) on center. The height at the top of the rail was 2.25 ft (0.7 m). Later tests between 1965 and 1968 on short sections of guardrail (2) established the need for a positive anchor at the ends of guardrail installations. As a result, end anchors became a part of the standard guardrail design. Operational experience has proved this barrier to be effective in California. This design was designated G4W (4).

In 1971, consideration was given to further changes in California's standard guardrail design that would decrease costs without impairing the effectiveness of the barrier. Other states were using 6 by 8-in. (152 by 203-mm) DF wood posts and wide flange (W) 6-in. by 8.5-lb/ft (152-mm by 12.7-kg/m) steel posts. The Southwest Research Institute had conducted successful tests on the steel post design (3). Previously, steel posts were not economically competitive in California, but fluctuations in the price and supply of wood posts in 1972 made consideration of alternative post materials desirable.

This report describes the results of four full-scale dynamic impact tests on guardrails that incorporated either 8 by 8-in. (203 by 203-mm) or 6 by 8-in. (152 by 203-mm) wood posts and blocks or W 6-in. by 8.5-lb/ft (152-mm by 12.7-kg/m) steel posts and blocks. These comparative tests were deemed necessary for three main reasons:

1. Guardrails with 6 by 8-in. (152 by 203-mm) wood posts and blocks or steel posts had never been tested under the more severe conditions considered representative of California freeways; therefore, they were used in California guardrail tests [±4,960-lb (2250-kg) vehicle, 65-mph (105-km/h) impact velocity, and 25-deg angle of impact].
2. Guardrails with the three types of posts had never been compared under identical test conditions.
3. Good accelerometer data had not been obtained in previous California guardrail tests.

Shortages of the W 6-in. by 8.5-lb/ft (152-mm by 12.7-kg/m) steel post have developed since the tests were conducted. It is felt, however, that the tests still have value for comparative purposes with other guardrail designs, for verification of the integrity of steel post barriers in place on highways, and for illustration of the value of positive end anchorage connections and backup plates between posts and beams.

TEST CONDITIONS

Guardrail Design and Construction

Figure 1 shows the guardrail design details. Each 75-ft-long (22.9-m) test guardrail was built approximately 1.5 ft (0.46 m) in front of the previous guardrail tested with posts staggered midway between the post location of the previous guardrail. This procedure ensured that soil conditions would be nearly identical for all test guardrails, that posts for each guardrail would be placed in undisturbed soil, and that post resistance in the soil would not be affected by post holes from previous guardrails that were staggered out of the way.

Wood posts were installed in accordance with common practice in California. The 8 by 8-in. (203 by 203-mm) posts were driven into 9-in.-diameter (228-mm) predrilled holes. To simulate the same soil condition, the 6 by 8-in. (152 by 203-mm) wood posts were driven into 8-in.-diameter (203-mm) pilot holes. Steel W 6-in. by 8.5-lb/ft (152-mm by 12.7-kg/m) posts were driven into the ground rather than into predrilled holes.

Figure 2 shows the cable-end anchor with a swaged fitting (replacing the cable clips) that was used in test 276. Note the strain gauges that were used on the anchor for test 276. The test equipment and procedure are given elsewhere (9).

Test 272

Test 272 was a control test on the metal beam guardrail using 8 by 8-in. (203 by 203-mm) wood posts and blocks (Figure 1). A 1970 Mercury sedan weighing 4,960 lb (2250 kg) impacted the barrier between posts 5 and 6 at 66 mph (106 km/h) and 26 deg. (Posts are numbered from the upstream end.)

There was little rise or roll imparted to the vehicle during impact until it was nearly parallel to the barrier. Then the vehicle rolled about 15 deg away from the barrier, and the right front end rose about 0.9 ft (0.27 m). The vehicle traveled smoothly through impact, had an exit angle of the vehicle's center of gravity (c.g.) of about 6 deg, and an exit heading angle of 0 deg so that the vehicle stayed close to the barrier and almost parallel to it. Figure 3 shows sequential photographs of the impact. The right front portion of the vehicle was so severely damaged that it could not be driven away. There was no intrusion of vehicle parts or barrier components into the passenger compartment. On impact, the dummy, restrained in the driver's position by a lap belt, was thrown sideways and downward toward the right passenger's seat. There were no apparent abrasions incurred by the dummy, and there was no damage to the interior of the vehicle caused by the dummy.

Two guardrail posts near the point of impact were destroyed, and pieces of the posts and their blocks were splintered and broken and thrown behind the barrier. Two other posts and their blocks were split. The metal beam was partially flattened and raised near the area of impact. Maximum displacement of the posts at ground level was 1 ft (0.3 m).

Test 273

Test 273 was performed on a guardrail identical to the guardrail in test 272 except that 6 by 8-in. (152 by 203-mm) wood posts and blocks were used in place of 8 by 8-in. (203 by 203-mm) wood posts and blocks. A 1970 Mercury sedan weighing 4,960 lb (2250 kg)

Figure 1. Test barrier details.

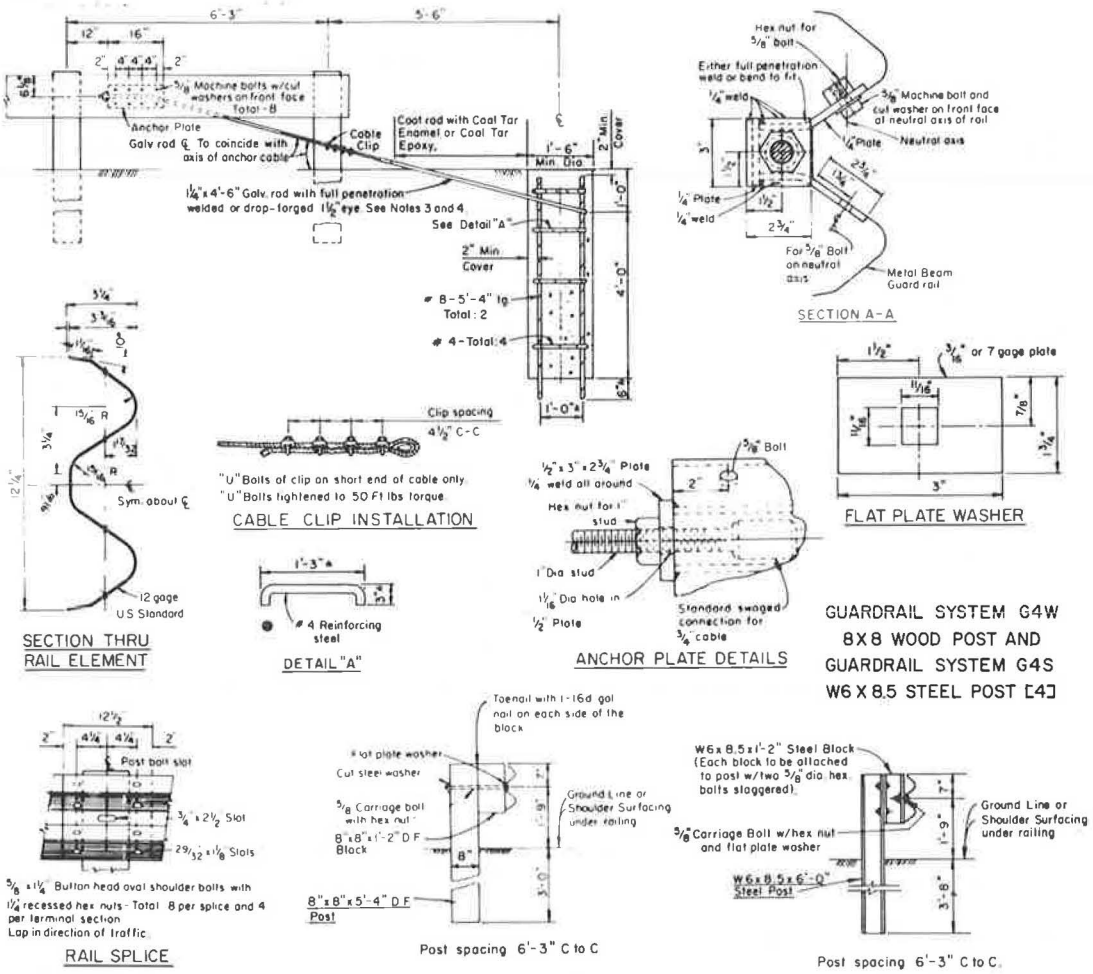

Figure 2. Cable-end anchor used on barrier for test 276.

impacted the barrier slightly downstream of post 4 at 68 mph (109 km/h) and 24 deg.

Vehicle behavior was similar to that in test 272. There was little rise or roll imparted to the vehicle during impact until it was nearly parallel to the barrier. Then the vehicle rolled about 17 deg away from the guardrail, and the right front end rose about 0.8 ft (0.24 m). The vehicle traveled smoothly through the impact. The exit angle of the vehicle's c.g. was 14 deg, which was the same as the exit heading angle of the vehicle. This angle gradually increased as the vehicle moved away from the guardrail. Figure 4 shows sequential photographs of the impact. Damage to the right front area of the vehicle was severe, and the car could not be driven away. There was no intrusion of vehicle parts or barrier components into the passenger compartment. Dummy behavior was the same as in test 272.

Two guardrail posts near the point of impact were destroyed. A third adjacent post was splintered, and one post near each end of the barrier was split. Three blocks were broken and thrown behind the barrier along with some of the splintered post debris. The beam was partially flattened and raised near the area of impact. Maximum displacement of the posts at ground level was 1.65 ft (0.5 m) perpendicular to the barrier at post 5.

Test 274

Steel W 6-in. by 8.5-lb/ft (152-mm by 12.7-kg/m) posts and blocks were used in the guardrail for test 274 (Figure 1) in place of wood posts and blocks. A 1970 Mercury sedan weighing 4,960 lb (2250 kg) impacted the guardrail between posts 4 and 5 at 63 mph (101 km/h) and 24 deg.

The vehicle penetrated the guardrail with little change in direction and spun around 180 deg as it slid to a stop. Vehicle forestructure damage was severe, and the car could not be driven away. There was no intrusion of vehicle parts or guardrail components into the passenger compartment. Figure 5 shows sequential photographs of the impact.

Shearing of the W-section beam occurred at the downstream edge of post 6. The beam was detached from post 6 and bent back around post 5. Downstream, the beam segment was bent where post 7 had been attached and at the upstream edge of post 8. All 13 posts were twisted and displaced; the top of post 1 was displaced 1.5 ft (0.46 m) downstream, and the top of post 13 was displaced 1.25 ft (0.38 m) downstream. Posts 5, 6, and 7 were twisted and bent down near the ground about their minor axes with virtually no displacement of the posts in the ground. Slippage of the cable through five cable clips occurred at the upstream anchorage. These clips had been torqued to 50 ft-lbf (67.8 J) twice, including once on the day before the test. The bolt between the beam and block pulled through the beam at posts 5, 6, 7, and 8. The block at post 6 was buckled flat, and local buckling of block flanges occurred at several posts near impact.

Test 276

The guardrail for test 276 also incorporated steel W 6-in. by 8.5-lb/ft (152-mm by 12.7-kg/m) posts and blocks and was the same as that for test 274 with two exceptions: (a) One-ft-long (0.3-m) steel W-section backup plates were placed behind the continuous guardrail beam at alternate steel posts where there were no beam splices, and (b) the cable clips at the cable-end anchors were replaced by a swaged fitting and clevis that connected to the standard eyerod that is embedded in the concrete footing at the ends of the barrier. A 1970 Mercury sedan weighing 4,960 lb (2250 kg) impacted the guardrail between posts 4 and 5 at 66 mph (106 km/h) and 25 deg.

Vehicle behavior was very stable during impact; there was virtually no vehicular roll or rise as redirection occurred. The exit angle of the vehicle's c.g. was about 16 deg and was the same as the exit heading angle of the vehicle. This angle decreased as the car skidded clockwise to a stop and came back toward the guardrail. Figure 6

Figure 3. Sequential views of test 272.

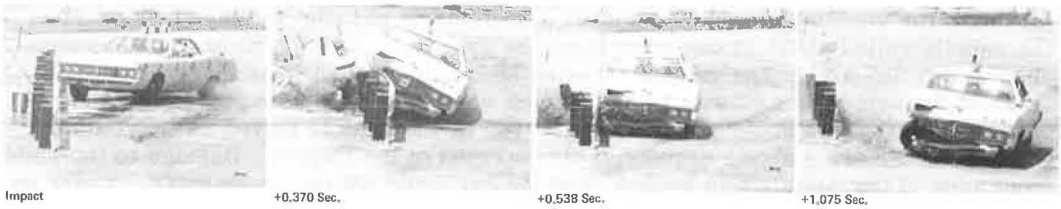

Impact | +0.370 Sec. | +0.538 Sec. | +1.075 Sec.

Figure 4. Sequential views of test 273.

Impact +0.032 Sec. | +0.204 Sec. | +0.418 Sec. | +0.776 Sec.

Figure 5. Sequential views of test 274.

Impact +0.052 Sec. | +0.134 Sec. | +0.296 Sec. | +0.550 Sec.

Figure 6. Sequential views of test 276.

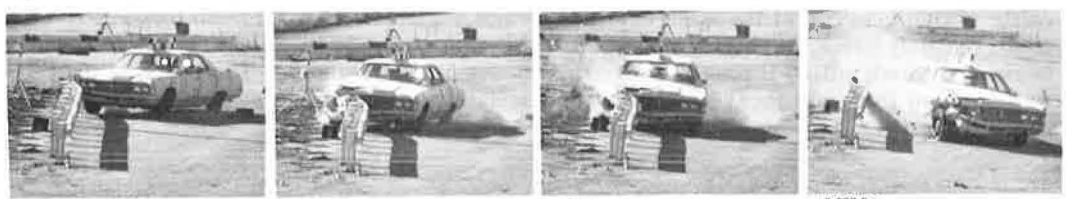

Impact +0.025 Sec. | +0.174 Sec. | +0.273 Sec. | +0.673 Sec.

Figure 7. Barrier damage, test 276.

shows sequential photographs of the impact. Vehicle damage was similar to that in tests 272 and 273. During impact, the dummy was thrown to the right and downward into the right passenger's seat, apparently without striking the dashboard. The dummy immediately bounced back into an upright position, struck the back of its head on the left door post, and came to rest against the left door.

Guardrail damage consisted mainly of moderate twisting and bending of posts 5, 6, and 7 although none of the posts was bent to the ground. Separation of the metal beam from the steel post block occurred only at post 6. Severe buckling of the blocks occurred at posts 5, 6, and 7. A maximum $^{3}/_{8}$-in. (9.5-mm) slippage of a beam splice occurred at post 5. Barrier damage is shown in Figure 7.

TEST RESULTS

The test results were weighed against the service requirements and performance criteria for longitudinal barriers (4) as follows:

> The order of emphasis for service requirements is first to safety, second to economics, and third to aesthetics.... If the barrier system contains the moving vehicle (i.e., structural strength), the vehicle decelerations are judged to be within human tolerance levels, and the vehicle post impact trajectory is acceptable; the candidate barrier is considered acceptably safe for in-service experimental use. After the system has been carefully monitored and evaluated in service and its effectiveness has been established, the system is judged to be operational.

Dynamic Performance Criteria for Safety

Structural Integrity of Barrier

The guardrails impacted in tests 272, 273, and 276 all met the requirements of containment. There were no indications that they were on the brink of failure. The guardrail impacted in test 274 was penetrated, and this was unacceptable. An analysis of that failure is described later. Figure 7 shows close-up views of posts near the impact area for test 276. The backup plates at posts 4 and 8 clearly resisted excessive bending of the W-section beams at the posts.

Sample borings were taken of the soil at the test site. The soil consisted of a layer of stiff, overconsolidated clay in the top 1.5 ft (0.46 m) and a layer of sandy clay with gravel and clayey sand with gravel (commonly called hardpan) for 1.5 to 4.5 ft (0.46 to 1.37 m) of depth. This stiff soil probably gave the barrier added apparent stiffness and forced the wood posts near impact to shear and the steel posts to bend rather than to yield in the soil. However, the major restraining force in the barrier appears to come from the W-section beam as evidenced by test 274 during which the cable anchor slipped and the W-section tensile strength could not be developed.

Vehicle Deceleration

Guideline values for maximum vehicle decelerations (at the center of mass) are given in Table 1 (6). The limits of deceleration given are not nominal limits for no injury but rather are maximum limits beyond which disabling injury or fatality may be expected. Detailed explanation of reasons for using the 50-msec time interval is given elsewhere (7).

Table 2 indicates, in accordance with the values given in Table 1, that, for all tests, values of vehicle deceleration in the longitudinal direction were well below the 10-g recommended limit for lap-belted passengers and slightly over the 5-g recommended limit for unrestrained passengers. The values of vehicle deceleration in the lateral direction, which are more critical for impacts into guardrail, slightly exceeded the recommended limit of 5 g for lap-belted passengers but were well below the 15-g limit

Table 1. Maximum vehicle decelerations.

Barrier Performance Rating	Maximum Vehicle Decelerations[a] (g)		
	Lateral	Longitudinal	Total
Limits for unrestrained passenger	3	5	6[b]
Limits for passenger restrained by lap belt	5	10	12
Limits for passenger restrained by lap and shoulder belts	15	25	25

[a]For vehicle rigid body; maximum 500-g/sec onset rate; highest 50-msec average.
[b]Preferred range.

Table 2. Test parameters and results.

Test Series	Test No.	Vehicle Weight (lb)	Vehicle Speed (mph)	Kinetic Energy (ft-kips)	Impact Angle (deg)	Vehicle Deceleration[a] (g)		Gadd Severity Index	Maximum Permanent Guardrail Deflection[b] (ft)	Exit Angle[c] (deg)
						Lateral	Longitudinal			
Nordlin, Stoker, and Stoughton	272(G4W)	4,960	66	725	26	5.45	5.55	883	2.22	6
	273(G4W)[d]	4,960	68	770	24	6.95	6.75	1,130	2.33	14
	274(G4S)	4,960	63	661	24	4.75	5.80	279	Failure	—
	276(G4S)[e]	4,960	66	725	25	6.85	3.78	371	1.76	16
California Division of Highways, previous tests (1, 2)	107(G4W)	4,570	60	552	25	—	—	—	1.5	17
	108(G4W)[f]	4,570	59	534	25	—	—	—	1.5	19
	133(G4W)	4,540	56	477	30	—	—	—	2.8	7
	135(G4W)	4,540	59	534	28	—	—	—	1.6	24
Southwest Research Institute (3, 4)	101(G4W)	4,042	55.3	414	30.5	4.6	4.6	—	2.60	11.7
	103(G4W)	4,123	60.1	500	22.2	6.1	3.0	—	2.40	15.0
	119(G4S)[g]	4,169	53.4	400	30.2	4.4[h]	4.6[h]	—	2.67	19.8
	120(G4S)	3,813	56.8	413	28.4	6.6	3.9	—	2.90	8.0
	121(G4S)[i]	4,478	56.2	475	27.4	6.8[h]	3.7[h]	—	2.10	9.3
	122(G4S)[i]	4,570	62.9	607	25.3	7.8[h]	3.9[h]	—	2.90	9.0

Note: 1 lb = 0.45 kg, 1 mph = 1.6 km/h, 1 ft-lbf = 1.36 J, 1 ft = 0.3 m. G4W and G4S are defined elsewhere (4).
[a]Maximum averaged over a period of 50 msec. Values for guardrail tests 273(G4W) computed from high-speed movie film; other values computed from accelerometer data.
[b]Measured at top edge of rail.
[c]Direction that vehicle's c.g. was moving immediately following final vehicle contact with barrier.
[d]6 by 8-in. (152 by 203-mm) posts and blocks.
[e]Modified with backplates and clevis in anchorage.
[f]2-ft (0.6-m) beam height.
[g]No blockout.
[h]Peak decelerations.
[i]Double blockout.

Table 3. Vehicle rise and roll.

Test No.	Rise[a] (ft)	Roll[b] (deg)	
		Front of Vehicle	Rear of Vehicle
272	0.9	15	12
273	0.8	17	—
276	—	0	-1

Note: 1 ft = 0.3 m.
[a]Measured at target on right front fender.
[b]Measured at top of front and rear windshields in degrees away from a horizontal plane.

for passengers wearing shoulder and lap belts.

Table 2 also gives the results of other test series involving similar vehicle weights, impact speeds, and angles of impact (4). The number of tests for which 50-msec values of deceleration have been reported in the literature are rather limited. Southwest Research Institute recently reported results of tests on guardrail and median barrier terminals. Eight side-angle tests into these barriers have yielded 50-msec values of longitudinal deceleration ranging from 4.6 to 8.5 *g* and values of lateral deceleration ranging from 2.5 to 7.6 *g*, given test parameters similar to those in Table 2.

Values of the Gadd severity index (similar to the head-injury criterion now more commonly used) were computed and are also given in Table 2. In test 273 only, the index slightly exceeded the threshold value of 1,000, above which serious injury or death might be expected because of a concussion. This value is not reliable as a sole indicator of the chance of passenger injuries because of the large number of variables

related to the dummy and the vehicle interior.

Notwithstanding these limitations, it can be surmised that in these severe proof tests of the guardrails vehicle passengers had a fair chance of survival. Hence, in the large majority of actual highway accidents involving these guardrail systems, it can be predicted that passengers would sustain something less than serious injuries. The degree of injury would, of course, depend greatly on the type of passenger restraints.

Vehicle Post-Impact Trajectory

Barrier Deflection

The deflection of the rail in test 276 is less than that in tests 272 and 273. This may account for the relatively low longitudinal vehicle deceleration measured in this test. Table 2 indicates that the permanent barrier rail deflections recorded in this series were in the same range as those recorded for previous test series. It should be noted that the vehicle kinetic energy at impact for tests 272, 273, and 276 was appreciably higher than that for other tests shown in Table 2. Barrier damage in tests 272 and 273 was similar, and this indicates that the anchored metal beam, rather than the wood posts, was the critical restraining element.

Vehicle Crush

In a comparison of tests 272, 273, and 276, the damage to the right front portion of the vehicle was quite severe, was roughly similar for all tests, and was typical of that for other high-speed, oblique-angle guardrail crash tests. The right front wheel was disabled in all three tests.

Vehicle Rise and Roll

Analysis of the high-speed movie film produced the values of vehicle rise and roll given in Table 3. These values and the movie film demonstrate the stable condition of the test vehicles as they progressed through impact. The most stable condition occurred with the steel post guardrail.

Final Vehicle Position

Figure 8 shows the paths of the test vehicle after it impacted the test guardrails. There is no easy answer to explain the variance in post-impact trajectories. Various factors having an effect may include guardrail deflection, vehicle crush and damage to the wheel, time when brakes are actuated by remote control, amount of rise and roll, and paving surface conditions.

Barrier Debris

The steel post guardrail appears to have an advantage over wood post guardrail in that no barrier parts were dislodged in test 276. In tests 272 and 273, pieces of wood posts and blocks were thrown behind the barrier. Therefore, when guardrail is placed in narrow median or gore areas it may be preferable, from the debris standpoint, to use the steel post type of guardrail.

Cost

In the past, only wood posts were approved for use in guardrails in California. The use of steel posts had not been seriously considered because they were not cost competitive and the wood post type of guardrail had proved fully effective in full-scale tests and in operation. However, about the time this latest test series was conducted, the cost of wood posts and blocks was rising rapidly, and there was an apparent shortage. These rapid changes in supply and cost made it desirable to investigate the alternative use of steel posts in guardrails. The steel post guardrail used in test 276 was as effective as the wood post guardrail.

It does not appear that there would be any difference in maintenance and repair labor costs for the guardrail types tested in tests 272, 273, and 276. Cost and availability of replacement components are difficult to predict because of the current shortages of highway construction materials; this situation may continue into the future.

Aesthetics

Guardrails with 6 by 8-in. (152 by 203-mm) wood posts and blocks and W 6-in. by 8.5-lb/ft (152-mm by 12.7-kg/m) steel posts and blocks do not appear to offer any substantial improvement or downgrading of the appearance of guardrails using 8 by 8-in. (203 by 203-mm) wood posts and blocks. The steel post guardrail is slightly more streamlined and has uniformity of materials (all steel); the wood post guardrail may have a blockier, more substantial appearance, and perhaps a more rustic appearance that may be desirable in rural areas or other selected locations. However, bare steel posts made of any of the weathering steels could also be used to provide a rustic appearance.

Analysis of Test 274

The guardrail used in test 274 incorporated W 6-in. by 8.5-lb/ft (152-mm by 12.7-kg/m) steel posts and blocks. Penetration of the rail resulted when the vehicle impacted the barrier. The failure that led to the successfully revised barrier design used in test 276 is as follows:

1. The steel posts have about 90 times less torsional rigidity than wood posts, hence they absorbed little of the tensile load developed in the beam. Instead, they twisted and transmitted a large load almost instantly to the cable-end anchors.
2. Because of this large dynamic load (jerk), the cable slipped through the five cable clips at the upstream anchor.
3. Slipping of the cable relaxed the tension in the steel W-section beam and permitted severe pocketing, cold-working, and weakening of the metal beam.

To correct this condition, two changes were made to the barrier design for test 276: (a) A swaged fitting and clevis were used to replace the five cable clips on the cable-end anchorage to provide a positive anchorage and (b) twelve 1-ft-long (0.3-m) backup sections of W-section beam were placed behind the beam at alternate posts where beam splices did not occur. These backup sections reduced the tendency of the rail to hinge or tear along the hard sharp edge of the steel blocks and posts. The results of test 276 proved the effectiveness of these modifications.

Figure 9 shows the loads on the anchorage cables during impact and indicates more rapid load initiation times for tests 274 and 276 for which steel posts were used. Figure 9 also shows that the cables are not overdesigned.

The Southwest Research Institute also has conducted several successful tests on guardrail systems with W 6-in. by 8.5-lb/ft (152-mm by 12.7-kg/m) steel posts and blocks. Results of test 141 at the Southwest Research Institute seem to confirm the effectiveness of backup plates on a steel post guardrail system (8).

Figure 8. Vehicle trajectories.

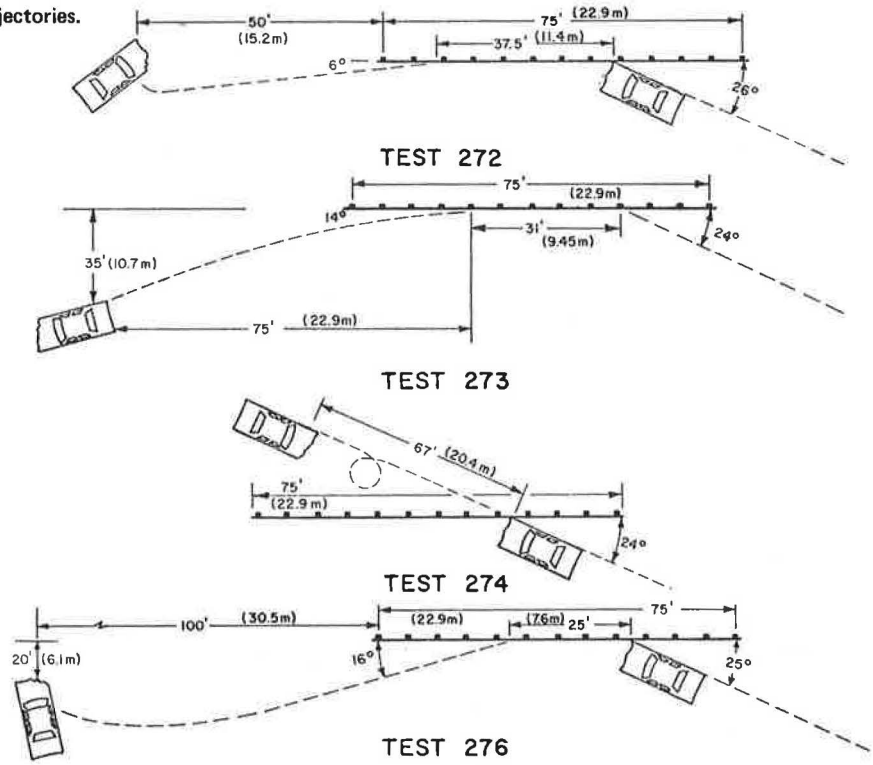

Figure 9. Upstream anchorage.

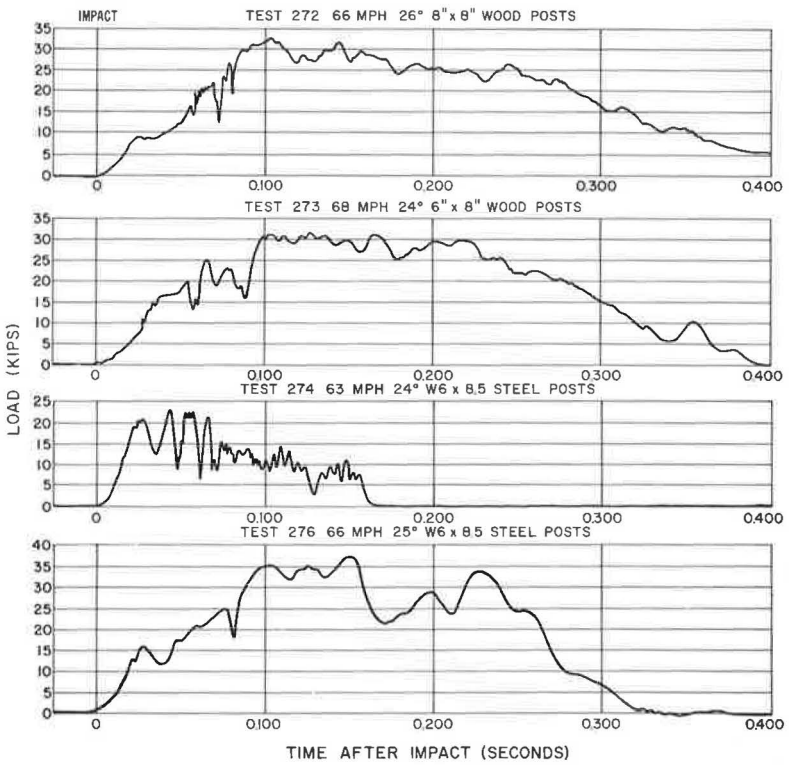

CONCLUSIONS

1. Metal beam guardrail using 6 by 8-in. (152 by 203-mm) DF wood posts and blocks effectively redirected a 4,960-lb (2250-kg) vehicle impacting the barrier at 68 mph (109 km/h) and 24 deg.
2. Metal beam guardrail using W 6-in. by 8.5-lb/ft (152-mm by 12.7-kg/m) steel posts and blocks effectively redirected a 4,960-lb (2250-kg) vehicle impacting the barrier at 66 mph (106 km/h) and 25 deg. However, the following two modifications of the standard wood post design were necessary: (a) a 1-ft-long (0.3-m), 12 gauge (2.66-mm) W-section backup plate was placed between the beam and block at alternate posts where beam splices did not occur, and (b) the cable clips at the standard end-anchor connection were replaced with a swaged fitting and clevis, and this resulted in a positive cable connection.
3. Guardrails using either 6 by 8-in. (152 by 203-mm) wood posts and blocks or W 6-in. by 8.5-lb/ft (152-mm by 12.7-kg/m) steel posts and blocks (as modified in test 276) were as effective as the guardrails using 8 by 8-in. (203 by 203-mm) DF wood posts and blocks, which were also tested using a 4,960-lb (2250-kg) vehicle impacting the barrier at 66 mph (106 km/h) and 26 deg.

ACKNOWLEDGMENTS

This paper was sponsored by the Federal Highway Administration, U.S. Department of Transportation. The contents of this report reflect the views of the Transportation Laboratory of the California Department of Transportation, which is responsible for the facts and the accuracy of the data presented. The contents do not necessarily reflect the official views or policies of the state of California or the Federal Highway Administration. This report does not constitute a standard, specification, or regulation.

The authors appreciate the efforts of the California Department of Transportation employees who assisted with the research: L. Staus, O. Box, V. Martin, J. Keesling, W. Crozier, D. Parks, R. Pelkey for testing and data reduction; R. Mortensen and L. Green for the photography; and R. Johnson, S. Law, and D. Gans for program instrumentation.

Special appreciation is also due W. R. Juergens and E. J. Tye of the Traffic Branch, California Division of Highways, who served as consultants on this project.

REFERENCES

1. E. F. Nordlin, R. N. Field, and R. H. Prysock. Dynamic Full Scale Impact Tests of Double Blocked-Out Metal Beam Barriers and Metal Beam Guard Railing. California Division of Highways, Series 10, Feb. 1965.
2. E. F. Nordlin, R. N. Field, and W. H. Ames. Dynamic Tests of Short Sections of Corrugated Metal Beam Guardrail. California Division of Highways, Series 13, Oct. 1968.
3. J. D. Michie, L. R. Calcote, and M. E. Bronstad. Guardrail Performance and Design. NCHRP Rept. 115, 1971.
4. J. D. Michie and M. E. Bronstad. Location, Selection, and Maintenance of Highway Traffic Barriers. NCHRP Rept. 118, 1971.
5. Committee on Guardrails and Guide Posts. Proposed Full-Scale Testing Procedures for Guardrails. Highway Research Circular 482, Sept. 1962.
6. N. E. Shoemaker and H. S. Radt. Summary Report of Highway Barrier Analysis and Test Program. Cornell Aeronautical Laboratory, Rept. VJ-1472-V-3, July 1961.
7. E. F. Nordlin, J. H. Woodstrom, and R. P. Hackett. Dynamic Tests of the California Type 20 Bridge Barrier Rail. California Division of Highways, Series 23, Oct. 1970.
8. NCHRP Research Results Digest 43, Oct. 1972.

9. E. F. Nordlin, J. R. Stoker, and R. L. Stoughton. Dynamic Tests of Metal Beam Guardrail. California Division of Highways, Series 27, April 1974.
10. N. J. DeLeys. Investigation of a Torsion Post-Beam Rail Type of Bridge Railing. Cornell Aeronautical Laboratory, Rept. VJ-2363-V-1, Nov. 1970.
11. M. D. Graham et al. New Highway Barriers: The Practical Application of Theoretical Design. Highway Research Record 174, 1967, pp. 88-183.

PENDULUM TESTS USING RIGID AND CRUSHABLE BUMPERS

M. E. Bronstad and J. D. Michie, Southwest Research Institute; and
R. R. White, Hi-Shear Corporation

The test program discussed in this paper consisted of 19 tests of a breakaway sign support using a 2,000-lb (907-kg) pendulum mass impacting the support at 20 mph (32 km/h). Use of both rigid and crushable bumpers permitted examination of these techniques compared with current momentum-change criterion. In addition, the effects of bolt-tightening torque on the slip-base release loads were investigated. Hi-Lok frangible nuts, which control tightening torque, were also evaluated for the design torque condition. Only in the crushable bumper tests were dramatically different results obtained for the various nut-tightening torques when momentum change was used as the criterion. Momentum change with the hard bumper was 65 ± 15 lbf-sec (289 ± 67 N-s) for all base-nut torque levels. Momentum change with the crushable bumper ranged from 88 lbf-sec (391 N-s) for design torque condition to 398 lbf-sec (1770 N-s) for the overtorqued condition. Repeatability of slip-base loads was generally good when both a calibrated torque wrench and the Hi-Lok torque control nuts were used. It was concluded that momentum-change criterion is insufficient in evaluating results of pendulum tests using a rigid bumper. Use of a bumper with vehicle crush characteristics appears to provide a superior experimental evaluation.

•DEVELOPMENT of breakaway sign and luminaire supports during the 1960s has contributed greatly to the safety of the roadside. In a Federal Highway Administration circular memorandum (1), an acceptance criterion was set for luminaire supports. This criterion was a vehicle momentum change of 1,100 lbf-sec (4893 N-s) or less based on full-scale crash tests. A later FHWA report (2) permitted dynamic laboratory tests (a ballistic pendulum of other equivalent means) to be used instead of the more expensive and generally less repeatable vehicle impact test. This laboratory test criterion specified a change in pendulum momentum of 400 lbf-sec (1779 N-s) or less.

Chisholm and Viner (3) in a recent FHWA report discussed the relationship between the two criteria. It is apparent from their work that correlation of pendulum tests and vehicle impact tests varies considerably. Factors that may be the cause of poor data correlation include different types of base supports (e.g., frangible, shoe, and slip), fracture or initiation force level, strain rate sensitivity of materials, vehicle crush properties, and insufficiency of momentum-change criterion. For an illustration, breakaway base supports A and B are evaluated by pendulum tests, and the idealized results are shown in Figure 1a; although the resistance forces are different, the momentum changes (i.e.,, area of force-time plot) are equal. These same base supports are then evaluated in vehicle crash tests (Figure 1b). For A, the vehicle crushes until resistance force is sufficient to initiate base-support fracture F_A at time T_{A_1} from time T_{A_1} to T_{A_2}; no further vehicle crushing occurs, and momentun change is caused by breaking and displacing the support. Characteristics for the B test are similar to those for the A test except addition of vehicle crushing is necessary to achieve the higher base-support initiation force F_B. The point to be made is that there is significant difference between the momentum change (or linear impulse) for the two plots of Figure 1b, even though pendulum tests based on momentum change alone (Figure 1a) may suggest equivalent base-support performance.

Figure 1. Comparison of vehicle and pendulum tests.

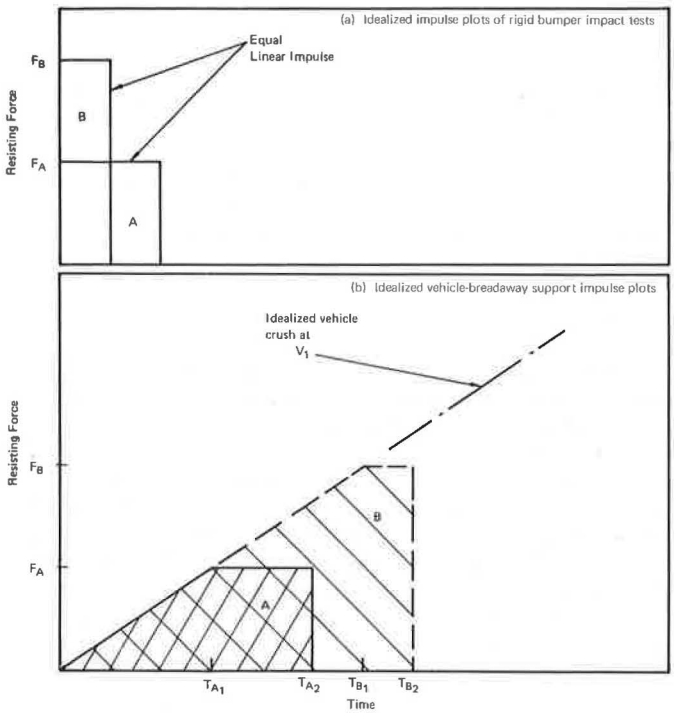

Figure 2. Sign support details.

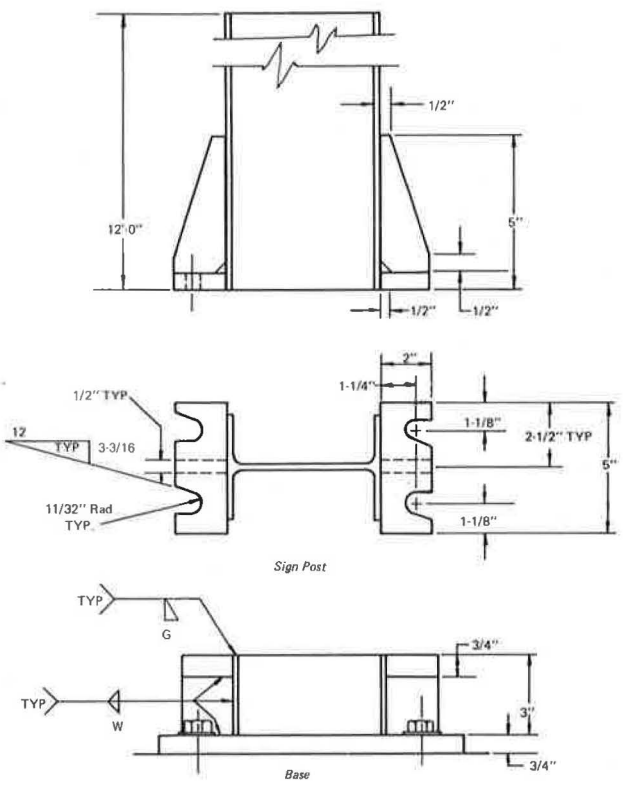

Figure 3. Acceleration versus time.

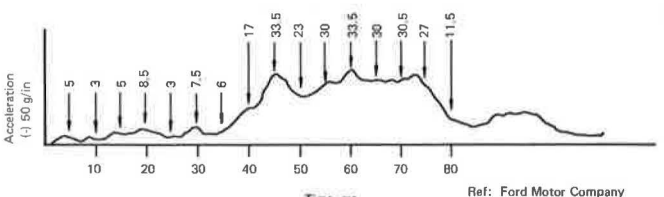

In view of the limitation of rigid bumper pendulum tests, a decision was made to investigate the use of a crushable bumper in pendulum tests to better simulate actual interaction of the vehicle and the breakaway support. This paper discusses and compares results of pendulum experiments using both rigid and crushable pendulum bumpers on a common breakaway sign support. In addition, effects of bolt torque control on slip-base loads and momentum change were studied.

TEST PROGRAM

Nineteen tests were conducted by using a 2,000-lb (907-kg) pendulum mass equipped with both hard and crushable bumpers. The deformable bumpers were designed to simulate vehicle crush and were constructed in stages using aluminum honeycomb as the energy-absorbing element.

A typical sign support specified by many states was selected as the impacted test article. A light section [W 6 in. by 8.5 lb/ft (W 15.2 cm by 12.3 kg/m)] was selected to minimize inertial effects on the data. Dimensions of the slip base are shown in Figure 2; the design nut-tightening torque for this slip-base support using $\frac{5}{8}$-in.-diameter (15.9-mm) ASTM A325 bolts is 450 lbf-in. (51 N · m).

Since a purpose of this program was to study the relative performance of pendulum bumpers, a complete sign assembly was not used. To compensate for resistance of the fuse plate (i.e., the upper breakaway hinge) in a sign support assembly, the height of the support was increased from the usual 7 to 12 ft (2.1 to 3.7 m).

CRUSHABLE BUMPER DESIGN

Several design requirements were established for the crushable bumper. A decision was made to design the bumper using time-acceleration data from an impact of a 1971 Ford Pinto (subcompact) automobile into a rigid pole at the vehicle centerline. Although the time-acceleration data were from tests conducted at 30 mph (48 km/h), it was felt that the bumper would yield good results at 20 mph (32 km/h). In addition, the bumper was to be inexpensive and lend itself to rapid fabrication. (Near the end of the program, the bumper was further simplified, and this resulted in cost savings.)

Aluminum honeycomb material was selected for the bumper assembly because the material is readily available, the crushing strength is predictable, the material cost is relatively low, the density is quite low (so that a change in bumper configuration would have a negligible effect on the pendulum weight), and the honeycomb material can be supplied in a wide range of crushing strengths.

Selection of the proper honeycomb densities required determination of impact force versus vehicle displacement for the full-scale automobile. Accordingly, the acceleration-time curve for the 1971 Pinto was integrated, and an average acceleration was determined for each 5-msec interval and used in developing a simplified force-time curve. (Only the first 80-msec of the curve were used, since it was felt that the slip-base sign would fail within that time span.) Based on these force-time data, a force-displacement curve was calculated and was the basis of the dimensional and density design of the bumper. Steps used in formulating the force-displacement property are shown in Figures 3, 4, 5, and 6. Figures 3, 4, and 5 apply to a 1971 Pinto impacting a rigid pole at 30 mph (48 km/h) at the vehicle centerline. Figure 7 shows the bumper configurations. The final bumper design is shown in Figure 7b.

Column instability occurred with the initial crushable bumper configuration in those tests with high base-nut torques. To provide lateral support to the bumper column, guide channels were added to the bumper design as shown in Figure 7d. It should be noted that this design allowed a much more rapid and economical test procedure.

Figure 4. Dynamic force versus time.

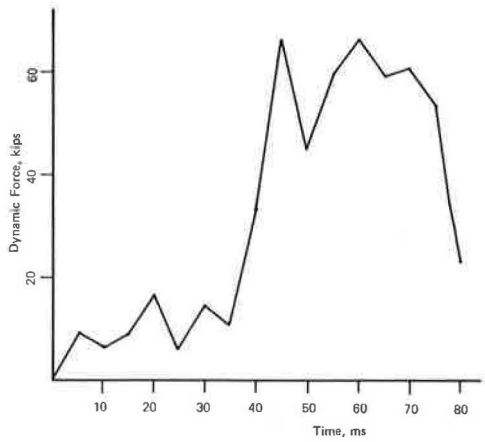

Figure 5. Dynamic force versus vehicle displacement.

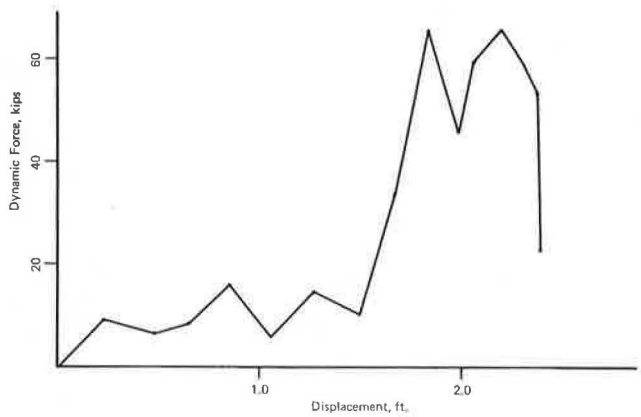

Figure 6. Predicted force response of honeycomb bumper.

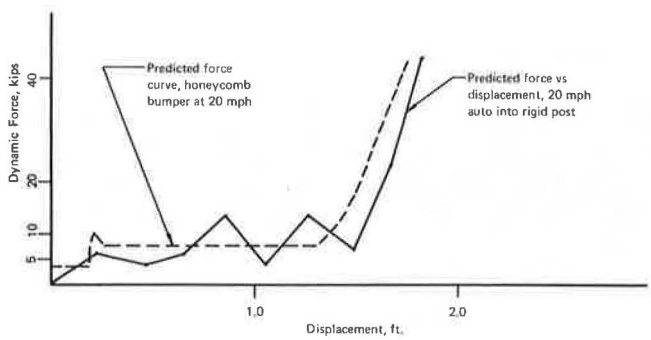

TEST PROCEDURE

The sign base was installed on a rigid foundation as shown in Figure 8. The sign support was attached to the base for each test using four $^{5}/_{8}$-in.-diameter (15.9-mm) galvanized ASTM A325 bolts. Heavy hex nuts (ASTM A325) used for the 0, 900, and 1,350-lbf-in. (0, 102, and 153-N·m) torque tests were installed with a calibrated torque wrench by using the installation method specified on typical state plans. The CHL14-10 Hi-Lok nut used for the 450-lbf-in. (50.8-N·m) torque tests is designed to provide the bolt preload of a heavy hex nut installed at that torque. During installation, the

Figure 7. Bumper configurations.

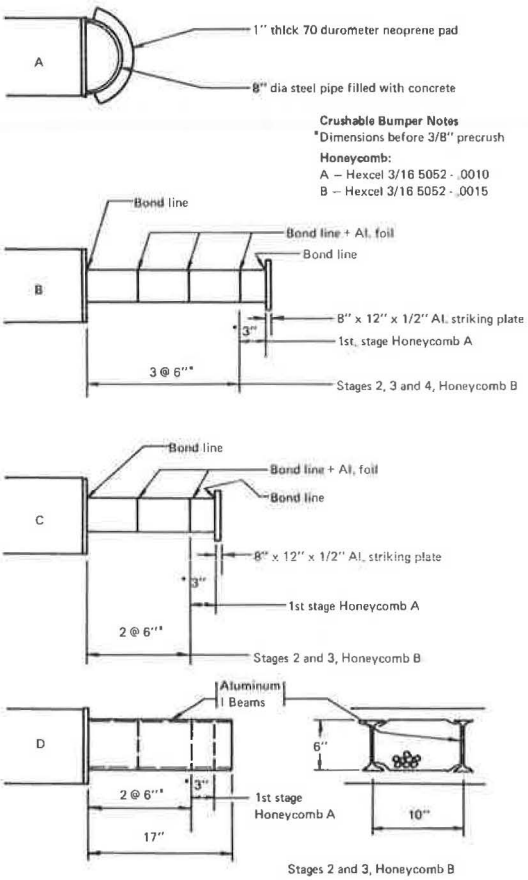

Figure 8. Test installation.

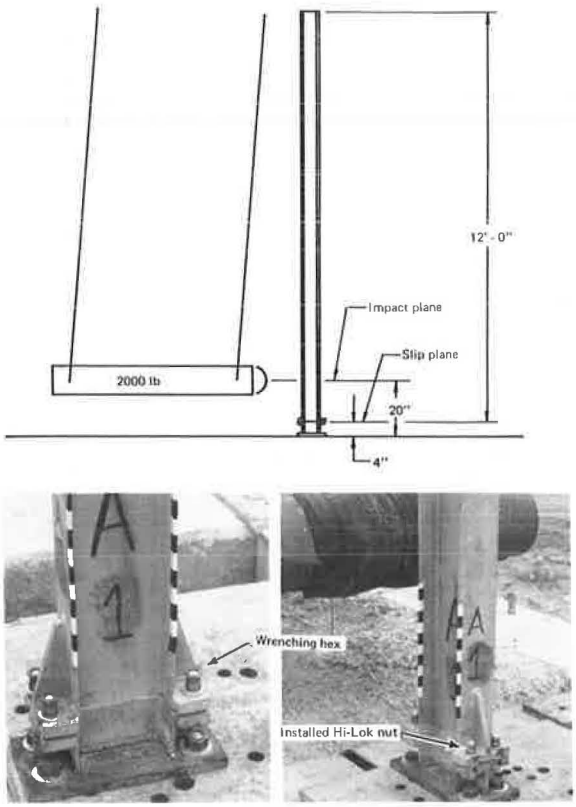

Figure 9. Test program bumpers.


Bumper A

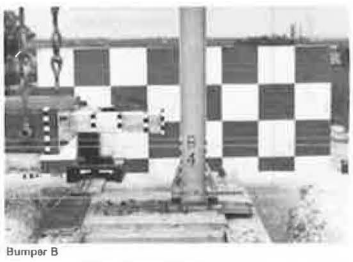
Bumper B

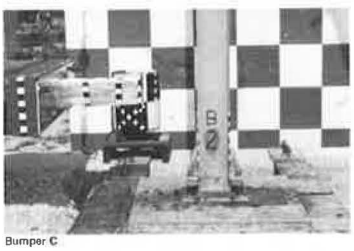
Bumper C


Bumper D

unique wrenching hex automatically shears off at the nut's torque-off groove when a predetermined design torque is reached.

Four different bumper configurations were used as shown in Figures 7 and 9. Buckling of the deformable bumpers B and C led to a redesign, configuration D, which performed as desired.

The 2,000-lb (907-kg) pendulum mass was hoisted to the appropriate drop height for a 20-mph (32-km/h) impact and was released. Impact data were obtained from a high-speed camera and accelerometers mounted on the pendulum mass. Data recorded by high-speed tape recorders were replayed and recorded (unfiltered) on oscillograph charts. A summary of the data acquisition systems is given in Table 1.

TEST RESULTS

Results of the tests are given in Table 2; an example of a data trace for test B-4(2) is shown in Figure 10. When the hard bumper was used, the peak force generally increased as nut torque increased, although linear-impulse (change-in-momentum) values were within a range of 65 ± 15 lbf-sec (289 ± 67 N-s).

The crushable bumper tests used three bumper configurations. Buckling of the bumpers occurred in tests B-5, B-6, B-7, B-8, and B-9. Bumpers in tests B-1(2), B-2, B-3, and B-4(2) performed as designed. Figure 11 shows the bumpers after testing. The successful performance (no buckling) of the C configuration bumper in tests B-2 and B-3 can be attributed to the low resistance afforded by the sign support installed with the Hi-Lok nuts. In tests with the same bumper design but with higher installation torques (tests B-5 and B-7), instability of the bumpers occurred because of the higher loads.

Comparison of results in tests B-2 and B-3 with the C bumper indicates good repeatability when the Hi-Lok nuts were used. Test B-1(2) with the improved bumper yielded similar force and impulse values. The hard bumper-Hi-Lok nut tests A-1 and A-2 demonstrated excellent repeatability for peak force and impulse values. Other torque test values were more erratic, although the two 900-lbf-in. (102-N·m) torque test results were in close agreement.

Figures 12 and 13 contain sequential photographs of the test series.

CONCLUSIONS

1. A crushable bumper has been designed and evaluated for use in evaluating breakaway or yielding highway structures. The bumper approximates the front end crush properties of a subcompact car (i.e., 1971 Ford Pinto) striking a rigid pole at 20 to 30 mph (32 to 48 km/h). The design is simple, economical, and easy to use. Use of the crushable bumper should improve the effectiveness of pendulum tests in predicting safe roadside structures.
2. Momentum change criterion alone is insufficient in evaluating results of pendulum tests using a rigid bumper. Base-support initiation force, which is less predictable, may be a necessary qualification to the change-of-momentum criterion. The crushable bumper appears to be a preferable alternate.
3. In a comparison of impulse values from the hard bumper tests with those from crushable bumper tests, the difference in impulse values for a range of base torques is demonstrated only with the crushable bumper tests.
4. Repeatability of the slip-base test results was generally good for a specified torque. Installation of the sign support using Hi-Lok torque control nuts provides control over the slip-initiation load comparable to that obtained with a careful installation of conventional units using a calibrated torque wrench and can be inspected visually.

Table 1. Electronic data acquisition system.

Component	Function	Equipment	Description
Transducer	Converts a physical phenomenon to an electric signal	Accelerometer	Kistler 815A7, ±250*g*; frequency response -5 percent at 1 Hz and ±5 percent at 6000 Hz
Tape recorder	Provides permanent, high-quality magnetic tape record of test data	CEC VR-3300 magnetic tape recorder-reproducer	14-channel FM recorder Tape speeds: $1\frac{7}{8}$ to 60 in./sec Extended bandwidth: DC to 20 kc Center frequency: 108 kc Signal/noise: 55 dB minimum Input sensitivity: 0.5 to 10.0v rms Linearity: 0.5 percent of full scale
Oscillograph	Provides analog traces of raw and filtered data	CEC 5-124A oscillograph	8-channel oscillograph with independent galvonometer and galvonometer circuits; typical galvonometers used are CDC 7-326 (within ±5 percent flat frequency response from 0 to 3000 Hz) and CDC 7-361 (0 to 5000 Hz)
Preamplifier	Scales and amplifies transducer signal	Southwest Research Institute design	Completes transducer circuit and amplifies signal by factor of 5 for tape recording

Note: 1 in. = 2.54 cm.

Table 2. Summary of test data.

Specimen No.	Bumper Configuration[a]	Slip-Base Nut	Slip-Base Nut Torque (lbf-in.)	Peak Acceleration (*g*)	Peak Force (kips)	Impact Duration (sec)	Linear Impulse (lbf-sec)
A-1	Hard A	Hi-Lok	450	11.8	23.7	0.008	63
A-2	Hard A	Hi-Lok	450	11.5	23.0	0.006	60
A-3	Hard A	Heavy hex	1,350	15.0	30.0	0.006	57
A-4	Hard A	Heavy hex	1,350	13.4	26.9	0.007	75
A-5	Hard A	Heavy hex	900	12.6	25.1	0.006	63
A-6	Hard A	Heavy hex	900	12.7	25.5	0.007	69
A-7	Hard A	Heavy hex	0	9.8	19.5	0.007	50
A-8	Hard A	Heavy hex	0	11.8	23.6	0.007	57
B-1(2)	Crushable D	Hi-Lok	450	4.8	9.6	0.017	88
B-2	Crushable C	Hi-Lok	450	3.4	6.8	0.019	79
B-3	Crushable C	Hi-Lok	450	3.6	7.1	0.018	71
B-4(2)	Crushable D	Heavy hex	900	9.8	19.6	0.043	322
B-5	Crushable C[b]	Heavy hex	900	7.7	15.5	0.071	398
B-6	Crushable B[b]	Heavy hex	900	9.4	18.9	0.065	280
B-7	Crushable C[b]	Heavy hex	1,350	13.7	27.3	0.050	287
B-8	Crushable B[b]	Heavy hex	1,350	13.0	26.0	0.065	331
B-9	Crushable B[b]	Heavy hex	1,350	12.5	25.0	0.065	291

Note: 1 lbf-in. = 0.113 N-m. 1 lbf = 4.4 N.

[a]See Figures 7 and 9. [b]Bumpers buckled.

Figure 10. Data trace for test B-4(2).

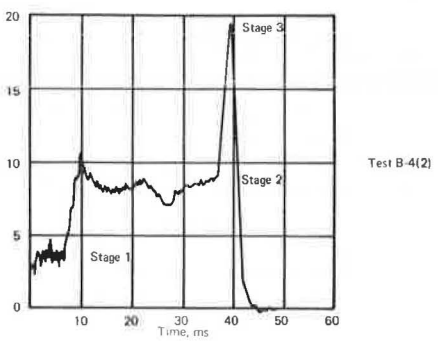

Figure 11. Bumpers after testing.

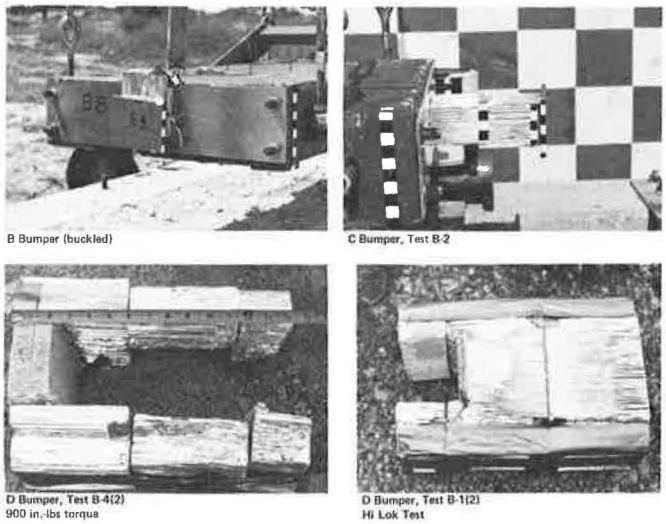

Figure 12. Sequential results of tests on bumpers A, B, and C.

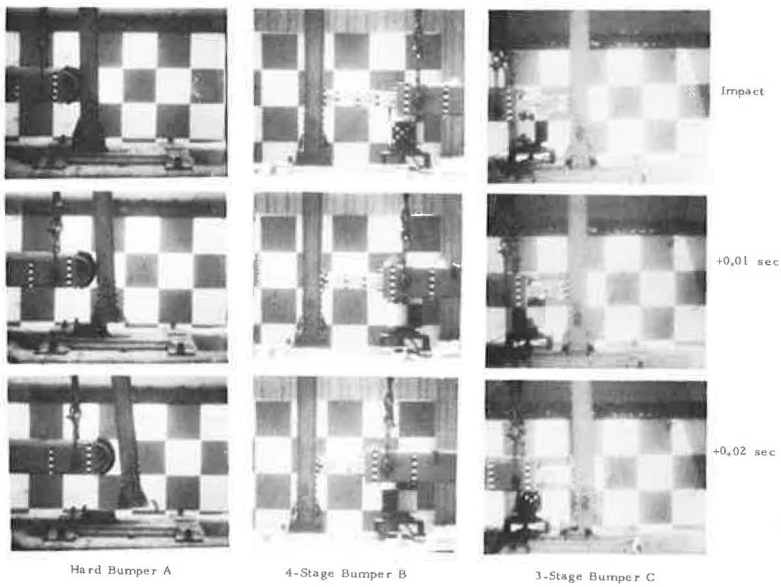

Figure 13. Sequential results of tests on bumper D.

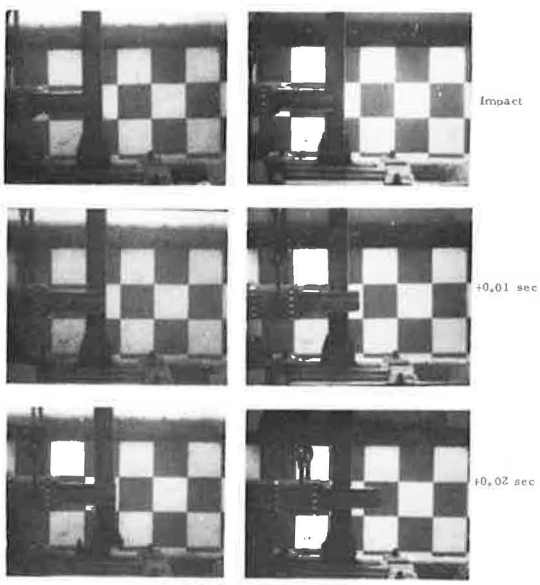

REFERENCES

1. Application of Highway Safety Measures, Breakaway Luminaire Supports. Federal Highway Administration, Circular Memorandum, June 5, 1968.
2. Application of Highway Safety Measures, Breakaway Luminaire Supports, Office of Traffic Operations, Federal Highway Administration, Notice TO-20, Nov. 16, 1970.
3. D. B. Chisholm and J G. Viner. Dynamic Testing of Luminaire Supports. Office of Research and Development, Federal Highway Administration, Final Rept., July 1973.

CONSTRUCTION OF FRANGIBLE-TUBE, ENERGY-ABSORBING BRIDGE BARRIER SYSTEM

Michael M. Kasinskas, Materials Testing Laboratory, and
Charles E. Dougan, Bureau of Planning and Research,
Connecticut Department of Transportation

ABRIDGMENT

The Connecticut Department of Transportation in cooperation with the Federal Highway Administration installed a frangible-tube, energy-absorbing bridge barrier system. The experimental barrier absorbs the impact forces of a colliding vehicle by using fragmenting aluminum tubes. This paper details the construction of the experimental barrier on a Connecticut bridge having concrete parapet walls.

•THE Connecticut Department of Transportation, in conjunction with the Federal Highway Administration, completed installation of a newly developed energy-absorbing bridge barrier system in July 1974. The basic concept of the barrier was conceived by the National Aeronautics and Space Administration for absorbing the impact experienced by space craft during lunar landings. FHWA, realizing the potential that NASA's energy-absorbing system had for highway-safety applications, contracted Southwest Research Institute (SwRI) of San Antonio, Texas, to investigate possible uses of this concept. Using the NASA concept, SwRI subsequently designed the energy-absorbing bridge guardrail discussed.

OPERATION OF ENERGY-ABSORBING SYSTEM

The operating principal of the SwRI design is based on the fragmentation of a series of aluminum tubes secured between a rigid bridge railing and a movable box beam. On impact between a vehicle and the box beam, the kinetic energy is absorbed in the fragmenting tubes at a rate that prevents the development of reaction force and that thereby reduces the possibility of the vehicle rebounding back into the traffic stream (1).

DESCRIPTION OF CONNECTICUT BRIDGES

In Connecticut, most bridges have concrete parapet walls 3.08 ft (0.94 m) high and 15 in. (38 cm) wide. At the base of the parapets, there is either a 6-in.-wide (15-cm) by 10-in.-high (25-cm) granite curb or an 18-in. (46-cm) sidewalk with the granite curb; at the top there is a steel railing 1.6 ft (0.49 m) high. Shoulders between the outside edge of the travelway and the approximate base of the parapet vary from 2 to 10 ft (0.6 to 3 m). The parapet ends are usually protected by a 1-ft (0.3-m) W-beam guiderail.

MODIFICATION OF INITIAL FRANGIBLE-TUBE BARRIER

There were substantial differences between the parapet-rail system used in the SwRI study (1) and the typical system currently used on Connecticut bridges. These differences required basic modification of the SwRI design (Figure 1). Some of these modifications were as follows:

1. Replacement of the rectangular guide with a standard 3-in. (7.6-cm) internal-diameter steel pipe of increased length to clear the 1.25-ft (0.38-m) concrete parapet;
2. Replacement of the 4-in. (10-cm) square sleeves with 4-in. (10-cm) round holes cored in the parapet;
3. Replacement of steel shims with wooden shims or spacers to minimize damage at lower levels, if the shims should become dislodged and drop; and
4. Deletion of the rub rail recommended by SwRI, since the existing granite curbing would serve as one.

TEST SITE DESCRIPTION

The structure chosen for the test installation is in the eastbound roadway of I-84 in the towns of Plainville and New Britain. The geometry of the bridge is as follows: L = 852.8 ft (260 m), R = 1,375 ft (419 m), and D = 4 deg 10 min. The concrete deck has a superelevated cross slope of ¾ in./ft (6.25 cm/m). The installation is on the high side of the road. The shoulder along the outside lane is 10 ft (3 m) wide with 6-in.-wide (15-cm) curbing at the parapet base.

CONSTRUCTION DETAILS

The contractor accomplished the work in two phases: core drilling and installation of the barrier system.

Core Drilling

The 4-in. (10-cm) core holes were drilled by using two conventional portable coring rigs with manual feed. The baseplate of each rig had a vacuum chamber on its underside for securing the rig in the desired position. A screw at each of the four corners of the baseplate permitted a small amount of adjustment when the bit was leveled. The guide on which the drill was mounted was attached to the baseplate at 90 deg in all directions.

The drilling operation required 10 working days to core 141 holes with a cumulative length of 176.25 linear ft (53.7 m); thus, drilling efficiency amounted to 17.625 linear ft (5.37 m)/day or 8.86 ft (2.7 m)/day/rig.

Figure 1. Top view of section through centerline of tubes.

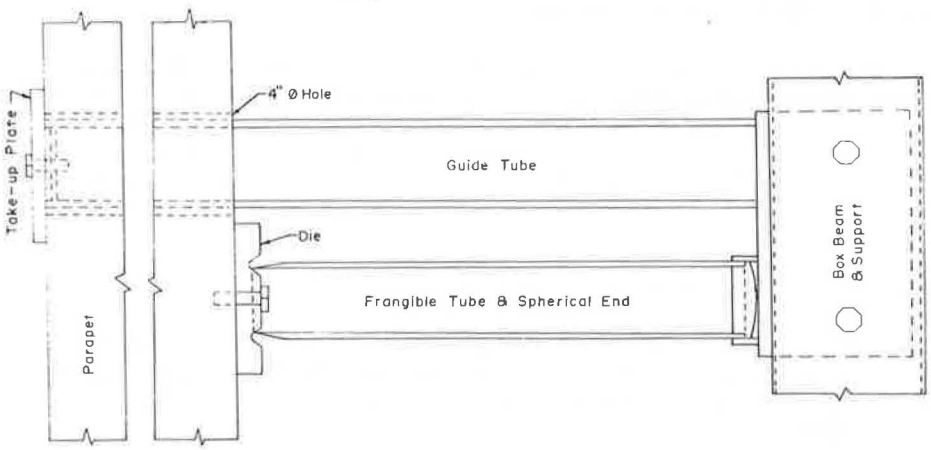

Figure 2. Components of frangible-tube system.

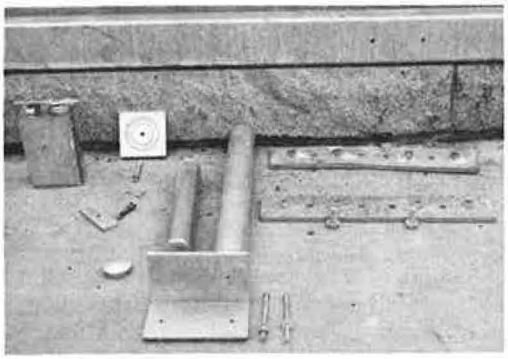

Figure 3. Fully installed unit of system on bridge.

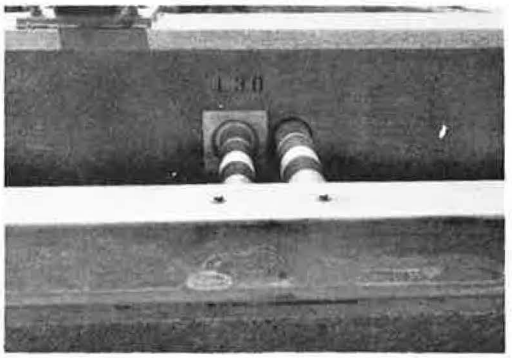

Figure 4. The completed system.

Installation

Before the barrier was installed, a backup system and transition section were installed at the west end of the bridge. The backup system consisted of a reinforced 1-ft (0.3-m) W-beam mounted on 6-in. (15-cm) I-beams driven 3.25 ft (0.99 m) into the embankment.

The radius of the bridge was sufficiently long to allow placement of the entire length of box beam in 18 to 19-ft (5.5 to 5.8-m) chord sections. The chords differed in those areas where twin conduits and junction boxes existed in the parapet. In these cases, the chords varied in length from 20 to 24 ft (6.1 to 7.3 m). The spacing between the frangible-tube units was 6 to 6.8 ft (1.8 to 2.1 m). Spacing differed to avoid expansion joints and electrical conduits.

Sufficient dies and frangible-tube assemblies were mounted on the parapet wall for each day of work. Before the aluminum tubes were mounted onto the die (Figure 2), they were coated with lubricant. The lubricant recommended by a local distributor was Molykote 557. This particular lubricant comes in liquid form and is described as an extreme-pressure lubricant with antiweld properties for cutting and forming metals. When the solvent evaporates, it leaves a thin film on the surfaces. The take-up plates were loosely bolted into position. A section of box beam with predrilled bolt holes was then placed on the mounted assemblies and loosely connected to the preceding section of box beam with a splice plate. Three units were used per section of box beam. After the initial installation, the alignment was corrected. The box beam was then bolted to the frangible-tube assemblies and the splice-plate bolts were secured (Figure 3). When all the units and box beam were in place, the units were leveled by using hydraulic jacks; wooden shims were inserted in the core holes at the top and bottom of the guides. When the units were leveled and the shims were in place, the take-up plates were secured.

SUMMARY

The entire project required 22½ working days to complete. As mentioned, 10 days were required for the drilling operation, and 10 days for the actual installation. The

remaining 2½ days were used in laying out the job, excavating and placing the concrete anchor block, and rechecking all the bolts for tightness.

Construction of the frangible-tube barrier system, as designed by SwRI and modified by Connecticut DOT (for Connecticut's needs) indicates that, with minor changes in design, the system can be installed without encountering major problems. In addition, the system has pleasant aesthetic features and blends in well with its environment (Figure 4).

ACKNOWLEDGMENT

The contents of this paper reflect the views of the authors, who are responsible for the facts and accuracy of the data presented. The contents do not necessarily reflect the official views or policies of the state of Connecticut or the Federal Highway Administration. The report does not constitute a standard, specification, or regulation.

REFERENCE

1. An Impact-Energy Attenuating Device Combined With Guardrail-Like Structures. Southwest Research Institute, Final Rept.

TEST AND EVALUATION OF A TIRE-SAND INERTIA BARRIER

E. L. Marquis and T. J. Hirsch, Texas Transportation Institute,
Texas A&M University; and
J. F. Nixon, Texas State Department of Highways and Public Transportation

Many rigid obstacles located on highways cannot be removed or made to break away and consequently are hazardous to motorists. Vehicle impact attenuators have been developed to protect the public from these obstacles. Most of these attenuators are expensive, and some obstacles remain unprotected since available funds are directed to protecting more cost-effective locations. An inexpensive vehicle impact attenuator composed of scrap tires and sand has been developed and tested at the Texas Transportation Institute. This inertia barrier uses a base that is crushable, plywood disks, scrap tires, sand, and a weatherproof covering. The principle of the conservation of momentum is used in the design. In addition, curves have been developed to assist the designer.

•THERE are many rigid obstacles on our nation's highways that cannot be removed or made to break away and that consequently are hazardous to the motoring public. Vehicle impact attenuators have been developed to protect the motoring public from impacting these obstacles directly. In general, most of these attenuators are expensive, and some obstacles remain unprotected since available funds are directed to protecting more cost-effective locations. This study was undertaken to develop an inexpensive and effective barrier that could be used to protect motorists from many hazards located near our primary and secondary roads.

Two previous studies had been made (1, 2) to show that a vehicle impact attenuator composed of scrap tires filled with sand was effective and feasible. The conclusions expressed in both reports were that the tire-sand inertia barrier was both effective and economical for selective locations and that the bases should be constructed so that they will not build up under the impacting vehicle and cause ramping. Three distinct possibilities of base designs meeting the criteria are possible:

1. The base could collapse on impact and slide under the impacting vehicle without causing ramping,
2. The base and sand container could be flexible laterally so that it would fragment on impact, and
3. The base could be stiff and light and an integral part of the module and thus could be knocked out of the way during impact.

Bases made of scrap tires with the annular space filled with empty metal beverage cans, those made of welded wire mesh, and those made of portions of used, 55-gal (208-liter) paint drums were investigated.

DEVELOPMENT OF DESIGN

The design of an inertia barrier is based on the conservation of momentum and has been documented by Hirsch (1) and Hirsch, Marquis, and Buth (2). D. L. Hawkins, when he was with the Texas Highway Department, first conceived of the idea of using scrap or salvage tires filled with sand as a vehicle impact attenuator in December 1965. At that time, he proposed using modules around high-level lighting standards and proposed this in a sketch.

The concept of the conservation of momentum is shown in Figure 1. The momenta before impact are equal to the momenta after impact. For rigid body plastic impact (i.e., the coefficient of restitution = 0),

$$V_o M = V_1(M + M_1) \tag{1}$$

where

V_o = the velocity of the vehicle before impact;
V_1 = the velocity of the vehicle and first mass after impact;
M = the mass of the impacting vehicle, W/g;
W = the weight of the vehicle;
M_1 = the mass of the impacted module, W_1/g;
W_1 = the weight of the impacted module; and
g = the acceleration due to gravity.

Multiplying both sides of the equation by g and solving for V_1 give

$$V_1 = V_o\left(\frac{W}{W + W_1}\right) \tag{2}$$

assuming that the first mass impacted, W_1, remains independent of the vehicle.

The vehicle speed after second mass impact is

$$V_2 = V_1\left(\frac{W}{W + W_2}\right) \tag{3}$$

The vehicle speed after the ith mass impact is

$$V_i = V_{i-1}\left(\frac{W}{W + W_i}\right) \tag{4}$$

If s is defined as the distance between the expendable mass centers, the average deceleration among the masses is

$$G = \frac{v_{i-1}^2 - v_i^2}{2gs} \tag{5}$$

For design purposes, the above equation may be solved for v_i as the minimum velocity to maintain an average specified deceleration G for spacing s and gives

$$v_i = \sqrt{v_{i-1}^2 - 2Ggs} \tag{6}$$

The weight of the module can be obtained by solving for W_i by

Figure 1. Principle of transferring vehicle momentum to expendable masses, assuming rigid body plastic impact.

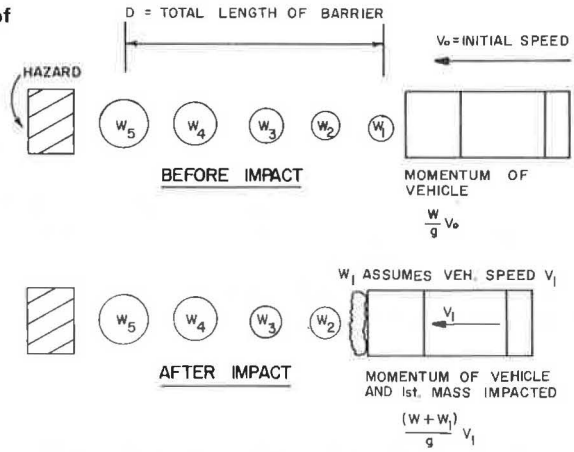

Figure 2. Design modules for tire-sand inertia barrier.

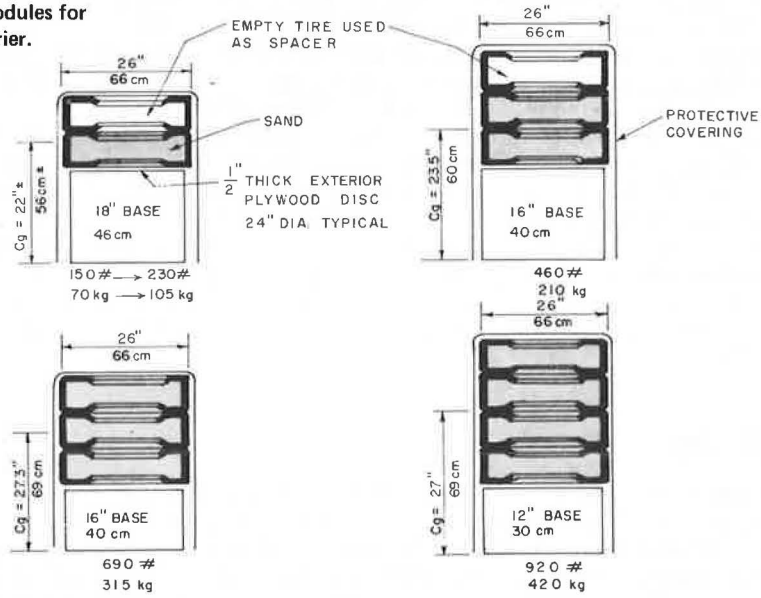

Figure 3. Design of a typical layout of tire-sand inertia barrier and estimated vehicle deceleration data based on initial impact of 60 mph (97 km/h).

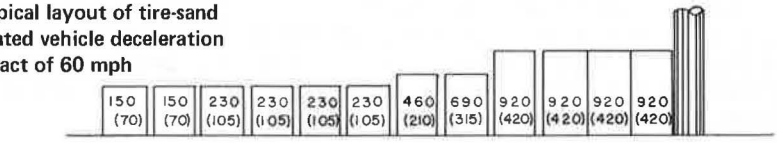

Numbers in Parenthesis are in Kilograms

ELEVATION

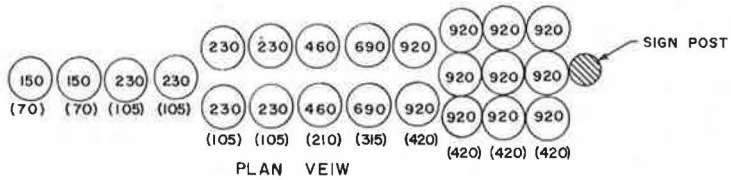

PLAN VEIW

2000 # (900 kg) Vehicle	G_{avg}	6.5	5.6	7.0	5.7	7.9	5.3	5.4	3.2	0.6		Avg = 5.6 g
	V_L mph	55.8	51.9	46.6	41.8	34.0	27.6	18.9	11.1	5.8		
	km/h	89.8	83.5	75.0	67.3	54.7	44.4	30.4	17.9	9.3		
4500 # (2040 kg)	G_{avg}	3.2	2.7	4.0	3.8	6.1	5.1	7.3	6.6	4.7	2.9	1.1	Avg = 4.0 g
Vehicle	V_L mph	58.0	56.2	53.5	50.8	46.1	41.8	34.7	26.6	18.9	11.7	7.3	
	km/h	93.3	90.4	86.1	81.7	74.2	67.3	55.8	42.8	30.4	18.8	11.7	

$$W_i = \frac{W(V_{i-1} - V_i)}{V_i} \quad (7)$$

It is apparent that theoretically the vehicle cannot be stopped completely by this principle. Practically, however, it is usually adequate to design the inertia barrier to reduce the vehicle speed to about 10 mph (16 km/h).

The remaining energy is dissipated by the ploughing action (1, 2) from sand and additional modules placed in the vehicle path.

Statistical Data

Since scrap automobile tires vary in size and weight, statistical data were needed for design purposes. Hirsch (1) collected one hundred twenty-four 14 and 15-in. (36 and 38-cm) used automobile tires from a local disposal area to determine their average weight, diameter, and weight and height filled with sand. The method of filling each tire was by hand so that the entire space was used. The average weight of the tires was 18.5 lb (8.4 kg), and the standard deviation was 3.8 lb (1.7 kg). The outside diameters of the tire ranged from 25.5 to 27.5 in. (65 to 70 cm) and averaged 26.25 in. (67 cm), which was adequate for design purposes. After these data were determined, the tires were filled with sand and were weighed. The procedure was to fill a tire, weigh it, and measure the thickness. A second tire was placed on the first, filled with sand, and the combination weighed and measured. The process was repeated until the stack was four tires high. The process was continued until 108 tires were processed. The average total weight of the tires filled with sand was 228 lb (103 kg); 230 lb (104 kg) were used for design, and the standard deviation was 23.54 lb (10.7 kg). The average height for tires filled with sand was 7.5 in. (19 cm). The average height for empty tires was 5.5 in. (14 cm).

Standard Modules

These statistical data led to the development of standard modules as shown in Figure 2. The lightest module [150 to 230 lb (68 to 104 kg)] is used on the nose of the barrier. This is the only module in which the average weight will vary. The variation may be accomplished easily by using a container of known volume and weight to measure the sand. The other three modules are progressively heavier up to a limit of four tires filled with sand, which have an average weight of 920 lb (417 kg). These modules may be used singly in each row or in multiples of two or three per row.

A typical barrier design and estimated vehicle deceleration data based on initial impact of 60 mph (97 km/h) are shown in Figure 3. The design presented conforms to the latest FHWA criteria for vehicle impact attenuators (5). The final row of modules is used to stop the vehicle by ploughing action.

Two successful supports were tested. The first was a wire cage that collapsed when impacted. The wire cage was constructed of 14 gauge galvanized welded wire fabric with 1 by 2-in. (2.5 by 5-cm) openings. Details (plan view) of construction are shown in Figure 4. The details of the second successful support are shown in Figure 5. This support is made of used, 55-gal (208-liter) steel drums that have the stiffening tops and bottoms removed and that then are cut vertically at 16 equidistant points. These cuts made the support weak laterally but still retained sufficient strength vertically to support the heaviest module. One 18-in.-high (46-cm) support was tested in a universal static testing machine. A compressive load of 2,300 lb (1043 kg) was slowly applied, held for several minutes, and then released. The support was undamaged, and at no time did it exhibit any tendency toward instability. From this test, it was concluded that there was no strength problem. This was proved in erecting the test installation.

In addition to equations 4, 5, 6, and 7, graphs have been developed to aid in the

Figure 4. Wire cage support details.

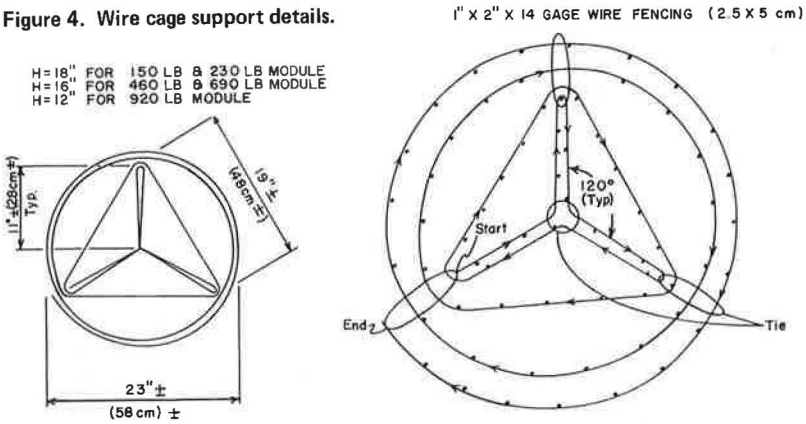

Figure 5. Steel drum support details.

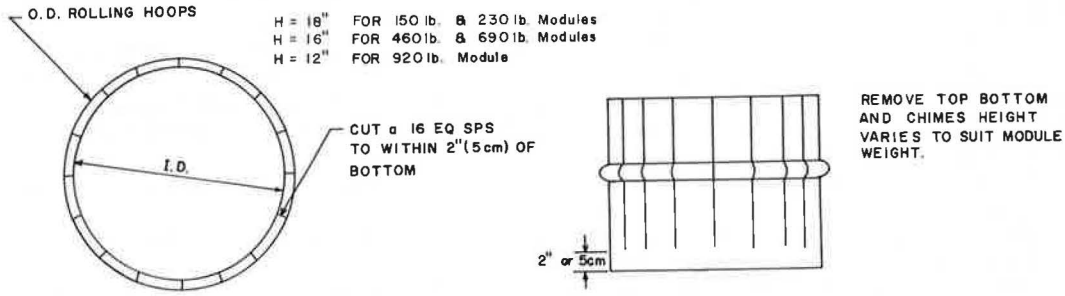

Figure 6. Sand-tire inertia barrier design curves for 2,000-lb (907-kg) vehicle.

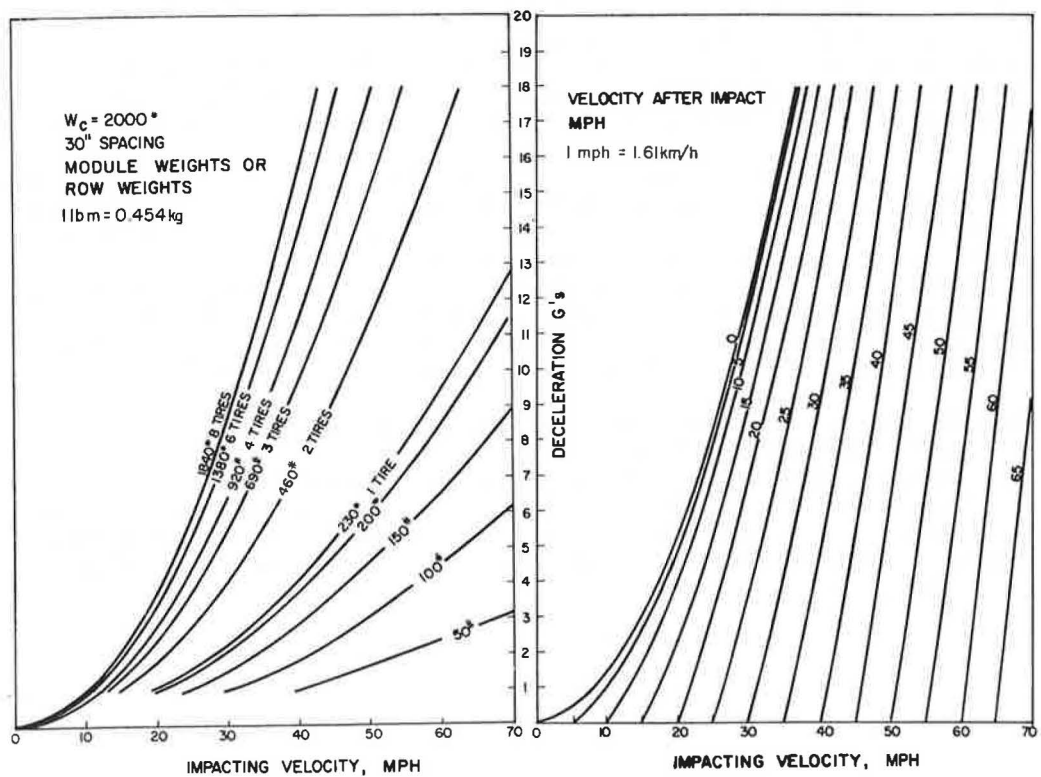

design of inertia barriers. These graphs based on the number of tires for a 30-in. (76-cm) spacing of modules are shown in Figures 6 and 7.

VEHICLE CRASH TESTS

Four additional vehicle crash tests were conducted for the Texas State Department of Highways and Public Transportation. Earlier tests on the tire-sand inertia barrier were conducted for the National Cooperative Highway Research Program (2).

In test 2146-I-3, the first one in the department program, the annular space of tires was filled with used beverage cans, and the tires were banded together to form a base. The tires containing sand were then lashed to the bases. The vehicle ramped during the test, and the idea of the tire base was abandoned.

In the next test, 2146-I-4, the bases used were the wire fabric cages, which were designed to collapse on impact and not produce an uplift force on the vehicle as they rolled under the vehicle (Figure 4). This test was conducted without the benefit of a backup structure.

The vehicle used for this test was a 1967 Dodge Monaco with a gross weight of 4,290 lb (1946 kg). Figure 8 shows the vehicle and barrier before the test.

The vehicle impacted the center of the barrier. The speed was 64 mph (103 km/h). The vehicle behaved as anticipated during impact. However, the majority of the mass was propelled to a place well ahead of the vehicle, and the vehicle stopped approximately 18 ft (5.5 m) after it passed the original end of the barrier. Figure 9 shows the vehicle and barrier after the test.

Two tires were hurled more than 100 ft (30 m) during impact. This occurred in previous tests (1, 2) with the tire-sand barrier.

The protective coverings were polyethelene sleeves of 4-mil (0.1-mm) thickness, such as those used by service stations.

In the third test, 2146-I-5, the barrier was constructed according to the design in Figure 3. The bases were fabricated from used paint drums modified in accordance with Figure 5, except that the top and bottom of the drum remained as an integral part of each base. The covering for the modules was made of 0.025-in. (0.6-mm) aluminum (the lightest readily available). The vehicle impacted the nose of the barrier at an angle of 15 deg with the barrier's longitudinal axis.

The vehicle used for the test was a 1961 Chevrolet weighing 4,090 lb (1855 kg) including the weight of the anthropometric dummy. The hood conformed to the current trend in American-made vehicles in that it extended to the windshield without an intermediate cowling.

The vehicle impacted the barrier in the center at 61.9 mph (99.6 km/h) and performed as mathematically predicted until the vehicle penetrated the barrier. The chimes and bottoms of the drums made the bases very stiff; they tended to build up under the vehicle, and the vehicle ramped. The hood came open but remained on the vehicle.

For the final test of the series, 2146-I-6, the typical barrier (Figure 3) was tested. The supports were made from steel drums designed according to Figure 5; that is, the tops or bottoms and chimes were removed. The protective covering was made from Armstrong Decolon vinyl rugs (linoleum) at a cost of approximately $\$0.11/ft^2$ ($\$1.18/m^2$).

The vehicle was a 1968 Chevrolet weighing 4,000 lb (1814 kg) including the dummy. Figure 10 shows the vehicle before and after the test.

The barrier was located in front of a simulated luminaire standard as shown in the top half of Figure 11. The vehicle impacted the center of the barrier at 43.1 mph (69.3 km/h). The vehicle performed as predicted except that there was a slight tendency to ramp that was evident toward the end of impact. Again, the hood came ajar but remained on the vehicle.

Figure 7. Sand-tire inertia barrier design curves for 4,500-lb (2041-kg) vehicle.

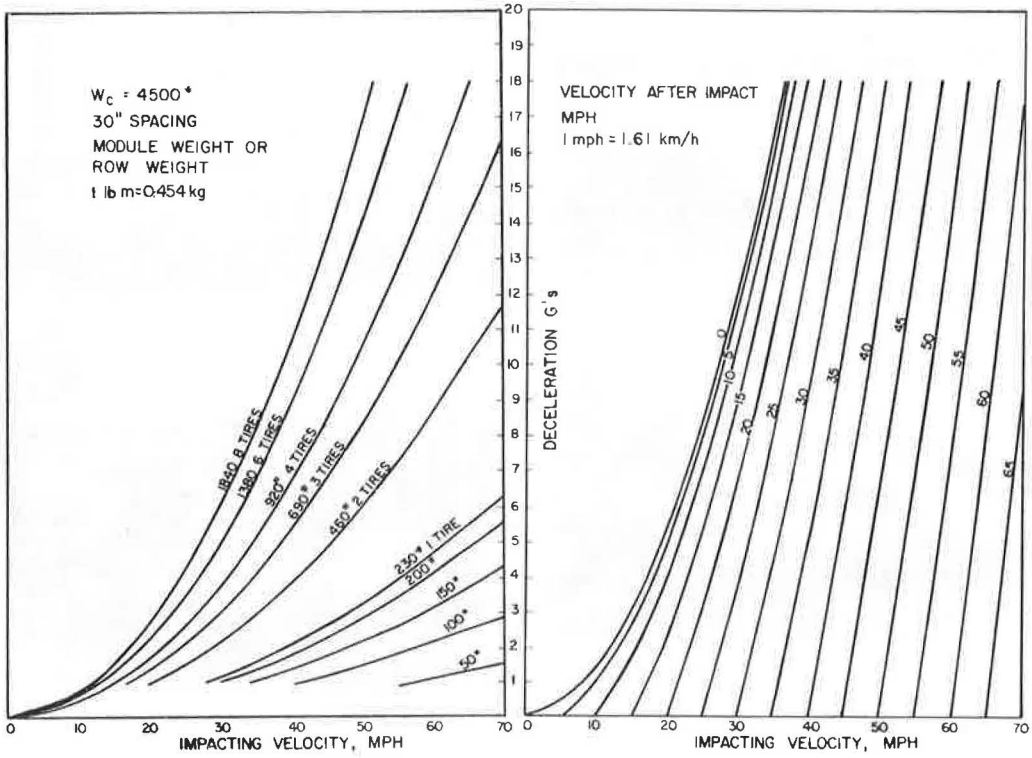

Figure 8. Test I-4 vehicle and barrier before impact.

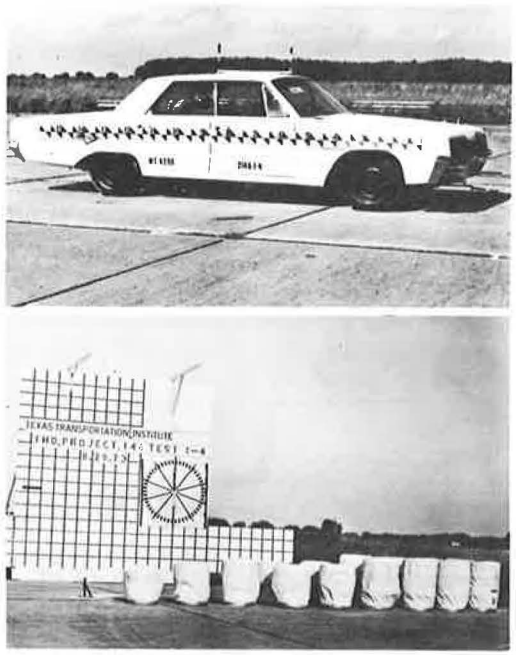

Figure 9. Test I-4 vehicle and barrier after impact.

Figure 10. Test I-6 vehicle before and after impact.

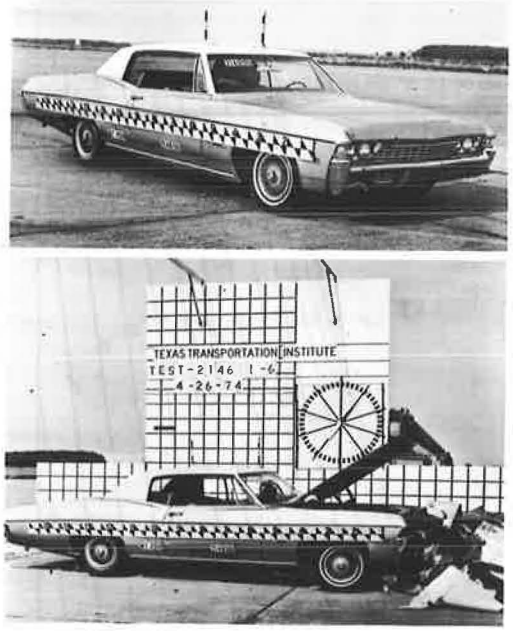

Figure 11. Test I-6 barrier before and after impact.

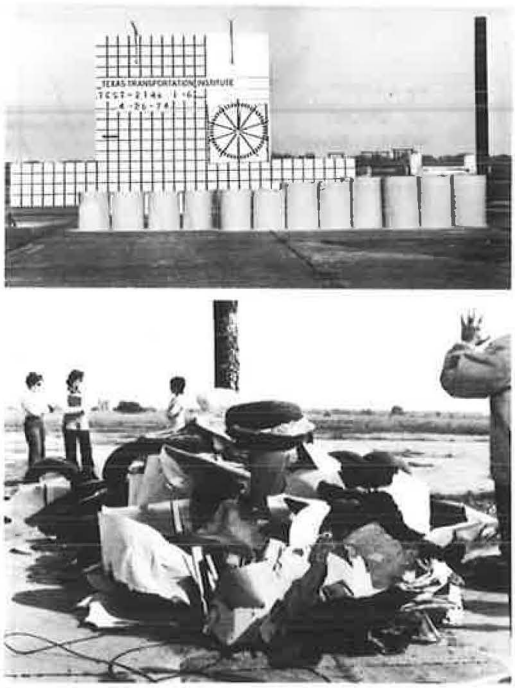

Table 1. Test data.

Item	Test I-3	Test I-4	Test I-5	Test I-6
Vehicle				
Make	Ford	Dodge	Chevrolet	Chevrolet
Year	1964	1967	1961	1968
Weight, lb	4,500	4,290	4,090	4,000
Impact angle, deg	0	0	15	0
Film data				
Initial speed, mph	62.2	64.0	61.9	43.1
Final speed, mph	0	0	28.7	0
Maximum forward motion, ft	Vehicle ramped	43.9		
Time, sec		2.25		
Accelerometer data				
Peak				
Longitudinal (*g*)	11.6		6.3	4.9
Transverse (*g*)	2.2		3.9	1.0
Average deceleration				
Longitudinal (*g*)	5.0		3.4	2.6
Over-time, sec	0.2		0.4	0.5
Maximum seatbelt force, lbf	1,395		460	290

Note: 1 lb = 0.45 kg. 1 mph = 1.6 km/h. 1 ft = 0.3 m. 1 lbf = 4.4 N.

DISCUSSION OF TESTS

The four full-scale tests were conducted on tire-sand inertia barriers with bases of four designs. Pertinent data from high-speed photography and accelerometers are given in Table 1. The stopping characteristics of the barriers were as predicted by the equations until the vehicle vaulted as in test I-3 or penetrated the barrier as in tests I-4 and I-5.

The base for the modules used in test I-3 was tires banded together as described earlier. The vehicle in test I-3 had traveled approximately 5 ft (1.5 m) when the first tires were dragged underneath the vehicle. The base of each module was crushed, and friction resistance with the ground caused the tires to move at a slower speed than the vehicle. This pulled the tires underneath the vehicle. The tires holding the sand were tied to the bases and were pulled under the vehicle. The result was that at about 0.172 sec or after the vehicle had traveled 10 to 12 ft (3 to 3.7 m) it began to climp up the modules. This chain of events caused the vehicle to end up with the front of the vehicle undercarriage resting on top of the concrete backup wall. The rear end of the vehicle was dragging the ground when it came to rest. None of the modules or individual tires had been sent flying as was the case in all previous tests (1, 2). It appears that tying the base tires to the container tires was instrumental in lessening the vaulting effects and in keeping the rear of the vehicle on the ground. The concept did not go far enough to prevent vaulting. Modules banded together so that sand that could not escape would probably move in front of the impacting vehicle. If so, the vaulting would be eliminated, but the total mass would move instantaneously and increase the severity of the impact. This is what would occur according to procedures recommended by Gadd (7). This solution would not necessarily be the best trade-off.

The wire cage used to support the sand mass in test 2146-I-4 collapsed on impact and rolled underneath the vehicle as intended. There was no tendency for the vehicle to ramp during this test. The vehicle behaved essentially according to the mathematical predictions until after the last module had been impacted. Since there was no backup wall to stop the tires or the sand mass, they were moved ahead for a considerable distance. The vehicle ploughing action into the debris (which is necessary to completely stop the vehicle) eventually brought the vehicle to a complete stop 43.9 ft (13.4 m) from the initial impact point. The majority of the tire and sand debris was located in the space 15 to 20 ft (4.5 to 6.0 m) in front of the vehicle. This required a total distance of 60 to 65 ft (18 to 20 m) to contain a vehicle with no hazard immediately behind the barrier. This distance can be greatly reduced by adding a few much heavier modules at the rear of the barrier. The required distance for the ploughing action and the space to collect debris would thereby be reduced since the heavier modules would help stop the bulk of the sand and tires from going beyond the back of the barrier. Regardless of the design, some additional space must be supplied behind the barrier for penetration and collection of debris when no rigid obstacle or backup wall is present.

The hood was forced open in test I-3. The hinges of the hood on the vehicle used in test I-4 were broken, which caused the hood to fall off (0.350 and 0.749 sec). Similar incidents have occurred in three previous tests on other projects, as well as in tests reported by California on a similar type of barrier (9).

Recent model American-made vehicles have been designed without the intermediate cowl between the hood and windshield. Researchers were concerned about the possibility of these hoods breaking loose from their hinges and penetrating the windshield. The two final tests were conducted using vehicles without the intermediate cowling. In both tests, the hoods flew open on impact but the hinges held, and the hoods remained with the vehicles. The hinges comply with the latest federal motor vehicle safety standards and are adequate to withstand the impact intensities without allowing the hinges to fracture.

The base used in test I-5 was fabricated from used, 55-gal (208-liter) steel paint drums and was similar to the base shown in Figure 5. The major difference from Figure 5 was that the end chimes and top or bottom of the drum were used as support for possible soft soil. These bases proved to be too stiff and caused the vehicle to ramp as it crossed through the barrier on a 15-deg impact angle.

The cover used in this test was 0.025-in. (0.6-mm) aluminum, the thinnest available. It also was too stiff to be of practical benefit.

The base used in test I-6 was fabricated as shown in Figure 5 from used, 55-gal (208-liter) paint drums. The chimes and tops and bottoms were removed, and the base was not so stiff laterally as were the bases used in test I-5; these performed satisfactorily.

The protective cover used in this test is inexpensive and satisfactory. The linoleum

should last several months in the weather and appears to contain the tires so that the missile problem is reduced. Special care should be exercised to attach the top of the covering so that rain or atmospheric moisture will not penetrate the sand and change the impact characteristics of the modules.

The top speed of the vehicle was only 43.1 mph (69 km/h), and the deceleration values were low. Because the design was for a relatively flat deceleration curve, the longitudinal deceleration and the seatbelt pull were both much smoother for test I-6 and test I-5 than for previous tests in which a much harder nose was used.

CONCLUSIONS

Scrap tires filled with sand will make an effective inertia type of vehicle impact attenuator for selected locations. The sand-filled tires used in each module need to be supported on easily crushable bases such as treated cardboard cartons (2), wire cages developed on this project (Figure 5), or bases fabricated from used, 55-gal (208-liter) paint drums (Figure 6).

The center of gravity (c.g.) of vehicles on the road generally varies from a low of 18 in. (46 cm) to a high of 23 in. (58 cm) (8). The average height of the c.g. is about 20 in. (50 cm). The crushable bases should be sized to raise the c.g. of the module to approximately 20 in. (50 cm) or more except for the first module impacted.

The following conclusions can be made:

1. The theory of conservation of momentum will provide a satisfactory design method for the tire-sand inertia barrier;
2. The state of the art of inertia barriers is sufficiently advanced so that the tire-sand inertia barrier can be considered for selected use; and
3. Tire-sand inertia barriers should be installed only in locations where the effects of flying or rolling tires or flying or loose sand and other debris associated with the barrier would not become a secondary hazard to other traffic as is the case on elevated sections.

In all high-speed impacts to date, a considerable amount of sand has accumulated on the engine, which could make it temporarily inoperative; however, this same sand could minimize the probability of fire. Additional research is recommended to determine the effectiveness of the tire-sand barrier in protecting guardrail ends.

The research in this paper indicates that the tire-sand inertia barrier would be an economical and effective crash cushion for use in front of rigid obstacles along the roadside where the scattered sand and tires are not likely to fall on the paved roadway. The estimated total installed cost of the tire-sand inertia barrier is approximately $800 when the barrier is installed by state employees.

ACKNOWLEDGMENT

The contents of this report reflect the views of the authors, who are responsible for the facts and the accuracy of the data presented. The contents do not necessarily reflect the official views or policies of the Federal Highway Administration. This report does not constitute a standard, specification, or regulation.

REFERENCES

1. T. J. Hirsch. Vehicle Impact Attenuation. In Final Report on the Feasibility of Using Solid Waste in Highway Construction and Maintenance, Texas Transportation Institute, Texas A&M Univ., chap. 3.11, Oct. 1971.
2. T. J. Hirsch, E. L. Marquis, and C. E. Buth. Crash Cushions of Waste Materials. NCHRP Rept. 157, 1975.

3. T. J. Hirsch. Use of Mathematical Simulations to Develop Safer Highway Design Criteria. North Carolina Symposium on Highway Safety, April 12, 1973.
4. T. J. Hirsch. Crash Barriers—State of the Art. Western Association of State Highway Officials, Montana, June 20, 1973.
5. Use of Crash Cushions on Federal-Aid Highways. Federal Highway Administration Instructional Memorandum 40-5-72 HNG-32, Nov. 8, 1972.
6. Test and Evaluation of Vehicle Arresting, Energy Absorption, and Impact Attenuation Systems. Texas Transportation Institute, Texas A&M Univ., Nov. 30, 1971.
7. C. W. Gadd. Use of a Weighted-Impulse Criterion for Estimating Injury Hazard. Society of Automotive Engineers, SAE 660793, 1966.
8. E. E. Seger and R. S. Brink. Trends of Vehicle Dimensions and Performance Characteristics From 1960 Through 1970. Highway Research Record 420, 1972, pp. 1-16.
9. E. F. Nordlin, J. R. Stoker, and R. N. Doty. Dynamic Tests of an Energy-Absorbing Barrier Employing Sand-Filled Plastic Barrels. Highway Research Record 386, 1972, pp. 28-52.

SPONSORSHIP OF THIS RECORD

GROUP 2—DESIGN AND CONSTRUCTION OF TRANSPORTATION FACILITIES
W. B. Drake, Kentucky Department of Transportation, chairman

GENERAL DESIGN SECTION
F. W. Thorstenson, Minnesota Department of Highways, chairman

Committee on Safety Appurtenances
Eric F. Nordlin, California Department of Transportation, chairman
Gordon A. Alison, Dennis W. Babin, William E. Behm, W. C. Burnett, Duane F. Dunlap, Malcolm D. Graham, Wayne Henneberger, Jack E. Leisch, Edwin Lokken, Bruce F. McCollom, Jarvis D. Michie, Roy J. Mohler, Roger J. Murray, Robert M. Olson, William L. Raymond, Jr., Edmund R. Ricker, Neilon J. Rowan, F. G. Schlosser, Richard A. Strizki, Flory J. Tamanini, James A. Thompson, John G. Viner, Charles Y. Warner, M. A. Warnes, Earl C. Williams, Jr.

Lawrence F. Spaine, Transportation Research Board staff

The organizational units and the chairmen and members are as of December 31, 1974.